NASA CR-66704

COMPARISON OF SOIL EROSION THEORY WITH SCALED LM JET EROSION TESTS

By Robert E. Hutton

OCTOBER 1968

Prepared under Contract No. NAS1-7970 by
TRW SYSTEMS GROUP
Redondo Beach, California

for

NATIONAL AERONAUTICS AND SPACE ADMINISTRATION

NASA CR-66704

COMPARISON OF SOIL EROSION THEORY WITH SCALED LM JET EROSION TESTS

By Robert E. Hutton

Issued by Originator as Report No. 10608-6004-R0-00

Prepared under Contract No. NAS1-7970 by
TRW SYSTEMS GROUP
Redondo Beach, California

for

NATIONAL AERONAUTICS AND SPACE ADMINISTRATION

Page Intentionally Left Blank

ACKNOWLEDGMENTS

The author wishes to acknowledge and express his appreciation for the cooperation and assistance given by the Langley Research Center during the performance of this work; in particular, to Mr. W. D. Conner and Mr. N. Land for providing the data used in the study and for their constructive comments and suggestions. He also wishes to express his appreciation to Mr. R. Schreiner of TRW Systems for the constructive suggestions given throughout the study and the assistance given in employing the TRW On-Line Computer Facility. Finally, he wishes to express his appreciation to Dr. J. McMunn for his assistance in the performance of this study.

Page Intentionally Left Blank

CONTENTS

CONTENTS (Continued)

ILLUSTRATIONS

ABSTRACT

Predictions, based on an existing theory, of soil erosion caused by impingement of gases from a descending rocket in a vacuum environment have been compared with experimental data obtained in a vacuum sphere. A total of 143 comparisons at various time and surface locations were made which included experiments with varying nozzle, engine, and soil conditions. The experiments were made with a small, cold gas jet which was scaled to represent the Apollo-LM conditions. The comparisons indicated a limited degree of correlation between the theory and the experiments.

SUMMARY

Roberts' theory for a lunar environment was used to predict soil erosion caused by viscous shearing stresses exerted on the soil-gas interface by the impingement of rocket exhaust gases. Predictions were compared with the erosion observed in tests conducted by Land, Clark, and Scholl in a vacuum sphere at the Langley Research Center. In all tests the nozzle was released from a fixed height and allowed to descend to a hover position with the jet gases directed perpendicular to a simulated soil test bed. The comparisons indicated a limited degree of correlation between theory and test. At times the erosion depth was over-predicted, but more often it was underpredicted. The surface location of the maximum erosion depth was often in error, but this was usually a consequence that the minimum nozzle heights that occurred during the tests were below the critical height for which the theory is valid.

The comparison of predicted and observed erosion depths for 143 time and surface locations indicated the predictions to be accurate within a factor of two 43 percent of the time and to within a factor of four 87 percent of the time.

INTRODUCTION

When retro rockets are used to brake a vehicle for a soft landing on the lunar surface the action of the rocket gases on the soil surface may have a major influence on the success of the landing. In an effort to assess plume-soil interaction effects, a series of experiments were conducted at the Langley Research Center, and the results were presented in References 1 and 2. The experimental procedure followed in these experiments is also described in Reference 3. These experiments explored the influence of variations in engine parameters and approach conditions, as well as the influence of variations in surface parameters. A theory was also developed at the Langley Research Center by Leonard Roberts and presented in References 4 and 5 to describe the surface erosion caused by rocket gas impingement under perfect vacuum conditions. Reference 6 contains additional comments on the exhaust flow field and surface impingement phenomena.

The purpose of the present investigation is to compare theoretical erosion predictions based on References 4 and 5 with observed erosion results for each of the 32 tests presented in References 1 and 2. This comparison is needed so a judgement can be made concerning the accuracy of the theory, and a determination of factors of uncertainty which must be applied to erosion predictions made for various lunar exploratory missions. Differences between theory and experiment must be identified and used to guide future experimental and theoretical investigations directed towards a more basic understanding of the phenomena. Such an understanding will allow an improved formulation of analytical procedures for extending and extrapolating test data, and for erosion predictions for various engine and surface parameters and landing approach modes.

Although this investigation is concerned with the action of rocket gases on soil surface, related phenomena have been studied earlier in connection with the transport of sediment and sand by water and wind action. In Reference 7, Kadib conducted an experimental investigation of the movement of sand by wind action. He reviewed many of the earlier investigations concerned with wind

and water action on soil and sediment transport, and concluded that the basic principles governing both types of transport are the same. As a result of his wind tunnel tests, Kadib concluded the basic force, which produces the transport motion of the soil particle, is due to an average lift and a fluctuating lift caused by turbulence.

In Reference 8, Chepil also conducted an experimental investigation of the movement of soil grains by wind action. He found that both lift and drag forces were exerted on the soil grains. The magnitude of the lift and drag pressure impulses were statistically distributed according to a somewhat skewed normal error law. The ratio of lift to drag was about 0.85 and the standard deviation of the pressure was about 0.49 times the average pressure.

Although it is recognized that there is experimental evidence indicating statistical methods may be required to describe the soil erosion phenomena, the deterministic procedure advanced by Roberts gives a simple method which may provide estimates of the average erosion. Thus, an assessment of the accuracy of predictions made with Roberts' theory is required before the development of more involved prediction procedures. The study conducted here is simply to make this assessment.

SYMBOLS

Engine Parameters

γ = gas specific heat ratio (dimensionless)

M_e = Mach no. at exit (dimensionless)

R = gas constant ($ft^2/sec^2\ ^oR$)

T_c = chamber gas temperature (^oR)

μ_c = chamber gas viscosity ($lb\text{-}sec/ft^2$)

p_c = chamber gas pressure (psf)

k = hypersonic parameter (dimensionless) $= 2\dfrac{\text{exhaust kinetic energy}}{\text{exhaust internal energy}}$

Flow-Field Parameters

a = ratio of soil particle velocity to gas velocity (dimensionless)

C_D = particle drag coefficient (dimensionless)

C_f = shear stress coefficient (dimensionless)

C_ℓ = lift coefficient (dimensionless)

M_ℓ = local Mach number (dimensionless)

p_r = recovery pressure (psf)

p_s = stagnation pressure (psf)

p = surface pressure (psf)

q = dynamic pressure along the surface based on gas radial velocity u (psf)

R_D = particle Reynolds number (dimensionless)

R_θ = flow field Reynolds number (dimensionless)

u = gas radial velocity (ft/sec)

v = velocity of soil particle entrained in the flow (ft/sec)

μ = gas viscosity (lb-sec/ft^2)

ρ = gas mass density (slugs/ft^3)

τ = shear stress acting on soil (psf) = $q C_f$ (for rough turbulent flow)

A = cross sectional area of soil element (ft^2)

A_{coh} = cohesion parameter (Roberts recommends 5×10^{-17} lb-ft)

c = soil packing constant [= 1 minus porosity] (dimensionless)

D = soil particle size (ft)

α = soil internal friction angle (radians)

ζ = parameter in equation for "a" (dimensionless)

σ = soil mass density (slugs/ft^3)

τ_{coh} = soil cohesive stress (lb/ft^2)

τ^* = soil restraining shear stress (psf)

Miscellaneous Parameters

a_2 = parameter in h equation = 0.25, Appendix B (dimensionless)

$f(R_e)$ = functional relation between the measured drag on a spherical particle and Reynolds number R_e (Relation was taken from Figure 1.5 in Reference 14 and reproduced here in Figure D1)

g = acceleration of gravity (ft/sec^2)

h = height of nozzle exit plane (ft)

h_c = critical nozzle height (ft)

h_o = nozzle height at time t = 0 (ft)

h_1 = nozzle height at hover (ft)

$h_1(t)$ = nozzle height above uneroded surface during descent (ft)

K = factor multiplying C_f -- taken to be unity here (dimensionless)

N = factor relating measured and predicted maximum erosion depths = experiment ÷ theory, or the inverse whichever > 1 (dimensionless)

r = radial station measured from stagnation point (ft)

SF = scale factor = maximum ordinate value on oscilloscope (ft)

t = time (sec)

t_1 = time at which hover begins (sec)

T = final time (sec)

y = soil erosion depth (ft)

y_{max} = maximum value of y (along r) at each time increment (ft)

$\dot{y}$ = soil erosion rate (ft/sec)

V_v = descent velocity (ft/sec)

$\tan \beta$ = slope of erosion crater $\partial y/\partial r$ (radians)

COMPUTATIONAL PROCEDURE

Soil erosion predictions for each set of the system parameters listed in Appendix A are based on solutions of the governing partial differential equations presented in Appendix B. The solutions were obtained on a digital computer in which the operator has control of the computer during the computations. Upon operator command, the input or output data can be displayed on a cathode ray tube oscilloscope in the form of graphical or alphanumerical data, displayed graphically by a CalComp plotter, or typed by an output writer. The computational procedure to determine the erosion profiles for the 32 tests is described as follows:

The system parameters and measured erosion at discrete times and radial stations for a particular test are first input to the computer. To verify the data are input correctly, they are then displayed on the oscilloscope. A typical display of the input data is shown in Figure 1(a). Note that the numerical values are followed by an algebraic sign and two digits which correspond to the factor of 10 associated with the number. For example, the Mach number is 0.268×10 or 2.68 while the particle diameter is 0.162×10^{-2} or 0.00162 foot. The letters under the Key column merely indicate to the operator the location where the associated parameter is stored in the computer.

The integration step size, the times at which erosion profiles are to be stored, and the time for the computations to cease are then input to the computer. At the initiation of the computations it is assumed that time is zero and the soil surface is a flat horizontal plane. The computer first determines the erosion profile for the range specified (usually taken to be a 1-foot range from the stagnation point) for the first time increment, and then for successive time increments until the final time is reached.

At the time when descent ends, the corresponding erosion profile is displayed on the oscilloscope as shown in Figure 1(b). This display shows the erosion depth (ordinate) over a 1-foot radial range from the stagnation point (abscissa). Only one half the profile is displayed because theory assumes the profile to be symmetric about the stagnation point. Since depth is shown upward,

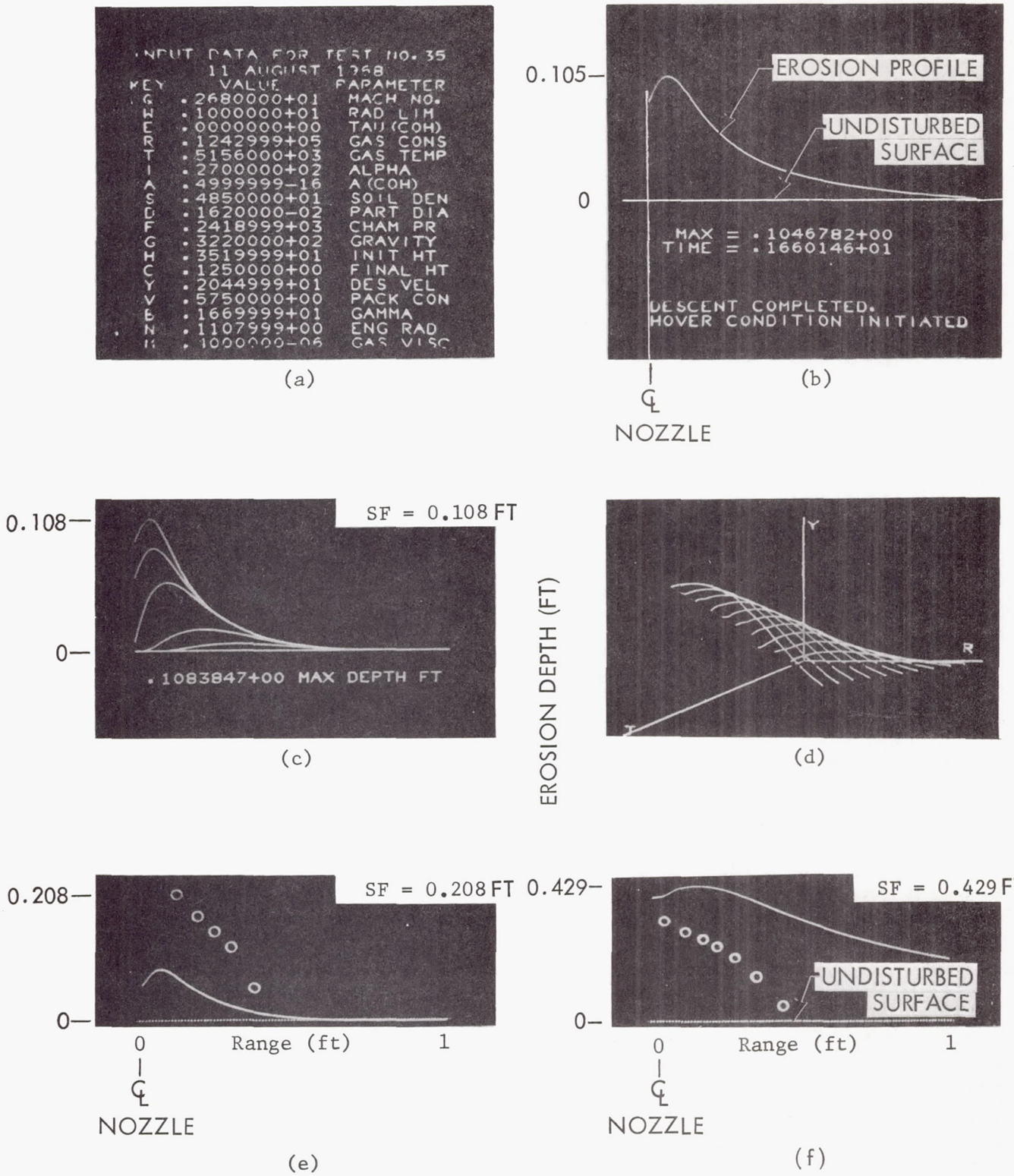

Figure 1. - Typical Computer Output Data

the half profile is viewed upside down. Figure 1(b) indicates the end of descent occurred at t = 1.660146 seconds, and the maximum erosion depth is 0.1046782 foot.

When the computations are finished, the stored erosion profiles can be recalled upon command at the operator keyboard and displayed on the oscilloscope. Figure 1(c) illustrates typical erosion profiles at five different times. The maximum erosion depth is 0.1083847 foot. Thus, the ordinate scale factor SF associated with this curve is labeled 0.108. A three-dimensional view of the erosion profiles can also be displayed upon command; an example is shown in Figure 1(d). Such curves were of little engineering value in this study and, therefore, are not presented in the detailed comparisons.

The measured erosion test points and the corresponding predicted erosion profile can also be recalled on command and displayed as shown in Figures 1(e) and 1(f). In Figure 1(e) the theoretical prediction (the curve) is less than the measured profile (the circles). The ordinate scale factor SF, in all data presented here and in the next section, represents the ordinate scale from the base line to the top data point presented measured in feet, regardless of whether it is a circled data point or the maximum erosion depth on a theoretical erosion profile. In Figure 1(e) the scale factor SF = 0.208 foot represents the depth to the highest data circle on the figure. In Figure 1(f), where the theoretical profile is higher than the measured erosion depths, the scale factor SF = 0.429 foot represents the depth to the highest point on the theoretical erosion profile. In all cases, the horizontal scale is from 0 to 1 foot while the vertical scale is established by the ordinate scale factor indicated.

It might be appropriate to mention two computational problems encountered in the solution of the erosion partial differential equation. The first difficulty is associated with the singularity at r = 0 (the stagnation point). At this point the radial gas velocity u is zero and the governing equations involve division by u. Difficulties are circumvented by simply determining the erosion at a neighboring point r = 0.01 and assuming the erosion at r = 0.01 is the same as at r = 0.

The second problem arises because the erosion rate expressed by Equation (B3) is a function of the local slope $\tan \beta = \partial y / \partial r$. Thus, to determine the incremental erosion Δy occurring over the time interval t to $t + \Delta t$ requires a spatial differentiation of the erosion profile y at time t. Since differentiation is inherently a destabilizing procedure any "noise" is propagated as the profiles are determined at successive times. This difficulty is overcome by numerically smoothing the increment Δy before adding it to the profile y at time t to obtain the erosion profile at time $t + \Delta t$. This numerical smoothing procedure is described on page 295 of Reference 9. The smoothing procedure was tested on a simplified equation of the form of (B3) for which a closed form solution could be found. Comparisons of the solutions obtained both with and without the numerical smoothing procedure with the exact solution, indicated the procedure did indeed converge to the correct solution. These comparisons are presented in Reference 10 where this point is discussed more fully.

RESULTS

Detailed comparisons of theoretical predictions and measured erosion for each of the 32 tests are presented in the 32 figures in Appendix C. The results presented in this section are selected from the detailed comparisons to show the influence of several system parameters and to provide an overall assessment of the accuracy of theoretical predictions. An examination of the detailed comparisons in Appendix C and the results presented here show that theoretical predictions often differ substantially from measured results. Possible sources of these discrepancies are discussed in the next section.

Before examining various detailed comparisons the entire results are examined from the overall viewpoint provided by Figures 2 and 3. Figure 2 shows a comparison of the predicted and measured maximum erosion depth for each of the 32 tests at each of the times a profile was compared with measured results. The three parts of the figure illustrate the comparisons during the descent period, at the instant descent ends (at which time hover begins) and during the hover period.

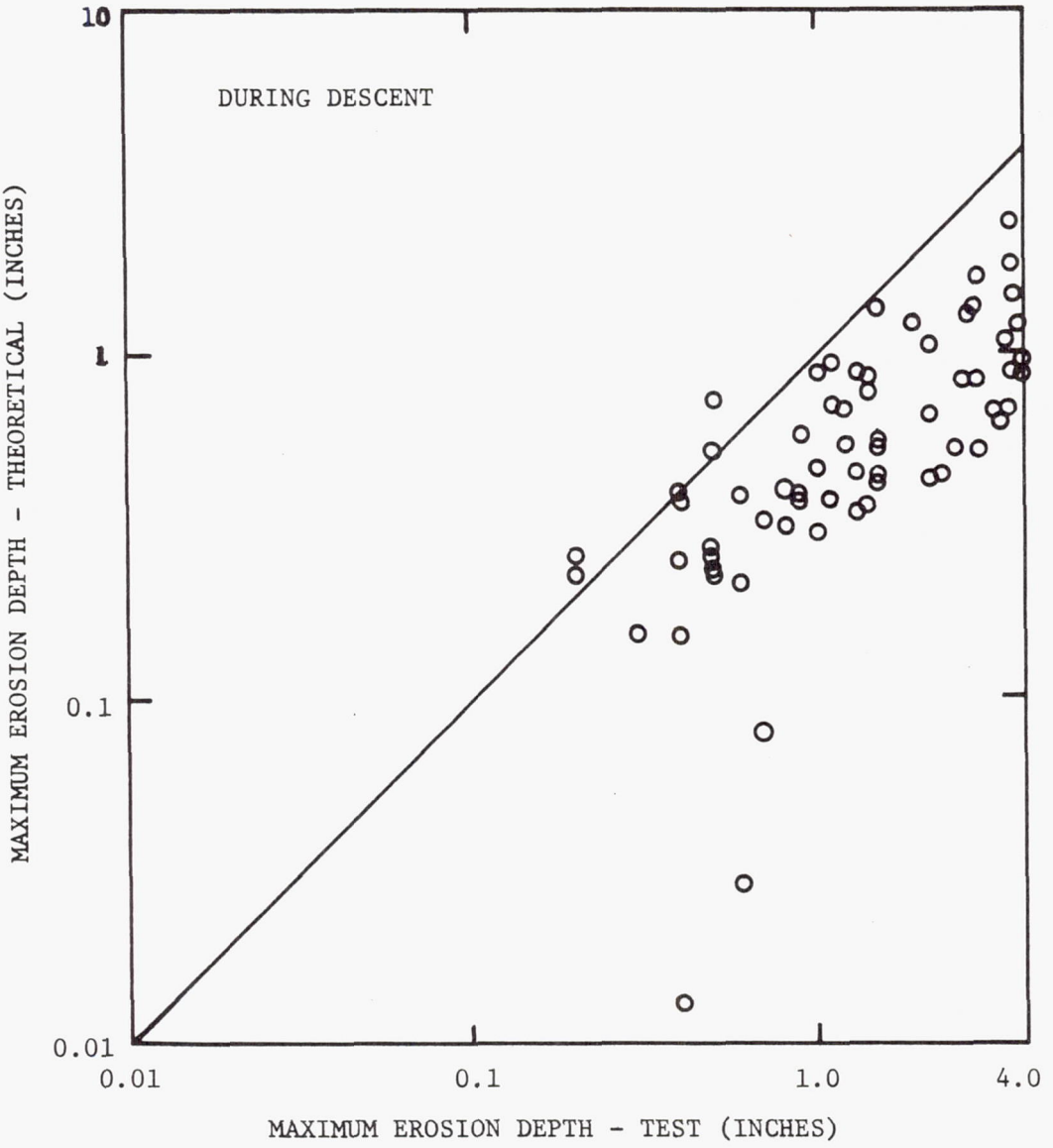

(a)

Figure 2. —Summary Comparison of Theoretical and Experimental Erosion Depths

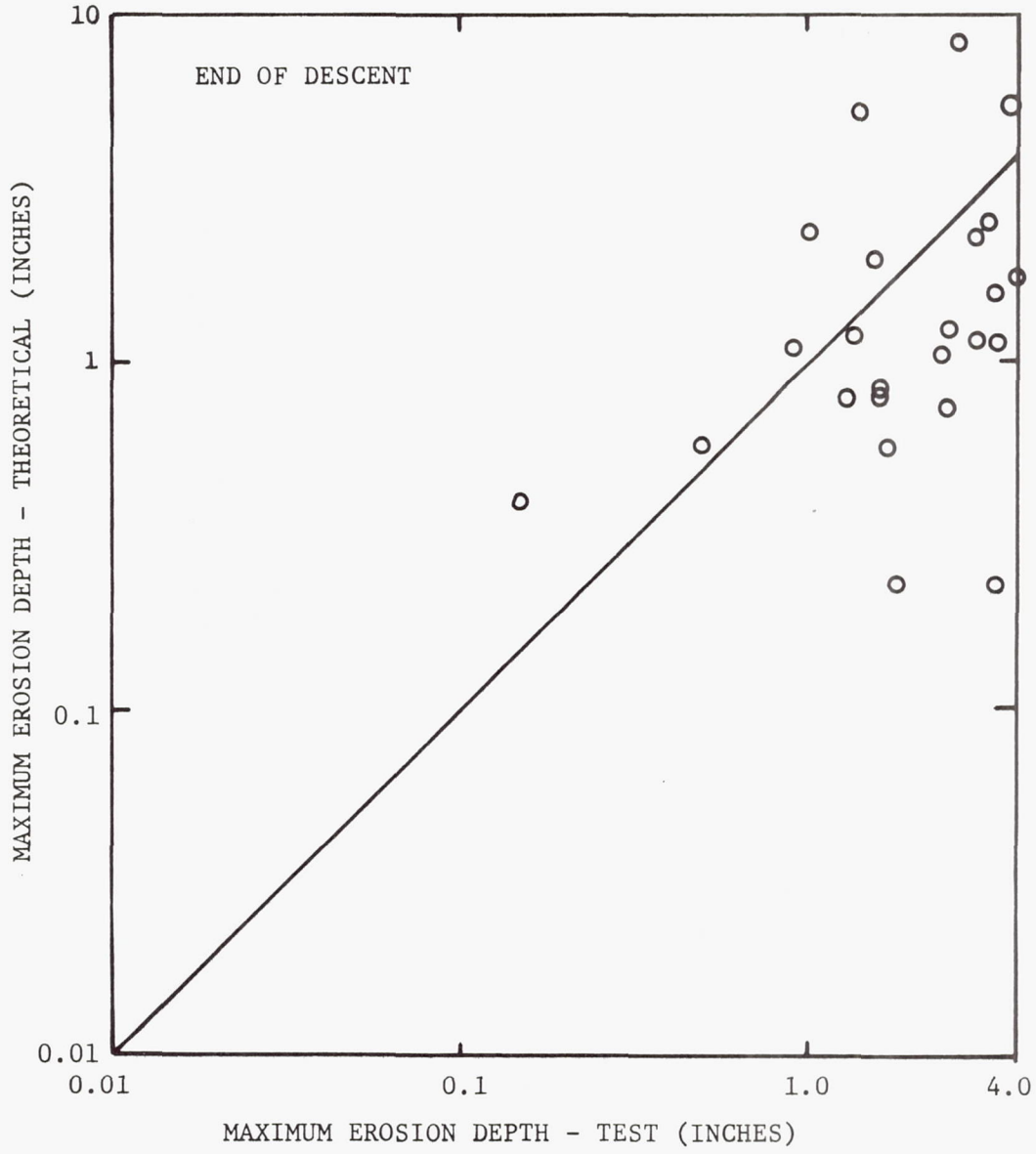

(b)

Figure 2. —Summary Comparison of Theoretical and Experimental Erosion Depths (Continued)

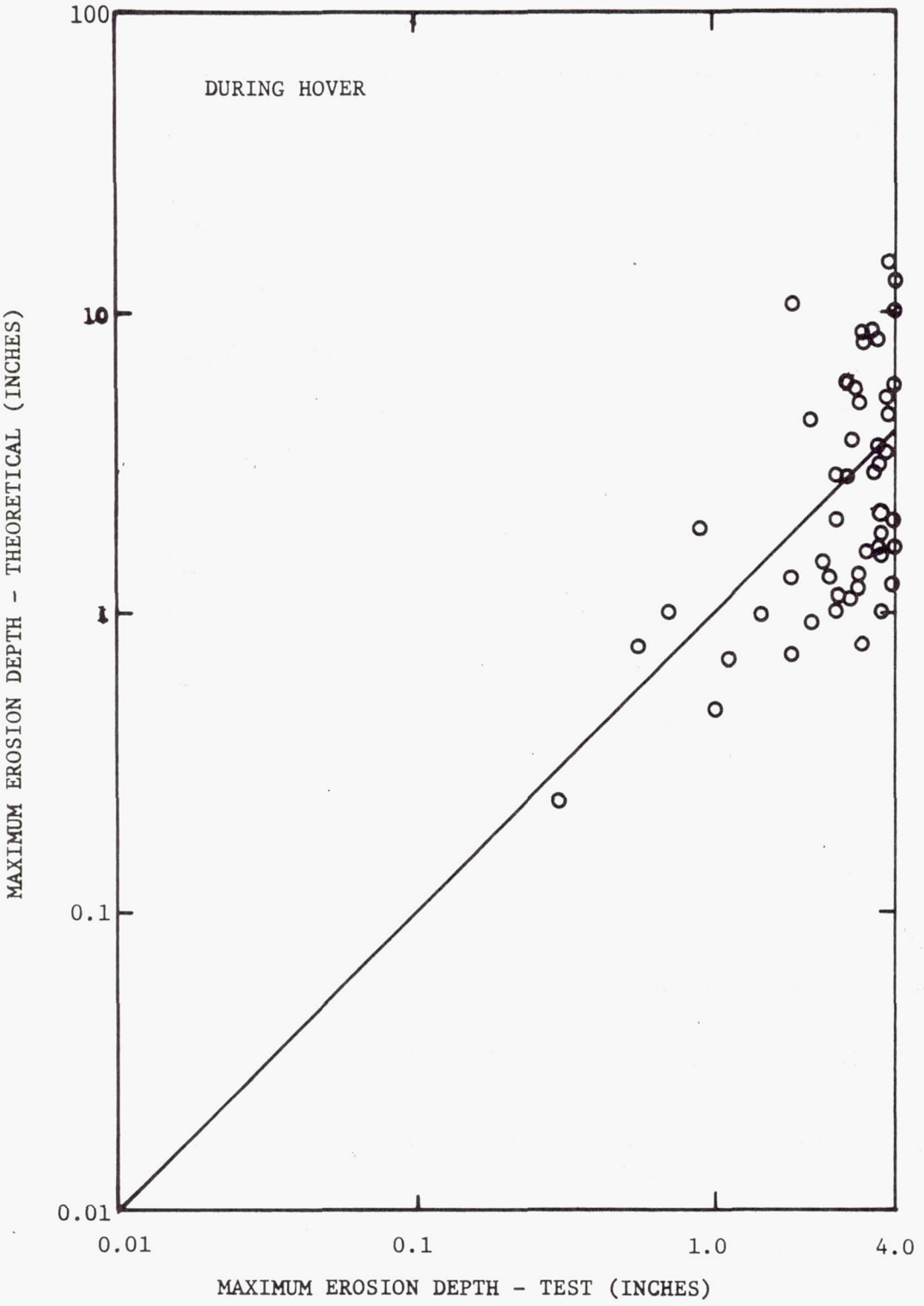

(c)

Figure 2. —Summary Comparison of Theoretical and Experimental Erosion Depths (Concluded)

Each of the 143 data points represents a plot of the theoretical maximum depth against the measured maximum depth. If theory was in complete agreement with test, these data points would lie along the straight line. Data points above the line represent overpredictions of depth, while points below the line represent underpredictions.

The figure indicates that during the descent period theory tends to underpredict the maximum erosion depth. But, as the nozzle approaches the surface and the hover period is entered, the predictions improve. For example, during the descent period 6 percent of the depths were over predicted while 94 percent were underpredicted. While at the end of the descent period 33 percent were overpredicted and 67 percent underpredicted. And, during the hover period, 40 percent were overpredicted while 60 percent were underpredicted. From the viewpoint of erosion predictions during a normal lunar landing, the comparison of importance is the one at the end of descent. For at this instant the thrust would normally be terminated. The comparison at this instant is only slightly biased in the direction of underpredicting the maximum erosion.

Figure 3 gives a quantitative measure of the amount the entire 143 predictions differed from measured results. In Figure 3, the factor N represents the ratio of predicted to measured maximum erosion depths when the depth is overpredicted; while for underpredictions, the factor represents the inverse ratio, i.e., measured to predicted. Thus, a factor N = 2 indicates the predicted values were either twice or one half the measured maximum depth. The vertical scale shows the percent of measurements falling within a given factor N. For example, the figure shows that 43 percent of the predicted values are within a factor of 2 and 87 percent are within a factor of 4 of the measured maximum erosion depth.

The detailed comparisons shown next give an indication of the influence of several system parameters and a quantitative comparison of theoretical predictions and measured results for individual tests.

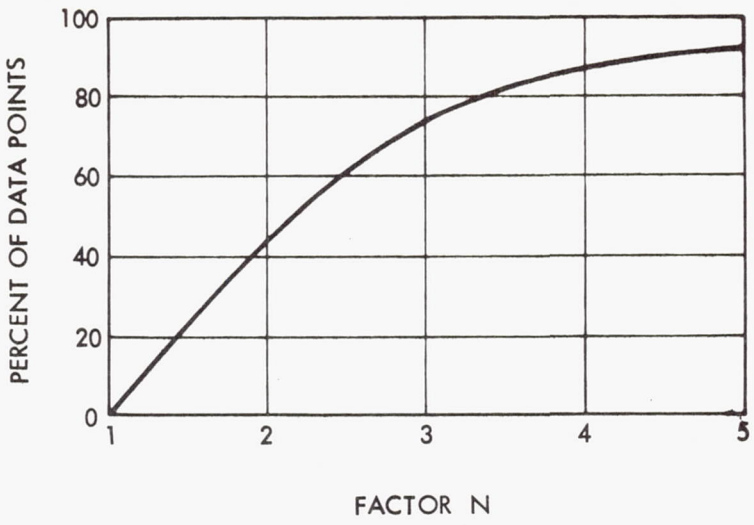

Figure 3. Percent of Erosion Depth Estimates Accurate to Within a Factor N

Figure 4 shows the measured and theoretical erosion rates at the point of maximum erosion depth at the end of descent for Tests 5, 6, and 8. The theoretical rates computed for these test conditions are those obtained from Roberts' theory in which the friction and drag coefficients are determined in accordance with the local Reynolds number. To indicate the trend over a wide range of soil particle diameters, the maximum erosion rate was also computed for a set of parameters representative of those for the 32 tests. This theoretical rate, which is indicated by the curve, is based on a 0.1-foot nozzle height, 100 psf chamber pressure and constant drag and friction coefficients of 2 and 0.2, respectively. The curve indicates that the soil erosion rate increases with particle diameter and then suddenly decreases to zero. In Roberts' theory this cutoff point is associated with the point where the frictional shearing resistance, which increases with particle size, is just equal to the maximum erosive shear stress. (It might be mentioned that in erosion theories that consider the erosive force as a lift on a particle, this cutoff point is associated with the point where the downward acting weight force is just equal to the lift on the particle; see, for example, Reference 7.) Figure 4 also shows the particle diameter range for the 32 tests. This range is below the theoretical cutoff point.

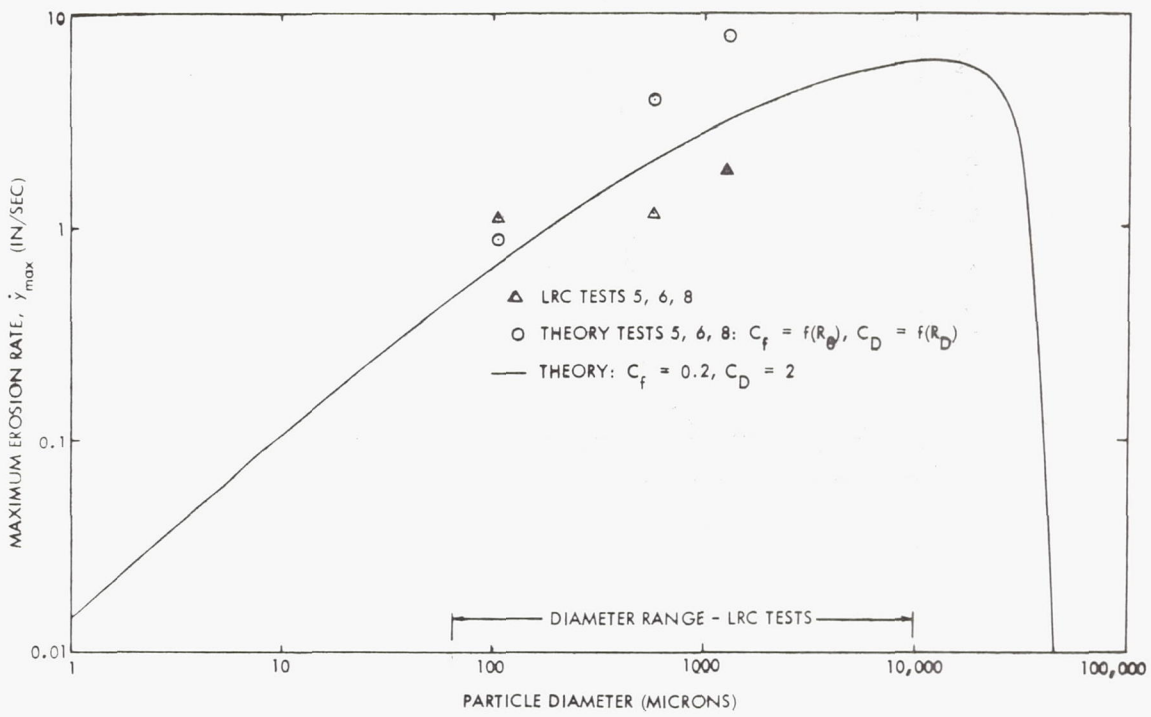

Figure 4. Typical Variation of Erosion Rate with Particle Diameter

Figure 5 shows the effect of particle diameter on the variation of the maximum erosion depth by superimposing Appendix C data. The depths are plotted against nondimensional time, which was obtained by dividing the actual time t by the descent time t_1. Hence, t/t_1 less than unity corresponds to the descent period; while t/t_1 greater than unity corresponds to the hover period.

Figure 5(a) compares Tests 5, 6 and 8. A comparison of the test parameters in Appendix A shows that all parameters are nearly constant in these three tests except for the particle diameters. Figure 5(a) shows that the quantitative agreement between theory and test is poor, but there is a qualitative agreement in that both theory tests show the erosion depth increases with increasing particle diameter. Figure 5(b) compares Tests 16 and 54. In these two tests the other parameters are not quite constant, but their differences are small compared to the differences in particle diameter. Here again, there is qualitative agreement in that larger particles erode faster. Figure 5(c) compares Tests 15 and 51. The results are similar to those in 5(a) and 5(b).

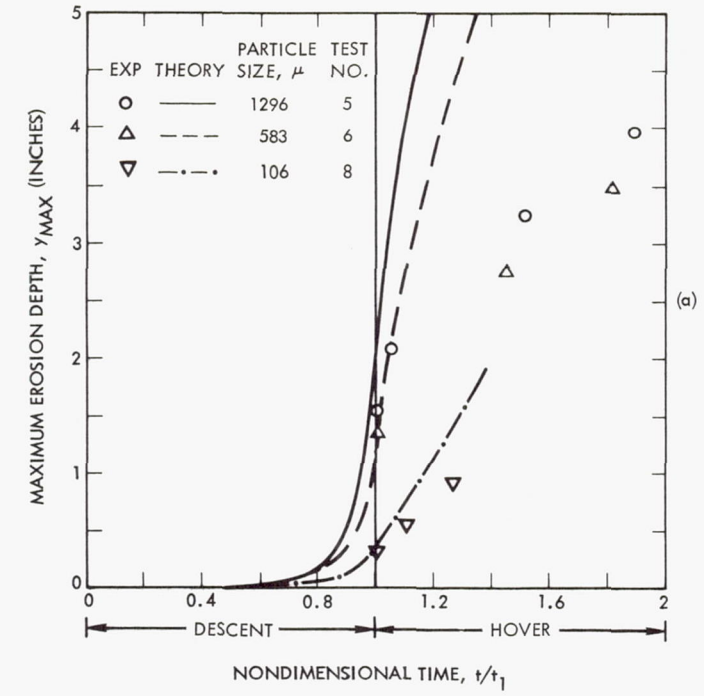

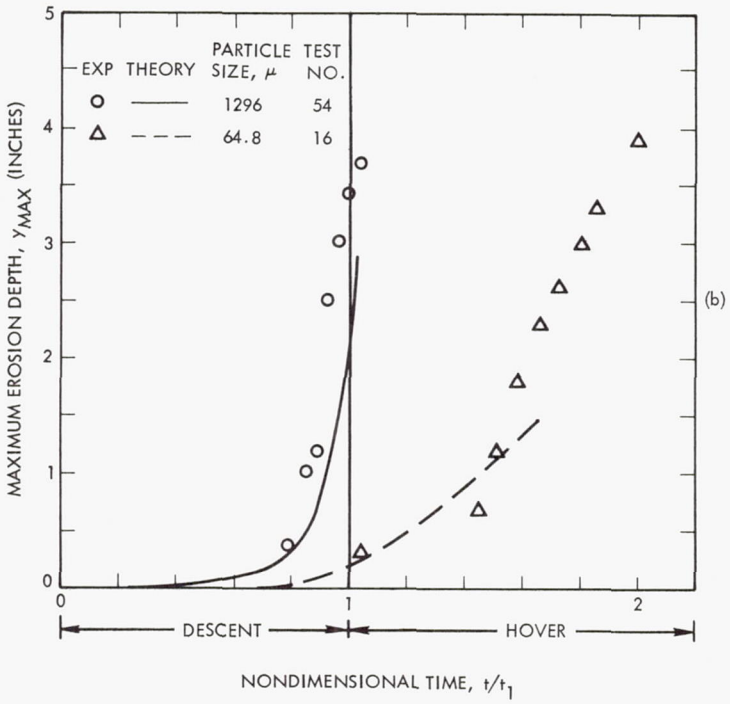

Figure 5. — The Effect of Particle Diameter on the Variation of Maximum Erosion Depth with Nondimensional Time

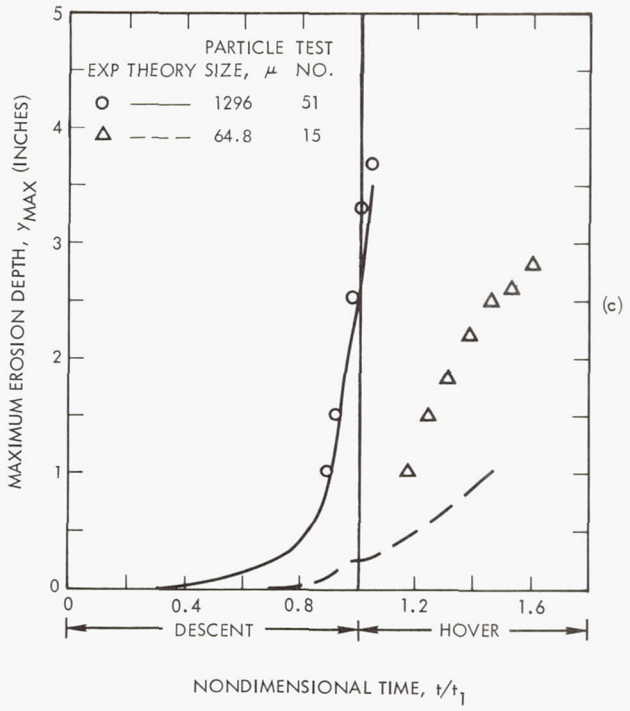

Figure 5. – The Effect of Particle Diameter on the Variation of Maximum Erosion Depth with Nondimensional Time (Concluded)

Figure 6 illustrates the influence of thrust on erosion by comparing the results for various chamber pressures. Figure 6(a) compares Tests 52, 54 and 55. Although the quantitative agreement is fairly poor, theory and experiment show the same trend. Theory predicts an increasing erosion with increasing chamber pressure (or thrust). Experimental results indicate the same general behavior. Differences between Tests 52 and 55 are minor and show different trends during the erosion period. Figure 6(b) shows the superposition of results from Tests 46, 47, 48 and 49, while Figure 6(c) shows a superposition of the results from Tests 24, 25 and 26. Both Figures 6(b) and 6(c) show the same behavior as Figure 6(a) in that both theory and test show an increase in erosion with increasing chamber pressure.

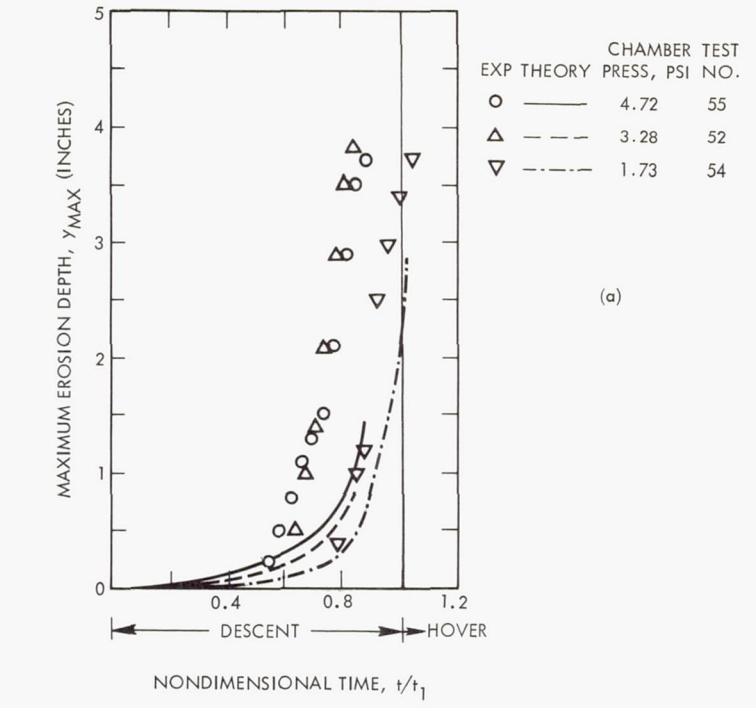

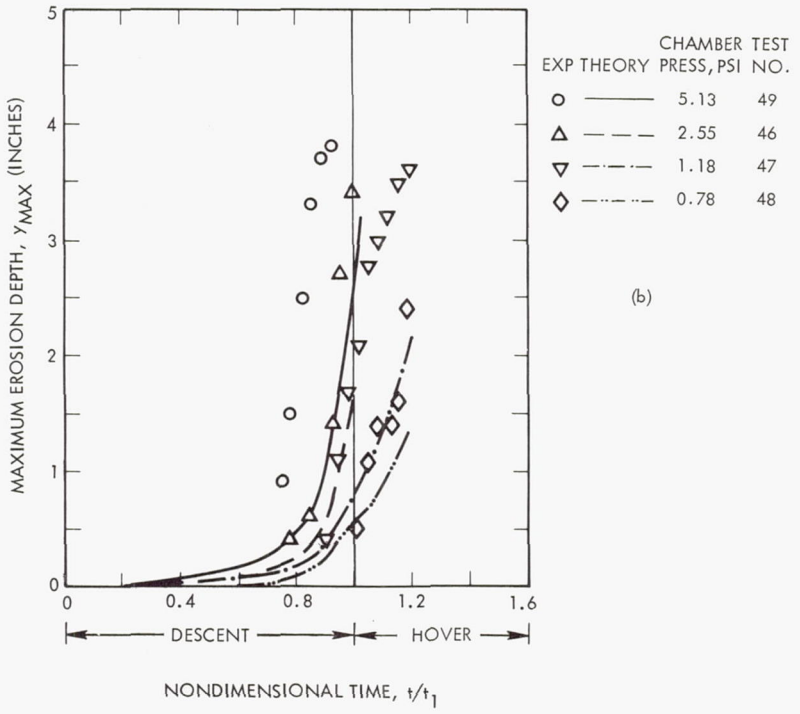

Figure 6. – The Effect of Chamber Pressure on the Variation of Maximum Erosion Depth with Nondimensional Time

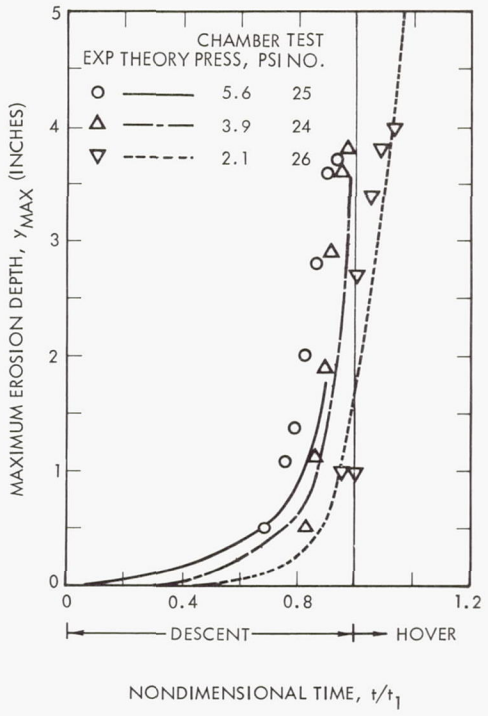

(c)

Figure 6. — The Effect of Chamber Pressure on the Variation of Maximum Erosion Depth with Nondimensional Time (Concluded)

Figure 7 gives an indication of the influence of descent velocity on erosion. The figure shows a comparison of Tests 31 and 32 in which the descent velocities are 5.351 and 1.873 ft/sec, respectively. Although the quantitative agreement is poor, both theory and test indicate the erosion depth is smaller at the end of the descent period for the faster descent.

This figure illustrates a behavior noted in several tests in which the increase in maximum erosion depth suddenly changes more slowly for a short time period. The variation in Test 31 near the time $t/t_1 = 1$ is an example of such a behavior. A possible explanation of this behavior is that the nozzle is descending rapidly, and simultaneously, the point of maximum erosion rapidly moves towards the stagnation point. The result is that over a small time increment, the maximum incremental erosion occurs at a point close to the current location of maximum erosion depth. This tends to "flatten out" the bottom of the erosion profile and produce only a minor change in the maximum erosion depth during the time increment. This behavior is also suggested in the Test 31 experimental results, but at an earlier time.

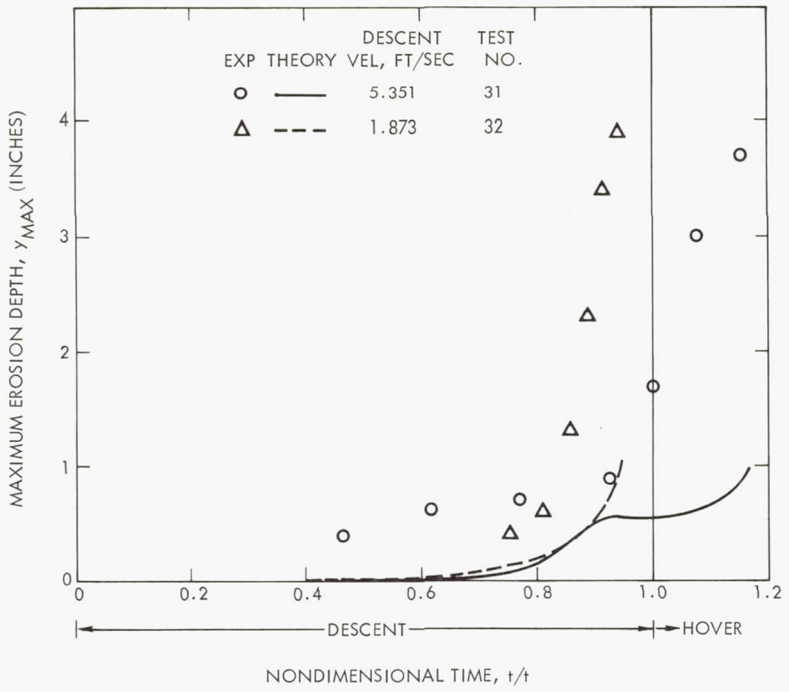

Figure 7. – The Effect of Descent Velocity on the Variation of Maximum Erosion Depth with Nondimensional Time

DISCUSSION

The preceeding section showed a varying degree of agreement between theory and experiment. The question naturally arises concerning the source of disagreements between theory and test and how the predictions can be brought into closer agreement with experimental results. This section discusses several of the known and possible sources of disagreement, while the next section considers recommended procedures for refining the predictions.

Even though some disagreement between theory and experiment must be due to experimental error, it is believed that the major discrepancy is due to deficiencies in the theory, and to a less degree, uncertainties in the input parameters. Only factors influencing errors in the theoretical predictions are discussed here.

1. INFLUENCE OF IDEALIZATION IN THE THEORY

a. Rocket Gas Emanates From a Point Source

Since the erosion theory is based on gases emanating from a point source, it is meant to be applicable only when the nozzle exit radius r_e is small compared to the nozzle height. Roberts indicates the approximate limit of applicability of the theory is at the nozzle height h_c given in Equation (B14). For the engine used in these experiments h_c = 0.248 foot. Thus, the assumption of a point source is not an error in the theory, but rather a limitation placed upon its applicability. Test 15 results will be used to illustrate the effect on soil erosion predictions at low nozzle heights. In Test 15, the hover height is 0.0469 foot which is even smaller than the nozzle exit radius r_e = 0.1108 foot. Thus, for this test the theory should not be applicable or, at least, have limited applicability at and shortly above the hover height.

The influence of a low nozzle height can be inferred by examining the dynamic pressure (the pressure assumed to produce erosion) as the nozzle height decreases. According to the theory, the dynamic pressure increases continually as the nozzle approaches the surface until the nozzle reaches the critical nozzle height. After this time, the peak pressure remains constant, but the point of maximum dynamic pressure continues to move towards the stagnation point. Since maximum surface erosion occurs in the region close to the peak dynamic pressure, the region where erosion takes place continues to move towards the stagnation point as long as the nozzle height decreases. This behavior is graphically portrayed in Figure 8. This figure shows the dynamic pressure distribution for four nozzle height. These heights correspond to the hover nozzle height in Test 15, the critical nozzle height and two higher nozzle heights. Starting with the highest nozzle height, the figure shows that the peak dynamic pressure moves towards the stagnation point with decreasing nozzle height. The value of the peak pressure increases until the critical nozzle height is reached, and thereafter remains constant.

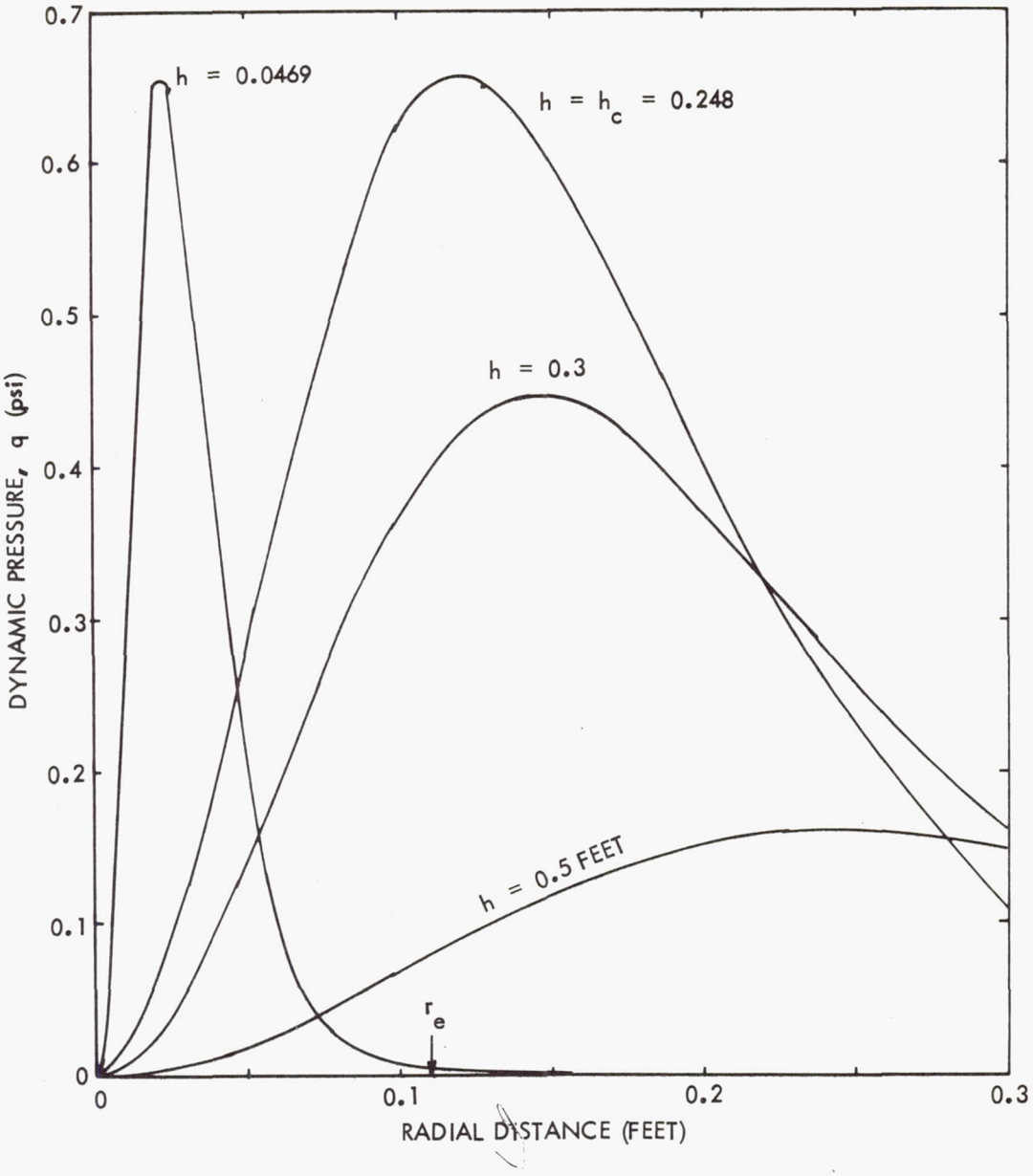

Figure 8. — Variation of Dynamic Pressure With Nozzle Height (Test 15 Parameters)

The radial location of the nozzle exit radius is also shown on the figure. Observe that the dynamic pressure developed at a radial station equal to the nozzle exit radius is quite small for the hover nozzle height. Since the dynamic pressure is small, negligible erosion or no erosion would be predicted at and beyond the point directly below the nozzle lip. Physically, it would be expected that the pressure directly below the nozzle would be nearly constant (if the exit velocity distribution is uniform) and that erosion would occur over and somewhat beyond this radial location.

The preceding behavior was noted in the computations performed in several of the tests. Consider, for example, the predictions for Test 15. Observe that after hover, the subsequent increments in surface erosion only occur near the stagnation point. The flow predictions at these very low nozzle heights are probably in error.

The conclusion drawn from these observations is that Roberts' theory must be modified to extend the range of applicability to lower nozzle heights before direct comparisons of theoretical and experimental erosion profiles can be made when the nozzle height is significantly less than Roberts' critical nozzle height.

b. Erosion Only Due To Gas Viscous Forces

The erosion theory used here assumes surface erosion only results from viscous shear stresses exerted on the surface. Another mechanism contributing to erosion is the lift forces acting on soil particles. Both types of forces should be proportional to the dynamic pressure. In the case of lift forces, the proportionality factor would be a lift coefficient C_ℓ, while the factor for the shear stresses is the shear coefficient C_f. Thus, even if lift was considered, the form of the basic equations should not be altered and the friction coefficient C_f used in Roberts' theory could be considered as an effective coefficient, which accounts both for lift and shear acting on the particle.

Since these erosive forces depend on the dynamic pressure, which is zero at the stagnation point, no erosion takes place directly below the nozzle center line. Yet, test data show that often the erosion is a maximum at this point, and that the erosion crater is dish shaped; in fact, the shape of the erosion crater is much like the distribution of surface pressure. This suggests that the gas stream impacting the surface is not only turned by the surface, but also dislodges soil particles by transfering some of the gas momentum normal to the surface to momentum of soil particles.

c. Real Flow Phenomena

Tests have often indicated that gas flow conditions can deviate substantially from an idealized flow condition. Many of such phenomena take on even added importance when the nozzle height is small. In a real nozzle, it is known that the flow may not be uniform across the nozzle. Also at certain nozzle heights, oblique shocks are formed which drastically influence the surface loadings. An example of these phenomena was observed by Stitt in Reference 11.

Clark, in Reference 12, also showed that the surface pressure could deviate from the bell shaped pressure distribution predicted by Roberts' theory. In this reference, it is pointed out that when the nozzle reaches a height where the jet peripheral escape area becomes less than the jet exit area, the nozzle chokes and static pressures within the nozzle increase about an order of magnitude. This should occur for the nozzle used in this test series when the nozzle height $h = r_e/2 = 0.055$ foot.

Most likely when the nozzle is close to the surface and a substantial crater has formed, the flow field must differ from that for a flat surface. It is doubtful that the theoretical flow field adequately accounts for this change. The question of how much the flow field is altered because of the entrainment of soil particles is another question unanswered at present.

d. Soil Erosion is a Deterministic Process

Roberts considers erosion to be a deterministic process, and therefore, predictions from his theory provide estimates of the average erosion. Clearly random variations in the soil parameters, surface roughness and fluctuations in gas flow must produce random variations in the surface erosion. In Reference 8, it was found that the lift and drag forces acting on surface particles varied randomly. Peak pressures were about 2.5 times the average pressure, while the standard deviation was about 0.49 times the average pressure. Thus, the random nature of this phenomena may account for a large portion of the differences between theoretical predictions of the average erosion and that observed in a given experiment.

e. Friction Coefficient Depends on Reynolds Number

At the beginning of this investigation, preliminary computations were performed to determine the friction coefficient C_f required for Roberts' theory to agree with tests. The computations and conclusions are discussed in Appendix D. These preliminary investigations showed that C_f must vary randomly for theory to be in complete agreement with test. This random variation most likely was due to random variations in the forces. The assumption that C_f depends on Reynolds number in the same manner as the drag coefficient measured on spherical particles may be an over simplification. However, the values used for C_f based on drag measurement on spherical particles gave values representative of those computed from data in Reference 8. Table 4 of Reference 8 lists average drag stresses measured on different particles in airstreams of various velocities. The value of C_f, computed according to τ/q ranged from 1.8 to 9.9 for a standard density air. Values in this range are representative of those computed in Appendix D.

2. INFLUENCE OF SYSTEM PARAMETERS

a. Cohesion

Often the theoretical prediction of incipient erosion occurred at a much higher nozzle height than observed in test; and as a result, the associated erosion occurred at larger distances from the stagnation point than observed during the entire test period. An examination of the governing equations shows that a small amount of cohesion serves to delay the erosion to lower nozzle heights and confines the erosion to regions closer to the stagnation point. The fact that theory generally predicted erosion at distances from the stagnation point beyond where it occurred in tests does not necessarily reflect a defect in the theory, but may have been a result of the soil having a small effective cohesion. Material is presented here to indicate the influence of cohesion on the nozzle height at incipient erosion and the corresponding radial location where erosion begins.

Figure 9 shows the variation of maximum erosive shear stress $\tau_{max} = C_f q_{max}$ (computed from Equations (B7) and (B18)) with nozzle height for chamber pressures of 100 to 500 psf. The remaining set of engine parameters used to develop Figure 9 are representative of all the tests. This figure was based on C_f = constant = 0.2, a representative value recommended by Roberts in Reference 5. (Note that if C_f were 1 rather than 0.2, the curve labeled 500 psf would correspond to 100 psf, since $\tau_{max} = C_f q_{max}$, and q is directly proportional to the chamber pressure.) Figure 9 shows that the shear stress increases as the nozzle height decreases until a critical nozzle height is reached. For the test parameters, this height is 0.248 foot and corresponds to the height where the stagnation pressure is equal to the nozzle recovery pressure. Below this nozzle height Roberts' theory assumes the stagnation pressure remains constant and equal to the recovery pressure given by Equation (B13).

Figure 10 shows the variation of the restraining shear stress τ^* (which must be exceeded before erosion begins) as functions of the soil particle

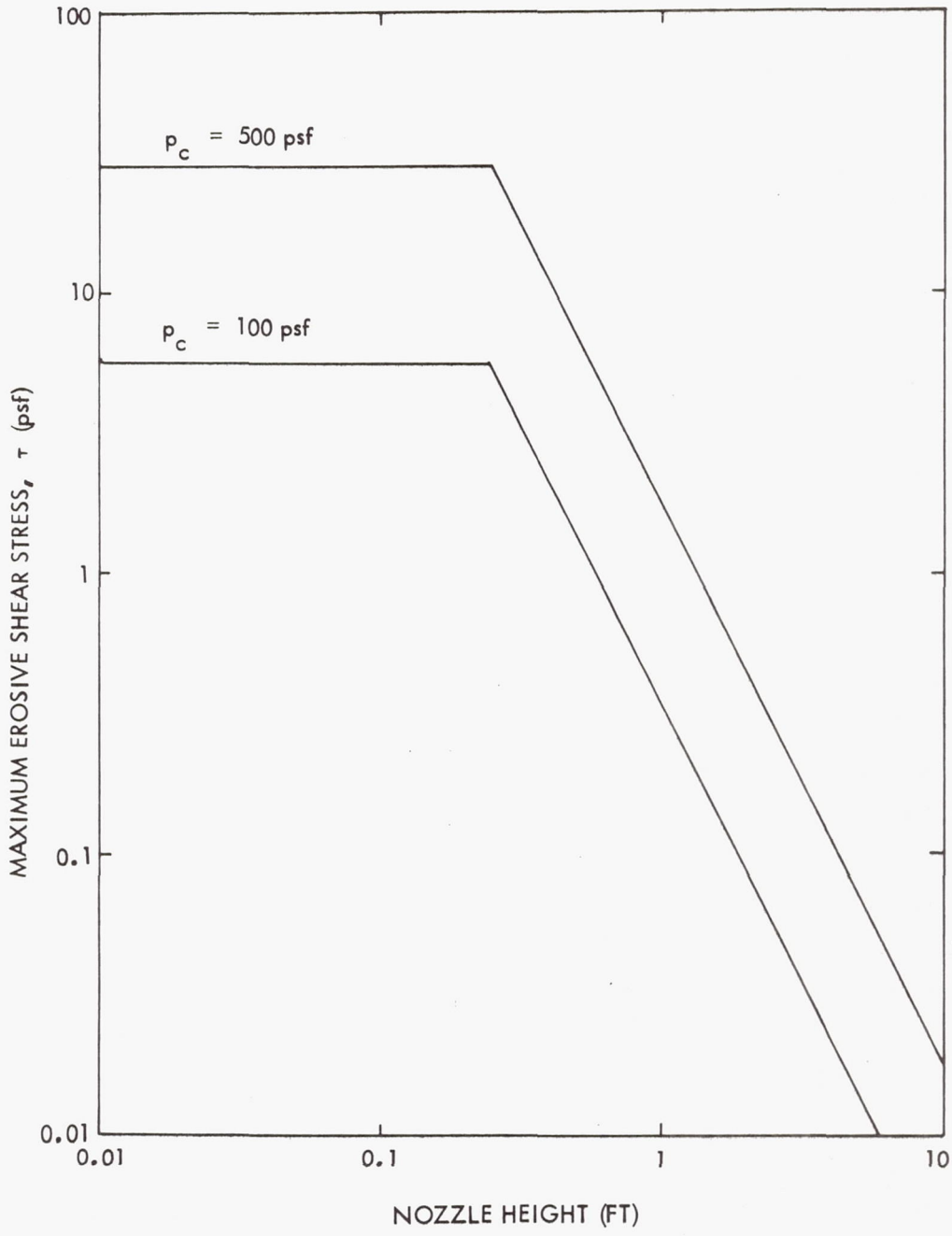

Figure 9. —Variation of Erosive Shear Stress With Nozzle Height

diameter. This figure was developed from Equation (B19) for a flat surface and for $\tau_{coh} = 0$ and $A_{coh} = 5 \times 10^{-17}$ lb-ft. The smaller diameter particles (less than about 12 microns) are essentially restrained by the cohesive stress, while the larger particles are restrained by the internal friction force between soil particles resulting from the gravitational force field. The soil parameters used to develop Figure 10 are representative of all tests with glass beads. In the particle diameter test range of 65 to 10,000 microns, the restraining force was essentially due to the gravitational force field. For example, the restraint for the 65-micron particles is about 0.01 psf. The contribution from the $A_{coh}D^{-3}$ term for these particles is only about 5×10^{-6} psf.

Figure 11 shows the relation between nozzle height and particle diameter at incipient erosion. This figure was obtained from Figures 9 and 10 by equating τ_{max} to τ^*. Nozzle heights below the curves in Figure 11 are those heights where erosion takes place.

The radial location corresponding to the point of incipient erosion can be determined from Equation (B8). Consider, for example, 65-micron diameter particles. Figure 11 indicates incipient erosion occurs at a 6-ft nozzle height for a chamber pressure of 100 psf. For $\gamma = 1.667$ and $M_e = 2.68$, Equation (B8) gives $r/h = 0.49$, and therefore, incipient erosion begins 2.94 feet from the stagnation point.

Consider now the influence of a small cohesion. Cohesion tests conducted on typical soils indicate that 1 psf is a relatively small cohesion value. Suppose the soil cohesion was 1 psf, a value large compared to the value 5×10^{-6} psf given by the formula $A_{coh}D^{-3}$. Adding 1 psf to the value 0.01 psf read from Figure 9 indicates erosion will not begin until the erosive shear stress exceeds 1.01 psf. Figure 9 indicates the corresponding nozzle height is 0.6 foot for a chamber pressure of 100 psf. The radial location of incipient erosion in this case becomes 0.294 foot. This illustration indicates a small cohesion between particles can have an influence on erosion predictions.

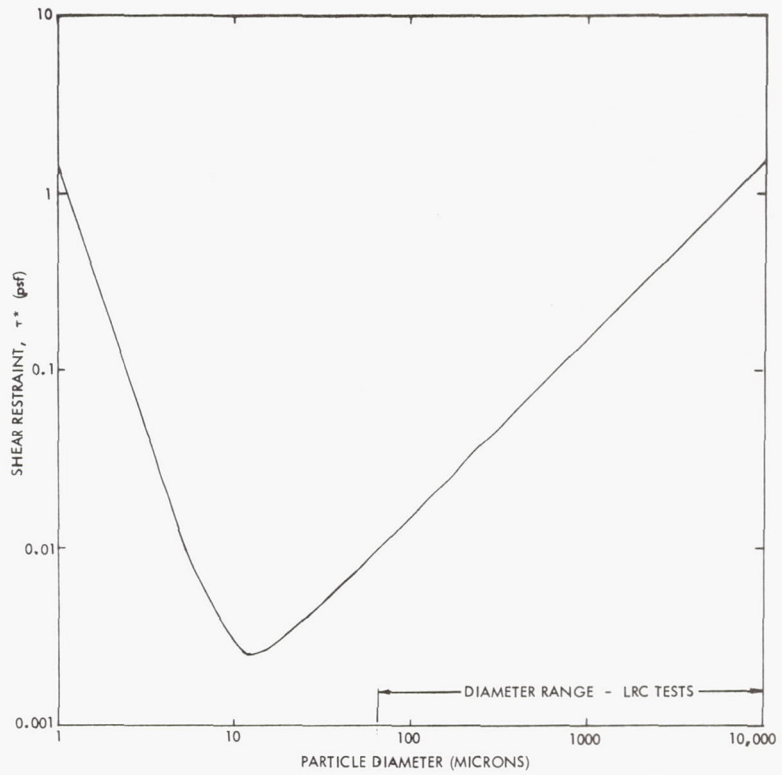

Figure 10.- Variation of Shear Restraint With Particle Diameter

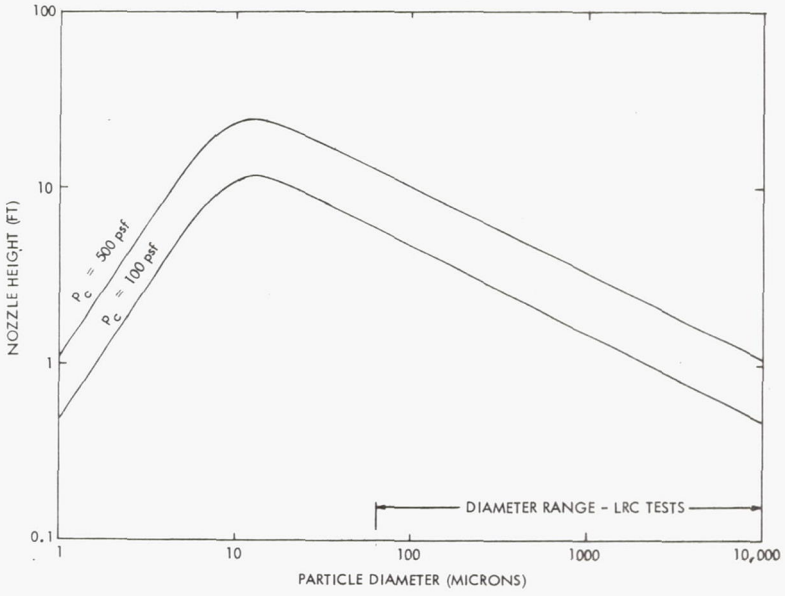

Figure 11.- Variation of Incipient Erosion With Nozzle Height and Particle Diameter

As a further illustration of the influence of cohesion on predicted erosion, consider the results shown in Figure 12. This figure shows the predicted erosion profiles for τ_{coh} = 0 and 0.01 psi, (1.44 psf) along with the corresponding measured erosion profiles. Since a unit of erosion depth is portrayed over a larger ordinate distance for τ_{coh} = 0 than for τ_{coh} = 0.01 psi, a visual indication of the influence of cohesion can best be observed by comparing the relative positions of the data points and the theoretical curves for each of the two values of cohesion. Even though the small amount of erosion delayed the beginning of erosion to lower nozzle heights and essentially to the range where erosion occurred during the test, the predicted erosion depths are substantially less than observed during the test.

b. Particle Diameter

Particle diameter has a significant influence on predicted erosion. The theoretical curve in Figure 4 illustrates the influence of particle diameter on the erosion rate. The figure shows that the erosion rate increases with increasing particle diameter until the gravity cutoff point is reached.

In 30 of the 32 erosion tests, the bed material was glass beads. This material closely approximates the assumption in the erosion theory that the soil particles are composed of spherical particles having the same diameter. For these tests, the actual particle diameter is very close to the measured average diameter, and therefore, errors in predicted erosion arising from uncertainty in particle diameter must be small. On the other hand in the tests on soils, the particles are not necessarily spherical and have a distribution of sizes. Thus, the effective particle diameter is not readily determined so that the influence of deviation from a spherical shape and effective size is not readily assessed.

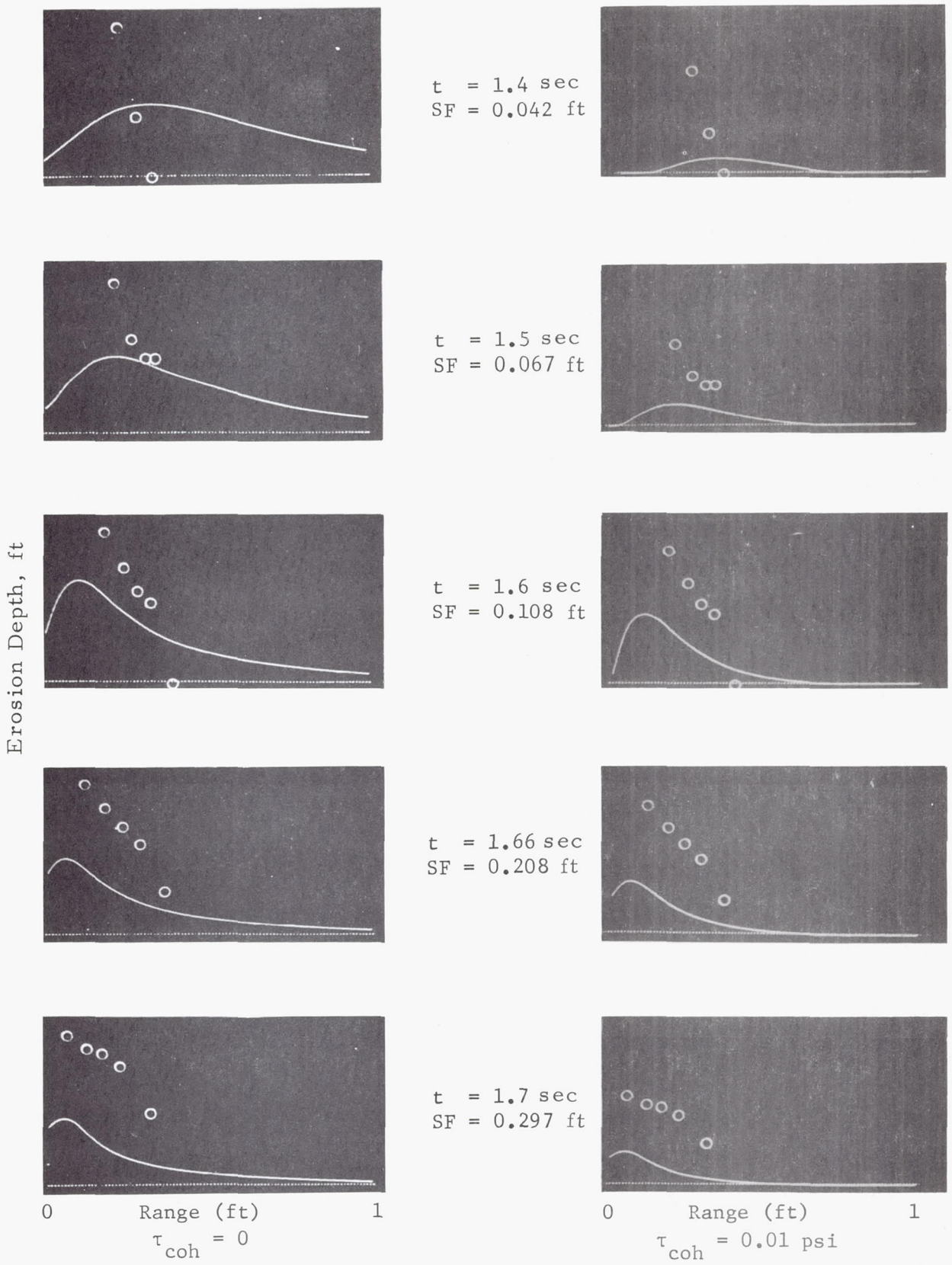

Figure 12.--Influence of Cohesion on Erosion Predictions for Test 35

c. Packing Constant

The packing constant for all of these tests was taken to be 0.575. Referring to Appendix A, Figure A2, it is observed that for aluminum oxide particles, the factor varies with particle diameter. It is easy to assess the influence on soil erosion predictions caused by over- or under-estimates in the packing factor because of the manner in which the factor enters the erosion equation. By referring to the equations in Appendix B one observes that the erosion rate varies inversely with the packing factor. Thus, if the packing factor was over-estimated by say 20% so that it should have been 0.46 rather than 0.575, then the erosion predictions would have been 20% higher. Such a change would have shifted the predictions higher in Figure 1 with the effect that the average prediction of maximum erosion rate would be closer to the measured erosion depths.

d. Internal Friction Angle

A 27-degree internal friction angle was used in the erosion computations. Figure A1 indicates the friction angle for various diameter aluminum oxide particles varies substantially with particle diameter. The influence of internal friction on the theoretical calculations can be determined from Equations (B3) and (B19). These equations indicate the rate of soil erosion is proportional to the difference in the shearing stress τ exerted on the surface by the gas and the soil resistance to shear τ^*. The internal friction angle α only enters into the τ^* term. Now, suppose α was increased from 27 to 40.5 degrees. If the frictional restraint is small compared to the cohesive restraint, this increase in α would not cause a significant increase in τ^*, and therefore, the change in α would not influence the erosion rate. If the frictional restraint is large compared to the cohesive restraint, the same increase in α would increase the value of τ^* by a factor of 1.65 (equal to tan 40.5/tan 27). Now, whether this increase in τ^* effects the rate of erosion depends on the relative magnitudes of τ and τ^*. If τ is large compared to τ^*,

the increase in τ^* has a negligible influence on the erosion rate. While, if τ is only a little larger than τ^*, a small change in τ^* has a large influence on the erosion rate.

The influence of changes in α in the theoretical erosion predictions can be examined quantitatively for parameters similar to those used in the erosion tests. Since most of the erosion occurs while the nozzle is at or near the hover position, the comparison will be made at a typical nozzle height of 0.1 foot. The influence of α on the erosion rate will, of course, be different at a much higher height. But, even so, the total erosion observed during a descent to hover will depend upon the rate of erosion during the final stages of descent. The surface loading conditions in this illustration are based on the same nominal engine conditions used in computing the theoretical erosion rate curve in Figure 4. For these conditions the maximum shear stress τ exerted on the soil surface is about 5.7 psf. A surface composed of 100 micron diameter particles produces shear restraints τ^* of 0.015 and 0.025 psf for α equal to 27 and 40.5 degrees, respectively. In either case, the maximum erosion rate is about 0.63 in/sec. On the other hand, a surface composed of 10000 micron diameter particles (the largest size used in the tests) produces shear restraints of 1.5 and 2.5 psf for α equal to 27 and 40.5 degrees, respectively. On this surface the maximum erosion rate is reduced from 5.9 to 4.4 in/sec as α is increased from 27 to 40.5 degrees. This 50 percent increase in α causes about a 25 percent reduction in erosion rate. These calculations indicate that near the hover nozzle height (where the erosion rate is largest) a 50 percent increase in internal friction angle has a negligible effect on the total erosion for the smallest particles used in the tests; and the same increase in α causes about a 25 percent decrease in the total erosion for the largest particles used in the test.

e. Soil Density

An examination of the soil erosion equations in Appendix B shows that the density enters the τ^* terms and also is in the denominator of the erosion rate expression, Equation (B3). For the smaller particles, a change in σ has no

effect on τ^*. Thus, if the density was decreased by 10 percent, the predicted rate would be increased by 10 percent for the smallest diameter particles. For the larger diameter particles, a decrease in density causes a detectable decrease in τ^*, and therefore, an additional increase in erosion rate. However, even for the largest diameter particles used in the experiments, a 10-percent decrease in density produces approximately a 10-percent increase in erosion rate.

f. Non Constant Descent Velocity

The erosion predictions were all based on a constant descent velocity. If the velocity actually varied during descent, the predicted erosion would be increased or decreased, depending on whether the descent velocity near the hover position was below or above the average value. An assessment of this effect can be inferred from Figure 4, which shows the variation of erosion rate with particle diameter for a 0.1-foot nozzle height and a 100 psf chamber pressure.

In Test 5, the descent velocity was 1.184 ft/sec, and the total drop time was 2.64 seconds. Suppose, for example, the velocity increased linearly with time during descent and consider the time required to reach a height of 0.233 foot (0.1 feet above the hover height). This time for Test 5 would be 2.5974 seconds, while for a constant descent velocity it would require 2.5566 seconds to reach the same position. For the constant descent case, the soil surface would be exposed to the erosive action of the gases 0.0408 second longer than for the nonconstant descent case during the remaining 0.1 foot of descent. A representative value of the erosion rate is given by the curve in Figure 4, which for the 1296 micron diameter particles in Test 5 is about 3 in/sec. Multiplying this rate by the time difference 0.0408 gives 0.12 inch. Thus, these computations indicate the erosion depth for the constant descent case would be about 0.1 inch deeper than for the nonconstant descent case.

3. APPLICABILITY OF THEORY

This investigation indicated a limited degree of correlation between theory and test. Apparently an uncertainty factor of about 5 should be applied to theoretical predictions of erosion depths. Although this factor may seem somewhat large, it is surprising that it is so small when one considers the experimental evidence of real phenomena not taken into consideration in the theory.

Tests have shown that turbulence gives rise to random fluctuations in both the lift and drag forces acting on surface particles. The theory assumes only a deterministic shear stress (drag) to be acting on the particles, and therefore, only provides an estimate of the average erosion. If the variation is small (small standard deviation) and the theory accounts for all first-order effects, the estimate of average erosion should be close to the erosion measured in test. And, conversely, if the variation is large or the theory neglects important effects, the estimates of average erosion could differ from test by an order of magnitude or more. During an actual lunar landing, additional sources of randomness would be anticipated, such as surface undulations and random variations in soil properties.

Examples of other real phenomena, which influence erosion, are indicated in the pressures measured when retro-rocket gases impinge on flat plates. For example, the surface pressure loadings presented in Figure 8 of Reference 11 show that the pressure often has one peak each side of the lower pressure measured at the stagnation point. This behavior was also observed by Clark in Reference 12. Stitt's data also showed that even for some nozzles in which a "bell shaped" surface pressure was observed (the type predicted by Roberts' theory) the pressures did not vary inversely as the square of the nozzle height. In fact in Figure 8C, the two bell-shaped pressure distributions for different nozzle heights are essentially the same, even though the nozzle heights ratios were $13.8/3.1 = 4.45$. According to Roberts' theory the pressures should differ by a factor of 20. In Figure 8B of Reference 11, two nozzle heights differ by a ratio of $14.1/2.2 = 6.4$, and

therefore, the pressures should differ by a factor of 41. However, Stitt's data show them to have the same stagnation pressure. Realizing that real flow conditions can produce surface loading conditions which differ substantially from Roberts' theory, a factor of uncertainty of about 5 for erosion predictions is not excessive.

It has been pointed out that the erosion theory was only meant to be valid when the nozzle exit radius is small compared to the nozzle height. Since in many of the tests the hover height was less than the nozzle exit radius, theory would not be expected to be in close agreement with test. However, above the critical height h_c the theory should be applicable. The critical nozzle height criteria are somewhat obscure because, generally by the time the nozzle reaches the hover position, erosion has occurred, and the distance from the nozzle to the soil surface directly below the nozzle is larger than h_c even though the height above the original surface is much less than h_c. As a result, it is difficult to determine at what time in any test the theory becomes invalid. In any event, at times when the nozzle is above the height h_c and when only small erosion has occurred, the theory should be applicable. However, the comparisons between theory and experiment indicated more disagreement during descent than during hover.

There are two major sources of potential error in the viscous erosion theory. These errors are in the predictions of surface loadings which cause the erosion, and the differential equation describing the erosion rate may not include all first order effects. It is believed that more accurate predictions are possible and can be made if some of the recommendations made here are followed.

CONCLUSIONS

Calculations of jet blast erosion, based on an existing theory, were made to compare with 32 experimental tests. These calculations and tests included variations in jet thrust, descent speed, and soil particle size. Comparisons

of the theoretical and experimental results lead to the following conclusions:

1. A comparison of predicted and observed erosion depths for 143 time and surface locations indicated the predictions to be accurate within a factor of two 43 percent of the time, and within a factor of four 87 percent of the time.

2. During descent the average predictions were biased on the side of underestimating the erosion with the average only slightly biased by the end of the descent period.

3. No single or simple modification to the existing theory improved the overall agreement with experimental data.

4. Both theory and experiment indicate a slow cautious descent can result in a large crater at touchdown, and the descent mode that results in the smallest crater would be a thrust-free drop from the greatest height the structure can safely tolerate.

RECOMMENDATIONS FOR FUTURE RESEARCH

This investigation indicated a need for additional experiments designed to provide a more basic understanding of the entire erosion phenomena before an improved erosion theory can be formulated. The recommendations outlined here involve both experimental and theoretical investigations concerned with surface loading conditions, the mechanism governing soil dislodgment and entrainment in the flowing gas, and the formulation of procedures for predicting soil erosion.

1. FLOW FIELD INVESTIGATION

a. Comparison of Theoretical and Measured Surface Loadings

Static and dynamic pressures should be measured on flat plates and surfaces having shapes similar to eroded soil surfaces for nozzle height and descent conditions in the tests. Also, shear stresses exerted on rough

surfaces should be measured. These measured loadings can then be compared with theoretical loadings to provide an assessment of gas flow-field theory. Tests have indicated surface loadings can change drastically with nozzle height and may differ by an order of magnitude from theoretical predictions. Hence, even if the differential equation governing soil erosion is exact, it would be expected that the predicted erosion would also differ from observed erosion by an order of magnitude.

b. Develop a Surface Loading Theory

Following Step a, an assessment of the accuracy of the theoretical surface loading predictions will be available and, if necessary, a modified or new theory can be formulated. One defect of the loading theory, which was clearly evident at low nozzle heights, was the influence of a nonzero nozzle exit radius. One modification required in the theory is to extend its applicability to lower nozzle heights. Roberts defined the azimuth angle to be $\tan \theta = r/h$. This resulted in the predictions of small surface pressures below the nozzle lip when the nozzle is close to the surface. A simple modification that comes to mind could be to define $\tan \theta$ to be $(r - r_e)/h$ when $r > r_e$ and 0 when $r < r_e$. This has the effect of making the pressure constant below the nozzle and to decay at radial distance greater than r_e. However, such a simple modification indicates that the gas radial velocity and dynamic pressure is zero between $r = 0$ and $r = r_e$. This infers that gas impacts the soil normally between $r = 0$ and r_e and diffuses into the soil. Such a simple modification is not adequate, but something of this type may lead to a better prediction of loading below the nozzle for small nozzle heights.

c. Investigate Soil Erosion Mechanism

Experimental investigations should be devised and conducted to show the the rate at which soil is removed from a surface under the action of a known flow over the surface. These tests should also clarify how much erosion is due to viscous shear stresses and to soil dislodgment from the

normal impact of the gas. Such test results will aid in the formulation of the differential equation governing soil erosion. For example, this would resolve the question of whether it is adequate to merely account for the erosion from viscous action as in the existing theory, or must the erosion produced by normal surface stresses also be considered.

2. DEVELOPMENT OF SOIL EROSION THEORIES

Two procedures could be devised for predicting soil erosion caused by jet impingement. Both procedures utilize an upgraded differential equation governing the soil erosion caused by impinging gas loadings as developed from the results of Item c.

The first method is similar to the one presently used in that surface loadings are determined from engine conditions and the corresponding surface erosion determined from the governing erosion equation. The second method begins with experimental surface loadings obtained from tests conducted by firing onto flat and curved plates, or, from theoretical surface loadings based on more exact real gas theories which satisfy the appropriate boundary conditions for curved and flat plates. Then these loadings can be used in conjunction with the upgraded soil erosion differential equation to determine the suface erosion. In these procedures, it is tacitly assumed the surface erosion has a negligible influence on the gas flow field.

REFERENCES

1. Land, N.S. and Scholl, H.F., "Scaled LEM Jet Erosion Tests," NASA Langley Research Center Working Paper 252, 1966.

2. Land, N.S. and Scholl, H.F., "Further Scaled LEM Jet Erosion Tests," NASA Langley Research Center Working Paper 455, 1967.

3. Land, N.S. and Conner, D.W., "Laboratory Simulation of Lunar Surface Erosion by Rockets," Presented at 13th Annual Meeting, Institute Environmental Sciences, Washington, D.C., April 1967.

4. Roberts, Leonard, "The Action of a Hypersonic Jet on a Dust Layer," presented at the 31st Annual Meeting of the Institute of Aerospace Sciences, January 1963.

5. Roberts, Leonard, "The Interaction of a Rocket Exhaust with the Lunar Surface," Published in The Fluid Dynamic Aspects of Space Flight, vol. 2, Gordon and Breach Inc., New York, 1968.

6. Roberts, Leonard and South, Jerry C., "Comments on Exhaust Flow Field and Surface Impingement," AIAA Journal, Vol. 2, No. 5, p. 971, May 1964.

7. Kadib, A.A., "A Function for Sand Movement by Wind, "Hydraulic Engineering Laboratory Report HEL 2-12, University of California, January 1965.

8. Chepil, W.S., "Equilibrium of Soil Grains at the Threshold of Movement by Wind, "Soil Science Society Proceedings, pp 422-428, 1959.

9. Hildebrand, F.B., Introduction to Numerical Analysis, McGraw-Hill Book Company, Inc., 1956.

10. Hutton, R.E., "An Investigation of Soil Erosion and Its Potential Hazard to LM Lunar Landing," TRW Systems EM Report 16-11, October 1966.

11. Stitt, L.E., "Interaction of Highly Underexpanded Jets with Simulated Surfaces," NASA TN D-1095, December 1961.

12. Clark, L.V., "LM Base Pressures and Retro Nozzle Choking During Simulated Lunar Touchdown," NASA LWP-632, July 29, 1968.

13. Deresiewicz, H., "Mechanics of Granular Media," Columbia University Department of Civil Engineering Technical Report No. 25, February 1967.

14. Schlichting, H., Boundary Layer Theory, Pergamon Press, New York, 1955.

APPENDIX A

SYSTEM PARAMETERS

All parameters used in this investigation are presented in this appendix. Table A1 lists the chamber pressure p_c and temperature T_c, while Table A2 lists the times at the end of nozzle descent and thrust cutoff. Figures A1 and A2 present experimental data provided by the Langley Research Center regarding the internal friction angle α and packing factor c for glass beads, aluminum oxide and graphite particles. In the erosion computations performed during this study, the friction angle and packing constant were taken to be 27 degrees and 0.575, respectively. The use of a constant packing factor, which is independent of particle diameter, is consistent with the theoretical values obtained in Reference 13. In this reference, it was found that for a given type of packing, the packing factor is independent of particle diameter.

Table A3 gives a complete list of parameter values for the 32 tests. Most of the parameter values are given in References 1 and 2 where a detailed description of the tests is presented. The soil mass density σ was computed from the specific gravity listed in Reference 1. The packing factor c and friction angle α for gravel, Tests 9 and 10, were assumed to be the same as for glass beads. The value used for A_{coh} of 5×10^{-17} lb-ft is the value suggested by Roberts (Reference 5). The descent velocity V_v was computed from the descent time tabulated in Table A2, and the nozzle heights given in References 1 and 2.

In Table A3 the symbol E is used to denote the exponent of 10 by which the number is multiplied. For example, the gas viscosity for Test 1 is listed as 3.9E-7, which corresponds to the value 3.9×10^{-7} lb sec/ft^2. The soil particle density for the same test is 6.80×10^{-4} ft.

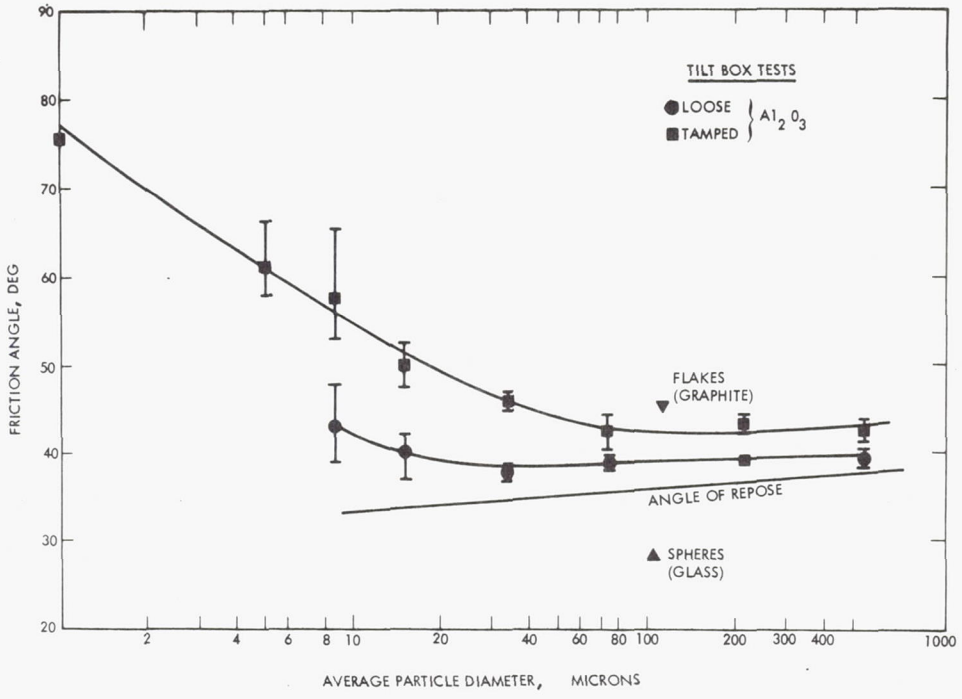

Figure A1. – Internal Friction Angle Data

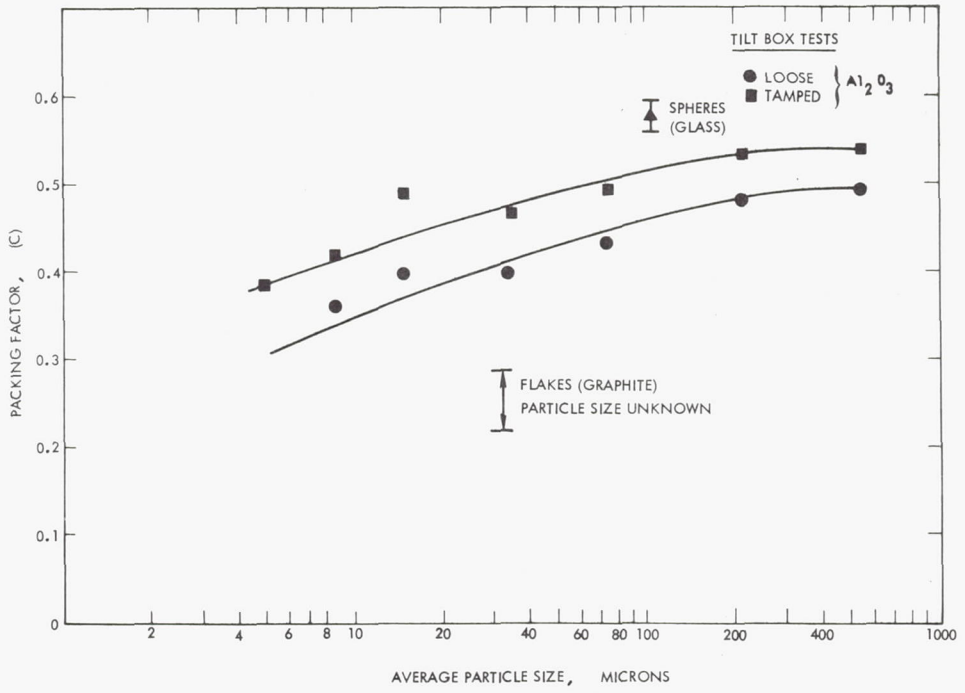

Figure A2. – Packing Constant Data

TABLE A1. - CHAMBER PRESSURES AND TEMPERATURES

Test No.	Pressure, psi p_c	Temperature ^oR
1	1.76	501.0
2	1.87	495.0
3	1.63	502.0
4	0.64	506.0
5	0.60	507.0
6	0.64	515.0
7	0.45	506.0
8	0.65	508.0
9	0.60	507.0
10	0.60	516.0
15	2.30	529.6
16	1.70	520.6
19	1.80	528.6
24	3.90	517.6
25	5.60	519.4
26	2.10	523.6

Test No.	Pressure, psi p_c	Temperature ^oR
28	2.45	510.6
29	1.75	515.6
31	1.55	523.6
32	1.65	530.6
35	1.68	515.6
37	1.83	523.6
38	1.95	527.6
39	1.87	513.6
46	2.55	510.6
47	1.18	517.6
48	0.78	523.6
49	5.13	527.6
51	1.73	510.6
52	3.28	506.6
54	1.73	507.6
55	4.72	508.6

TABLE A2. - TIMES AT END OF NOZZLE DESCENT AND THRUST CUTOFF*

Test No.	End of nozzle descent, sec.	Thrust cut-off, sec.
1	0.35	8.95
2	0.29	3.92
3	0.54	4.86
4	0.96	5.94
5	2.64	5.91
6	2.76	5.79
7	4.02	5.94
8	3.64	5.90
9	3.94	5.91
10	2.66	5.98
15	1.37	3.12
16	1.45	5.05
19	0.89	3.99
24	1.58	3.01
25	1.44	3.15
26	1.37	2.34

Test No.	End of nozzle descent, sec.	Thrust cut-off, sec.
28	1.56	3.00
29	0.82	2.00
31	0.65	2.00
32	1.86	1.99
35	1.66	2.03
37	1.55	2.00
38	1.58	2.02
39	1.69	2.00
46	1.41	2.00
47	1.42	1.98
48	1.44	1.99
49	1.47	2.01
51	1.39	1.99
52	1.42	2.01
54	1.30	2.00
55	1.37	1.99

*Time given is model time.
Zero time is start of nozzle descent.

TABLE A3. - SOIL EROSION PARAMETERS
(Model Dimensions)

PARAMETER	TEST NUMBER 1	2	3	4	5	6	7	8
ENGINE (Gas Type)	He	He	He	He	He	He	He	He
γ (dimensionless)	1.67	1.67	1.67	1.67	1.67	1.67	1.67	1.67
M_e (dimensionless)	2.68	2.68	2.68	2.68	2.68	2.68	2.68	2.68
r_e (ft)	0.1108	0.1108	0.1108	0.1108	0.1108	0.1108	0.1108	0.1108
R ($ft^2/sec^{2o}R$)	12,430	12,430	12,430	12,430	12,430	12,430	12,430	12,430
T_c (^oR)	501.0	495.0	502.0	506.0	507.0	515.0	506.0	508.0
μ_c (lb sec/ft^2)	3.9E-7	3.8E-7	3.9E-7	3.9E-7	4.0E-7	3.9E-7	3.9E-7	3.9E-7
p_c (psi)	1.76	1.87	1.63	0.64	0.60	0.64	0.45	0.65
p_c (psf)	253.4	269.3	234.7	92.2	86.4	92.2	64.8	93.6
SOIL	Glass	Glass	Glass	Glass	Glass	Glass	Glass	Glass
D (ft)	6.80E-4	6.80E-4	4.25E-3	4.25E-3	4.25E-3	1.91E-3	1.06E-3	3.50E-4
D (microns)	207.	207.	1296.	1296.	1296.	583.	324.	106.
σ (slug/ft^3)	4.85	4.85	4.85	4.85	4.85	4.85	4.85	4.85
c (dimensionless)	0.575	0.575	0.575	0.575	0.575	0.575	0.575	0.575
α (deg)	27	27	27	27	27	27	27	27
α (rad)	0.471	0.471	0,471	0.471	0.471	0.471	0.471	0.471
A_{coh} (lb-ft)	5E-17	5E-17	5E-17	5E-17	5E-17	5E-17	5E-17	5E-17
τ_{coh} (psf)	0	0	0	0	0	0	0	0
MISCELLANEOUS								
g (ft/sec^2)	32.2	32.2	32.2	32.2	32.2	32.2	32.2	32.2
h_o (ft)	2.07	2.07	3.26	3.26	3.26	3.26	3.26	3.26
h_1 (ft)	0.138	0.296	0.240	0.112	0.133	0.133	0.117	0.128
t_1 (sec)	0.35	0.29	0.54	0.96	2.64	2.76	4.02	3.64
V_v (ft/sec)	5.520	6.117	5.593	3.279	1.184	1.133	0.782	0.860
a_2 (dimensionless)	0.25	0.25	0.25	0.25	0.25	0.25	0.25	0.25

TABLE A3. - SOIL EROSION PARAMETERS (Continued)
(Model Dimensions)

PARAMETER	TEST NUMBER							
	9	10	15	16	19	24	25	26
ENGINE (Gas Type)	He	He	He	He	He	He	He	He
γ (dimensionless)	1.67	1.67	1.67	1.67	1.67	1.67	1.67	1.67
M_e (dimensionless)	2.68	2.68	2.68	2.68	2.68	2.68	2.68	2.68
r_e (ft)	0.1108	0.1108	0.1108	0.1108	0.1108	0.1108	0.1108	0.1108
R ($ft^2/sec^2{}^oR$)	12,430	12,430	12,430	12,430	12,430	12,430	12,430	12,430
T_c (^oR)	507.0	516.0	529.6	520.6	528.6	517.6	519.4	523.6
μ_c (lb sec/ft^2)	3.9E-7	4.0E-7	4.0E-7	4.0E-7	4.0E-7	4.0E-7	4.0E-7	4.0E-7
p_c (psi)	0.60	0.60	2.30	1.70	1.80	3.90	5.60	2.10
p_c (psf)	86.4	86.4	331.	244.8	259.	561.6	806.4	302.4
SOIL	Gravel	Gravel	Glass	Glass	Glass	Glass	Glass	Glass
D (ft)	1.57E-2	2.59E-2	2.13E-4	2.13E-4	3.12E-2	3.27E-3	3.27E-3	3.28E-3
D (microns)	4795.	7905.	64.8	64.8	9525.	997.9	997.9	1000.
σ (slug/ft^3)	5.23	5.23	4.85	4.85	4.85	4.85	4.85	4.85
c (dimensionless)	0.575	0.575	0.575	0.575	0.575	0.575	0.575	0.575
α (deg)	27	27	27	27	27	27	27	27
α (rad)	0.471	0.471	0.471	0.471	0.471	0.471	0.471	0.471
A_{coh} (lb-ft)	5E-17	5E-17	5E-17	5E-17	5E-17	5E-17	5E-17	5E-17
τ_{coh} (psf)	0	0	0	0	0	0	0	0
MISCELLANEOUS								
g (ft/sec^2)	32.2	32.2	32.2	32.2	32.2	32.2	32.2	32.2
h_o (ft)	3.26	3.26	3.52	3.52	3.52	3.52	3.52	3.52
h_1 (ft)	0.112	0.117	0.0469	0.0730	0.0515	0.0781	0.0622	0.0730
t_1 (sec)	3.94	2.66	1.37	1.45	0.89	1.58	1.44	1.37
V_v (ft/sec)	0.799	1.182	2.535	2.377	3.897	2.178	2.401	2.516
a_2 (dimensionless)	0.25	0.25	0.25	0.25	0.25	0.25	0.25	0.25

TABLE A3. - SOIL EROSION PARAMETERS (Continued)
(Model Dimensions)

PARAMETER	TEST NUMBER							
	28	29	31	32	35	37	38	39
ENGINE (Gas Type)	He	He	He	He	He	He	He	He
γ (dimensionless)	1.67	1.67	1.67	1.67	1.67	1.67	1.67	1.67
M_e (dimensionless)	2.68	2.68	2.68	2.68	2.68	2.68	2.68	2.68
r_e (ft)	0.1108	0.1108	0.1108	0.1108	0.1108	0.1108	0.1108	0.1108
R ($ft^2/sec^2{}^oR$)	12,430	12,430	12,430	12,430	12,430	12,430	12,430	12,430
T_c (^oR)	510.6	515.6	523.6	530.6	515.6	523.6	527.6	513.6
μ_c (lb sec/ft^2)	3.9E-7	4.0E-7	4.0E-7	4.1E-7	4.0E-7	4.0E-7	4.1E-7	4.0E-7
p_c (psi)	2.45	1.75	1.55	1.65	1.68	1.83	1.95	1.87
p_c (psf)	352.8	252.0	223.2	237.6	241.9	263.5	280.8	269.3
SOIL	Glass	Glass	Glass	Glass	Glass	Glass	Glass	Glass
D (ft)	1.62E-3	1.62E-3	1.62E-3	1.62E-3	1.62E-3	1.62E-3	1.62E-3	1.62E-3
D (microns)	492.	492.	492.	492.	492.	492.	492.	492.
σ (slug/ft^3)	4.85	4.85	4.85	4.85	4.85	4.85	4.85	4.85
c (diminesionless)	0.575	0.575	0.575	0.575	0.575	0.575	0.575	0.575
α (deg)	27	27	27	27	27	27	27	27
α (rad)	0.471	0.471	0.471	0.471	0.471	0.471	0.471	0.471
A_{coh} (lb-ft)	5E-17	5E-17	5E-17	5E-17	5E-17	5E-17	5E-17	5E-17
τ_{coh} (psf)	0	0	0	0	0	0	0	0
MISCELLANEOUS								
g (ft/sec^2)	32.2	32.2	32.2	32.2	32.2	32.2	32.2	32.2
h_o (ft)	3.52	3.52	3.52	3.52	3.52	3.52	3.52	3.52
h_1 (ft)	0.0832	0.104	0.0418	0.0367	0.125	0.156	0.223	0.312
t_1 (sec)	1.56	0.82	0.65	1.86	1.66	1.55	1.58	1.69
V_v (ft/sec)	2.203	4.166	5.351	1.873	2.045	2.170	2.087	1.898
a_2 (dimensionless)	0.25	0.25	0.25	0.25	0.25	0.25	0.25	0.25

TABLE A3. - SOIL EROSION PARAMETERS (Concluded)
(Model Dimensions)

PARAMETER	TEST NUMBER							
	46	47	48	49	51	52	54	55
ENGINE (Gas Type)	He	He	He	He	He	He	He	He
γ (dimensionless)	1.67	1.67	1.67	1.67	1.67	1.67	1.67	1.67
M_e (dimensionless)	2.68	2.68	2.68	2.68	2.68	2.68	2.68	2.68
r_e (ft)	0.1108	0.1108	0.1108	0.1108	0.1108	0.1108	0.1108	0.1108
$R(ft^2/sec^2{}^oR)$	12,430	12,430	12,430	12,430	12,430	12,430	12,430	12,430
T_c (^oR)	510.6	517.6	523.6	527.6	510.6	506.6	507.6	508.6
μ_c (lb sec/ft^2)	4.0E-7	4.0E-7	4.0E-7	4.1E-7	4.0E-7	4.0E-7	4.0E-7	4.0E-7
p_c (psi)	2.55	1.18	0.78	5.13	1.73	3.28	1.73	4.72
p_c (psf)	367.2	169.9	112.3	724.3	249.1	472.3	249.1	679.6
SOIL	Glass	Glass	Glass	Glass	Glass	Glass	Glass	Glass
D (ft)	1.62E-3	1.62E-3	1.62E-3	1.62E-3	4.25E-3	4.25E-3	4.25E-3	4.25E-3
D (microns)	492.	492.	492.	492.	1296.	1296.	1296.	1296.
σ (slug/ft^3)	4.85	4.85	4.85	4.85	4.85	4.85	4.85	4.85
c (dimensionless)	0.575	0.575	0.575	0.575	0.575	0.575	0.575	0.575
α (deg)	27	27	27	27	27	27	27	27
α (rad)	0.471	0.471	0.471	0.471	0.471	0.471	0.471	0.471
A_{coh} (lb-ft)	5E-17	5E-17	5E-17	5E-17	5E-17	5E-17	5E-17	5E-17
τ_{coh} (psf)	0	0	0	0	0	0	0	0
MISCELLANEOUS								
g (ft/sec^2)	32.2	32.2	32.2	32.2	32.2	32.2	32.2	32.2
h_o (ft)	3.52	3.52	3.52	3.52	3.52	3.52	3.52	3.52
h_1 (ft)	0.0628	0.0628	0.0628	0.0673	0.0571	0.0577	0.0470	0.0520
t_1 (sec)	1.41	1.42	1.44	1.47	1.39	1.42	1.30	1.37
V_v (ft/sec)	2.452	2.435	2.401	2.349	2.491	2.439	2.672	2.531
a_2 (dimensionless)	0.25	0.25	0.25	0.25	0.25	0.25	0.25	0.25

APPENDIX B

ROBERTS' THEORY

The equations used to predict soil erosion caused by rocket gases impinging on soil surfaces are presented in this appendix. The presentation begins with a brief description of Roberts' development of the equations. This introduction is followed by a listing of the gas flow field equations and equations governing soil erosion. The appendix concludes with comments concerning several of the equations listed and graphical presentations of typical flow field variables predicted from Roberts' theory.

1. ROBERTS' DERIVATION

In References 4 and 5, Roberts first develops a description of the gas flow field caused by gases emanating from a nozzle located a distance h above a flat soil surface. He then develops a theory describing the rate at which the soil surface erodes under the action of the gas viscous forces generated while the gas flows symmetrically along the soil surface away from the stagnation point.

The development of the gas flow field equations begins with an assumption regarding the spatial variation of gas density as it emanates from the nozzle. Then, by applying perfect gas theory, analytical expressions are developed which describe the gas radial velocity and static and dynamic pressures along the flat rigid surface.

The static pressure is obtained by imposing the condition that the gas momentum normal to the surface is destroyed, while the gas momentum parallel to the surface is unaffected by the surface. It is then assumed the gas flowing parallel to the soil surface exerts viscous shearing stresses on the soil which may dislodge soil particles and entrain them in the flowing gas. In essence, this procedure considers the surface to be infinitely rigid

with respect to vertical pressure loading, but has a finite shearing resistance to the viscous shear stresses parallel to the soil-gas interface

The development of the equation governing the rate of soil removal caused by the viscous shearing stresses begins with the postulated impulse-momentum relation

$$(\Delta m)\ v = A\ (\tau - \tau^*)\Delta t \qquad \text{(B1)}$$

which relates the momentum imparted to a soil mass element Δm to the impulse caused by the viscous shear stresses. In Equation (B1), v is the velocity imparted to the elemental soil mass, A is the cross-sectional area of the mass element, τ is the viscous shear stress acting on the soil mass, and τ^* is the soil restraining shear stress due to friction and cohesion between the soil grains that must be exceeded before erosion can begin. The coordinate system used in this derivation is shown in Figure B1.

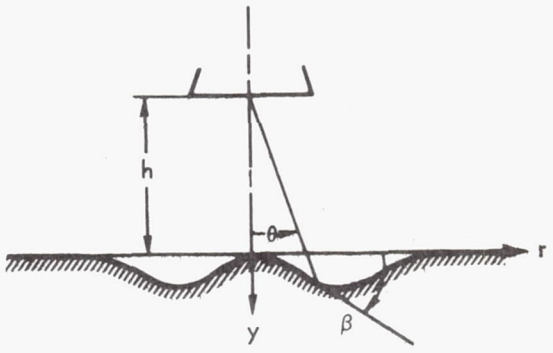

Figure B1.- Coordinate System

The element of soil mass and its velocity is then written as

$$\Delta m = \sigma c A(\Delta y)\cos\beta$$
$$v = au/2 \qquad \text{(B2)}$$

where σc is the soil bulk mass density (c is the packing factor which is also equal to 1 minus the soil porosity), Δy is the element of erosion depth, $\tan\beta$ is the slope of the surface, u is the radial velocity of the gas, and $(a/2)$ is the effective proportion of the gas velocity imparted to the soil particle. The partial differential equation describing the rate of erosion is obtained by taking the limit of Equation (B1). A list of the entire set of equations governing soil erosion follows.

2. GOVERNING EQUATIONS

Erosion Equation

$$\frac{\partial y}{\partial t} = \frac{2\,(\tau - \tau^*)}{au\ \sigma c\ \cos\beta} \tag{B3}$$

Flow Field Equations

$$u = \left\{ \frac{2\gamma}{\gamma - 1} RT_c \left[1 - \frac{p}{p_s}^{\frac{\gamma-1}{\gamma}} \right] \right\}^{\frac{1}{2}} \tag{B4}$$

$$M_\ell = \frac{u}{\sqrt{\gamma RT}} = \sqrt{\frac{2}{\gamma-1} \left[\left(\frac{p}{p_s}\right)^{\frac{1-\gamma}{\gamma}} - 1 \right]} \tag{B5}$$

$$q = \frac{\gamma}{\gamma-1} \left[1 - \left(\frac{p}{p_s}\right)^{\frac{\gamma-1}{\gamma}} \right] \left(\frac{p}{p_s}\right)^{\frac{1}{\gamma}} p_s \tag{B6}$$

$$q_{max} = \left(\frac{1}{\gamma}\right)^{\frac{1}{\gamma-1}} p_s \tag{B7}$$

$$\frac{r}{h} \text{ (at } q_{max}) = \sqrt{\gamma^{\frac{2\gamma}{(\gamma-1)\,(k+4)}} - 1} \tag{B8}$$

$$\frac{p}{p_s} = (\cos\theta)^{(k+4)} (\cos\beta)^2 \left[1 - \tan\theta \tan\beta\right]^2 \tag{B9}$$

$$\rho = \frac{2q}{u^2} \tag{B10}$$

$$\mu = \mu_c \left(\frac{p}{p_s} \right)^{\frac{\gamma-1}{2\gamma}} \tag{B11}$$

$$\tan \theta = \frac{r}{h} \ , \ \tan\beta = \frac{\partial y}{\partial r} \tag{B12}$$

$$\left.\begin{aligned} p_s &= \min \left\{ p_r \ , \ \frac{k+2}{2} \left(\frac{r_e}{h} \right)^2 p_r \right\} \\ p_r &= \frac{\left[1 + \gamma M_e^2 \right] p_c}{\left[1 + \frac{\gamma-1}{2} M_e^2 \right]^{\frac{\gamma}{\gamma-1}}} \end{aligned}\right\} \tag{B13}$$

$$h_c = r_e \sqrt{\frac{k+2}{2}} \tag{B14}$$

$$k = \gamma(\gamma-1) M_e^2 \tag{B15}$$

$$h(t) = h_1(t) + a_2 \, y(t)_{max} \tag{B16}$$

$$h_1(t) = \begin{cases} h_o - V_v t & 0 \le t \le t_1 \\ h_1 & t > t_1 \end{cases} \tag{B17}$$

Erosive Viscous Shear Stress

$$\tau = C_f q \tag{B18}$$

Soil Shear Stress Restraint

$$\tau^* = \sigma c D g \cos\beta \tan\alpha - \sigma c D g \sin\beta + A_{coh} D^{-3} + \tau_{coh} \tag{B19}$$

Momentum Factor

$$a^{-1} = .5 + \sqrt{.25 + \zeta^{-1}} \tag{B20}$$

$$\zeta = \frac{18\mu_c h}{\sigma D^2 \sqrt{RT_c}\,(k+4)} \left[1 + \frac{(k+2)DC_D p_r}{72\sqrt{2}\,\mu_c \sqrt{RT_c}} \left(\frac{r_e}{h} \right)^2 \right] \tag{B21}$$

Reynolds Numbers

$$\left.\begin{aligned} R_D &= \frac{\rho u D}{\mu} \\ R_\theta &= \frac{\rho u r}{\mu} \end{aligned}\right\} \tag{B22}$$

Particle Drag and Friction Coefficients

$$\left.\begin{aligned} C_D &= f(R_D) \\ C_f &= Kf(R_\theta) \end{aligned}\right\} \tag{B23}$$

Although most of the preceding equations, in conjunction with the definition of parameters, need no explanation, several equations need some clarification.

In Roberts' formulation, it was assumed the nozzle height was large compared to the erosion depth. This appears to be a valid assumption for most cases of erosion by retro-rocket gases during lunar landing. However, during some of the erosion experiments, the erosion depth was even larger than the nozzle height above the original uneroded surface.

As a result, the nozzle height equation (B16) is modified slightly through the introduction of the nondimensional factor a_2 to account for an effective increase in nozzle height as the erosion crater forms. Such a modification allows theory to predict a limiting crater depth for long hover periods, which, of course, would occur in a real situation. The value of a_2 used in the calculations performed here is 0.25. This value was selected empirically during the erosion computations performed in Reference 10, wherein this nozzle height modification was first introduced. In the earlier erosion computations it appeared that $a_2 = 0.25$ provided about the "best" agreement between theory and test.

The shear stress expression τ^* contains two terms $A_{coh}D^{-3}$ and τ_{coh} which account for the cohesion between soil grains. Both of these terms are not used simultaneously in the same erosion computations. They merely permit the accounting for soil cohesion in one of two ways. If a value of soil cohesion is known, then that value is assigned to τ_{coh} and A_{coh} is set equal to zero. Roberts suggested that the soil cohesion could be expressed in terms of the particle diameter; and from test data he estimated A_{coh} to be 5×10^{-17} lb-ft. When a nonzero value of A_{coh} is used, the value of τ_{coh} is set equal to zero.

The expression for ζ (B21), differs slightly from the expression listed in Reference 5 because of typographical errors in Reference 5. Reference 5 contains a factor e which should have been omitted. The factor k + 4 inside the brackets should have read k + 2. One further difference is that Roberts'

intermediate parameter F was omitted so that ζ is expressed here directly in terms of p_r.

The particle drag and friction coefficients are based on experimental data obtained from drag measurements on spherical particles. For the drag coefficient C_D, the length parameter in Reynolds number is based on the particle diameter. The friction coefficient C_f relates the shear stress acting on a surface particle to the local dynamic pressure. Since the shear stress depends on the local flow conditions at the particular point where the particle enters the flow, the appropriate length parameter in Reynolds number is the distance from the stagnation point to the particle location.

In Reference 4, Roberts writes the aerodynamic shear stress as $K\tau$ where the constant K depends on the nature of the flow over the surface and its action on surface particles. Roberts quotes Bagnold's investigations of wind-blown dusts which indicated K to be approximately 35 for rough turbulent flow. The inference is that C_f is taken as a constant, and the viscous shear stress is K times C_f. In the work presented here, C_f is not assumed to be constant but is expressed in terms of the local Reynolds number. In this manner the value of C_f is allowed to vary both with time and radial coordinate. Actually in the calculations, a factor K was multiplied by the value of C_f obtained from the corresponding local Reynolds number. In the calculations performed here, the value of K was set equal to 1. However, some calculations were made with other values of K to determine whether better agreement with test could be obtained. The conclusion was that a value of K different from 1 did give better agreement for some tests. However, the same constant would degrade the agreement in other tests. As a result, K was taken equal to 1 for all the comparisons presented here.

Figures B2 through B5 present graphs showing typical variations in flow field variables. These figures are included merely to illustrate typical flow field variables and how they vary with nozzle height and distance from the stagnation point. These data were obtained using Test 39 engine parameters.

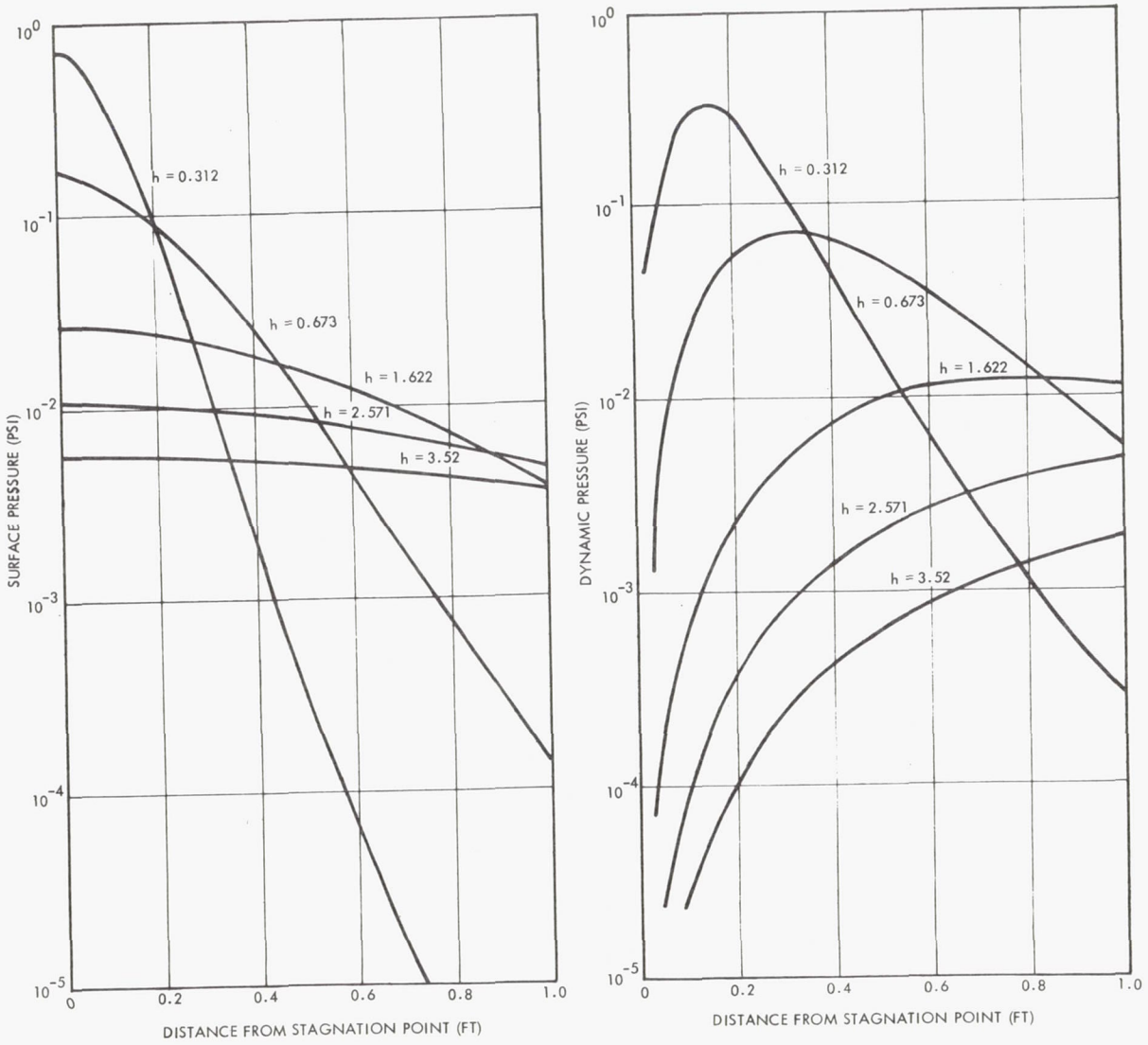

Figure B2.- Typical Variation of Static Pressure and Dynamic Pressure

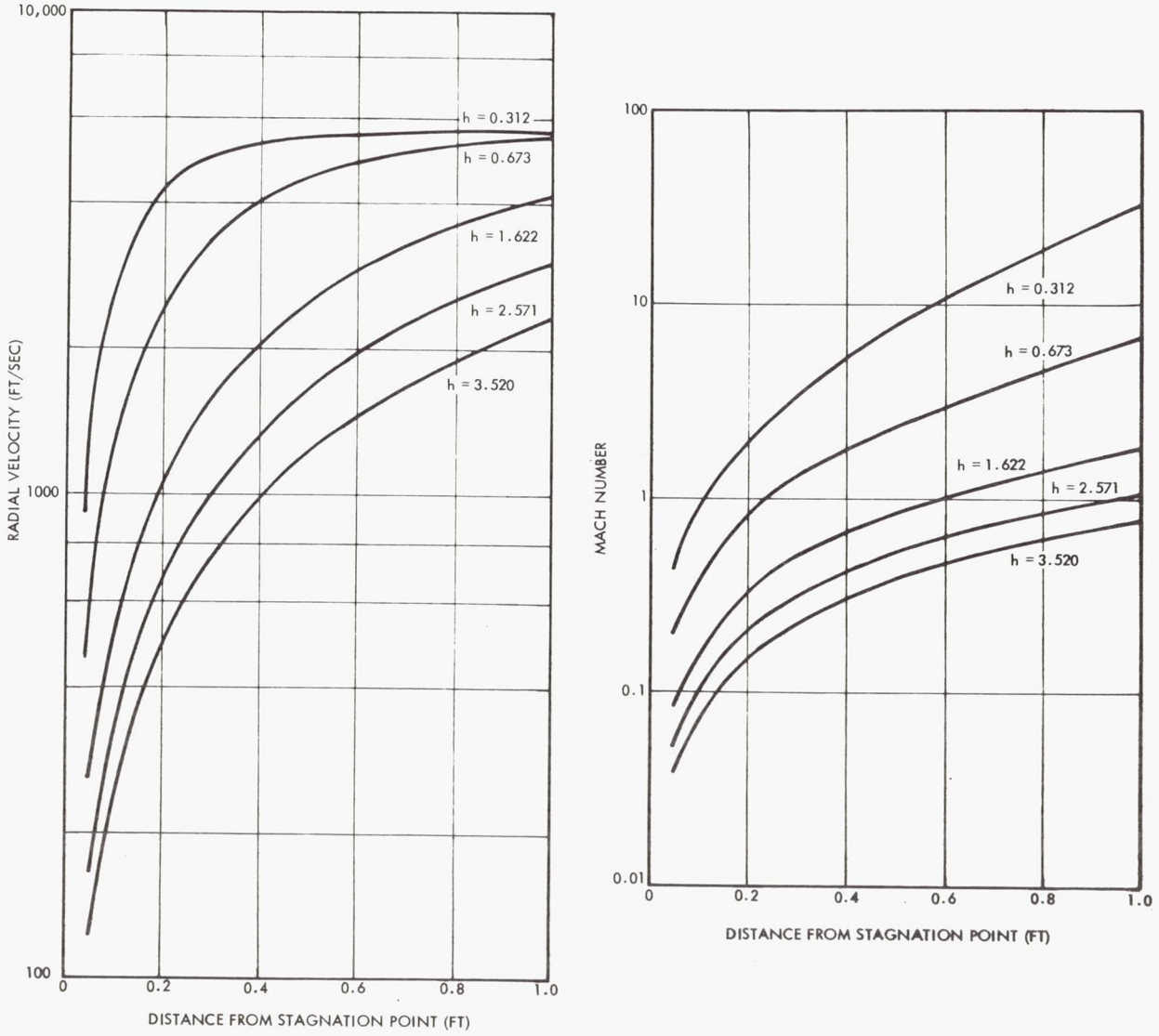

Figure B3.- Typical Variation of Gas Velocity and Local Mach Number

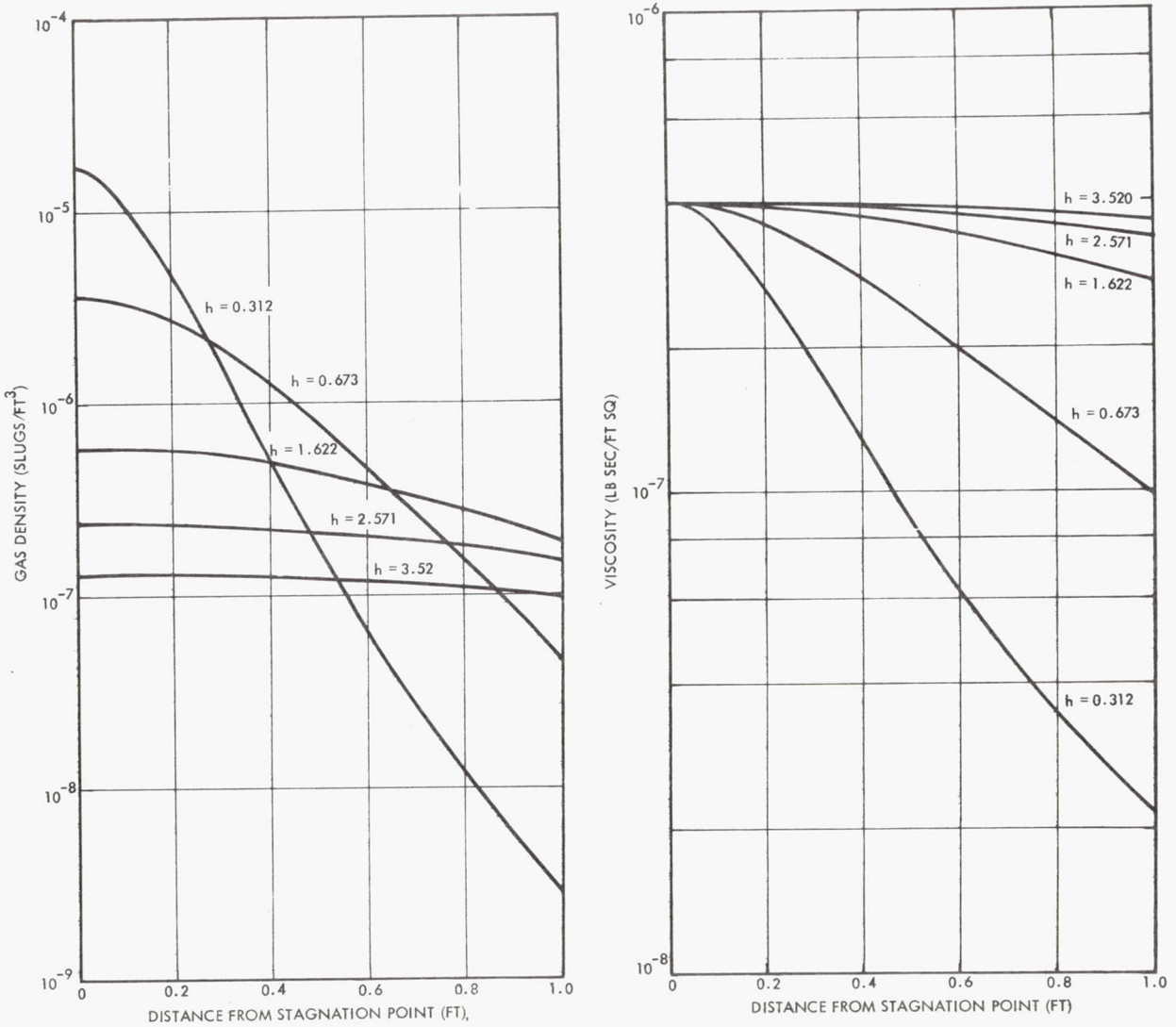

Figure B4.- Typical Variation of Gas Density and Viscosity

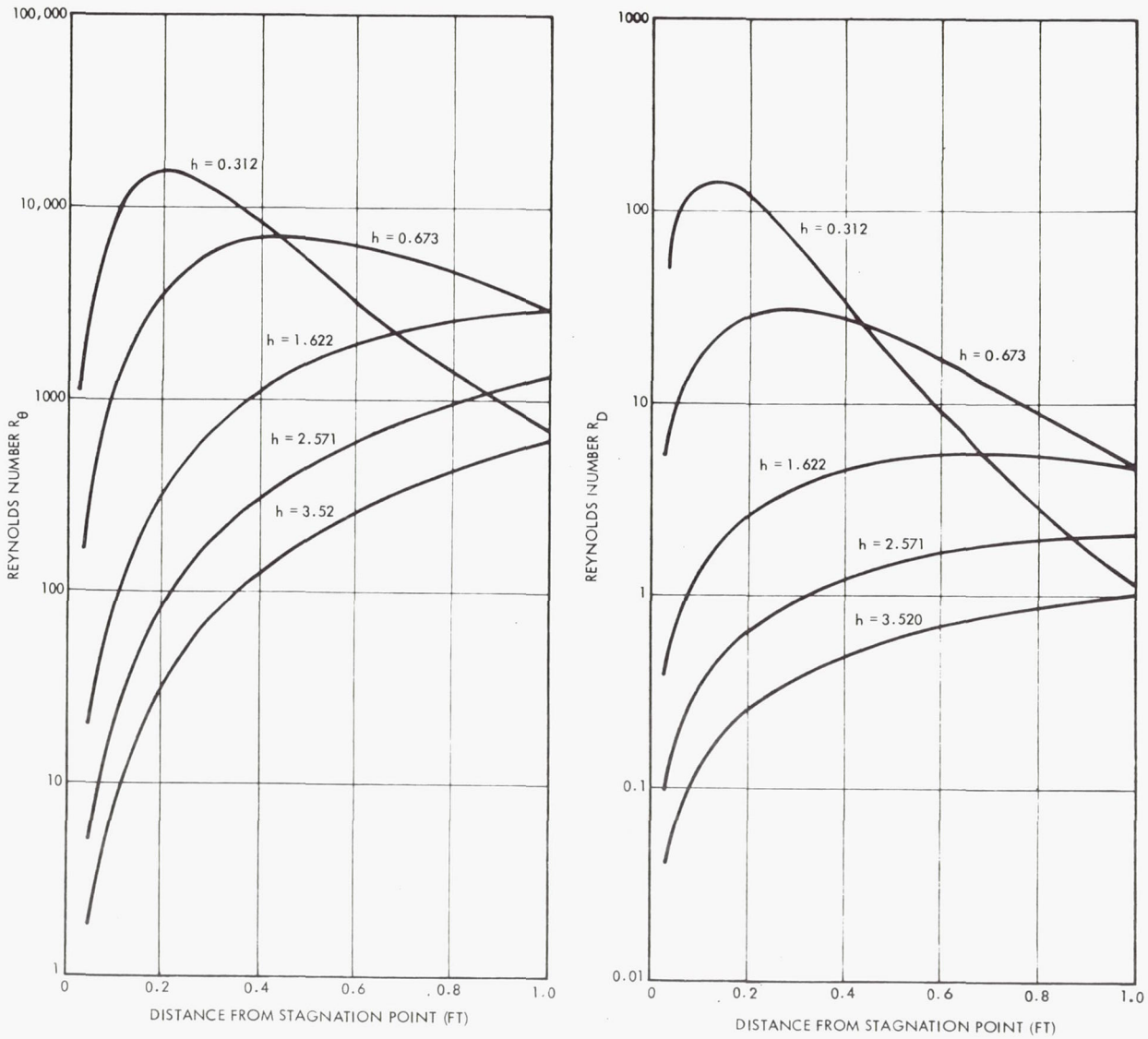

Figure B5. - Typical Variation of Reynolds Numbers

APPENDIX C

THEORETICAL AND EXPERIMENTAL EROSION RESULTS

The erosion observed in each of the 32 tests and the corresponding theoretical predictions are presented in this appendix. A separate figure containing three main parts is presented for each test.

Part (a) shows the theoretical erosion profiles and comparisons with the measured erosion depths at selected times. Contained in this part of the figure are theoretical profiles for several times all displayed to a common scale. These same profiles are individually displayed with measured depths superimposed for comparison. The scale factor SF (in feet) is different in each comparison plot because the erosion depth varies with time and the results are displayed at various expanded scales.

Part (b) shows the measured erosion profiles constructed from tabular data of the erosion depth at discrete times and radial locations provided by the Langley Research Center. No attempt was made to fair curves through the data points. Rather, straight lines were connected between the data points to provide a visual indication of the erosion profile. The numbers adjacent to the profiles correspond to the time in seconds (model time) after the beginning of engine descent.

Part (c) shows a curve of the variation in the maximum erosion depth with nondimensional time, with the measured maximum depths superimposed. Time was nondimensionalized by dividing the actual time by the descent time t_1. Thus, nondimensional time less than 1 corresponds to times when the nozzle is descending, while times greater than 1 correspond to the nozzle in the hover position. In part (c) of Test 1, no test data points are shown because it appeared that over a range of radial distances, the entire 4 inches of "soil" was already removed by the time the first profile is shown.

In examining the theoretical results in the 32 figures, it will be noted that the theoretical computations were often terminated well before thrust cutoff. This was because computations became meaningless whenever the predicted depth exceeded the soil bed depth of 4 inches. Also, computations were terminated when theoretical predictions began to deviate substantially from measured erosion. This often occurred at nozzle heights significantly below the critical nozzle height h_c. At these heights, theory predicts erosion only occurs over a narrow range between the stagnation point and a point directly below the nozzle lip. However, tests show erosion occurs well beyond the nozzle lip location.

THEORETICAL AND EXPERIMENTAL EROSION CONTOURS

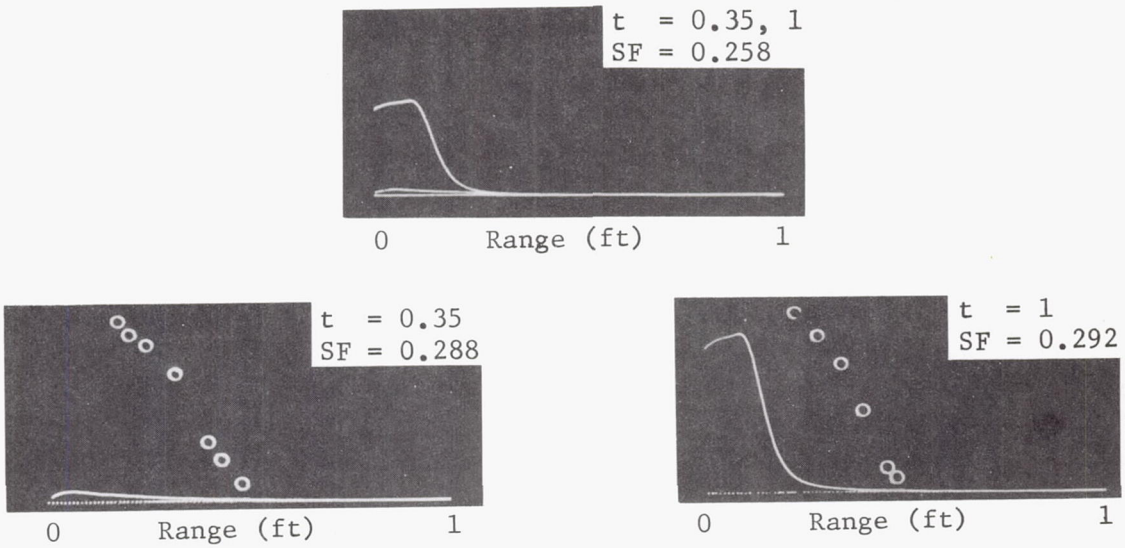

(a)
TEST 1

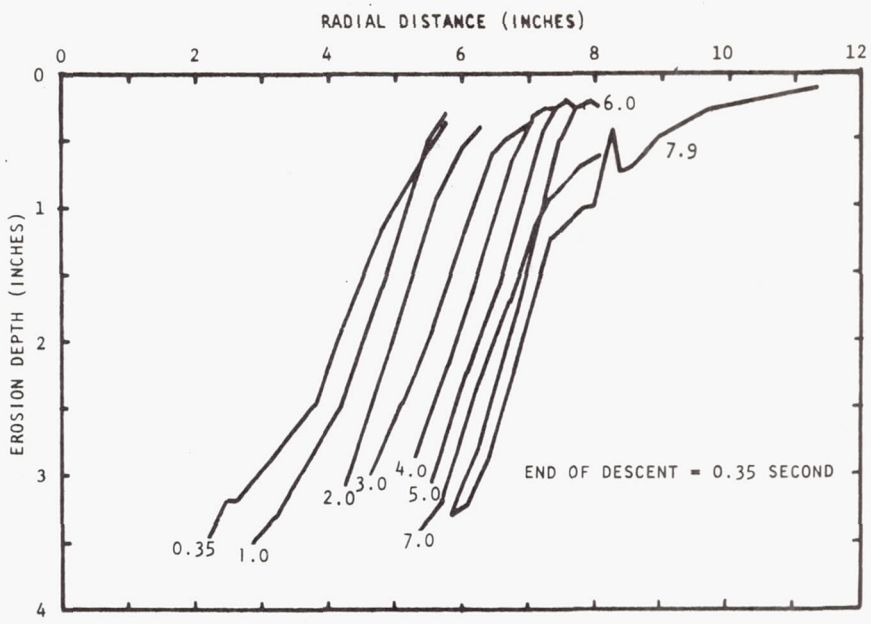

(b)

TEST 1

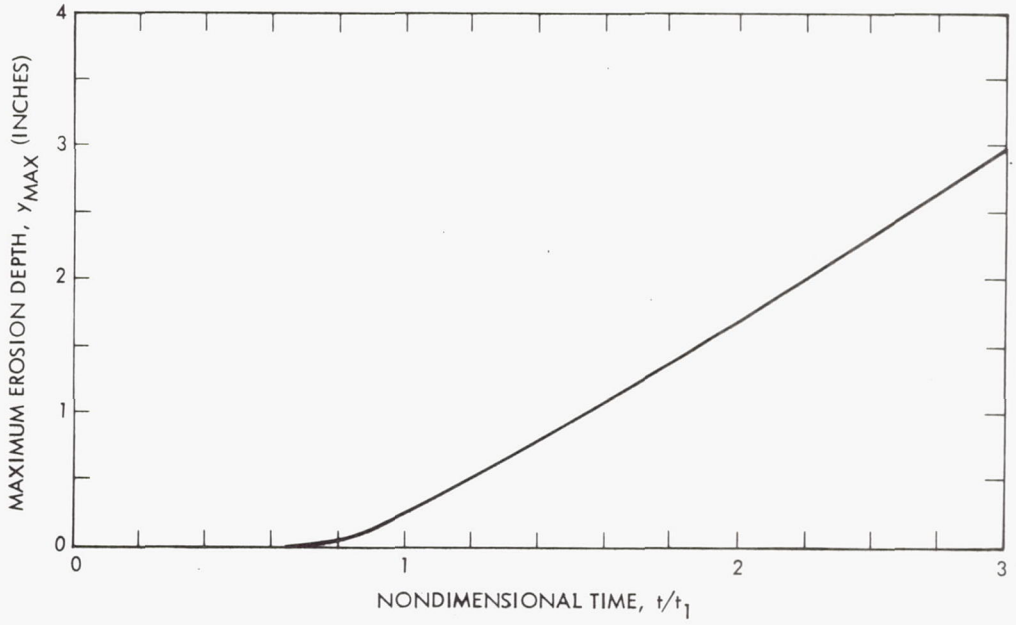

(c)

TEST 1

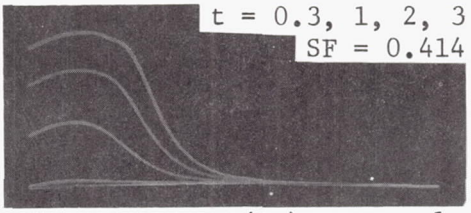
t = 0.3, 1, 2, 3
SF = 0.414
0
Range (ft)
1

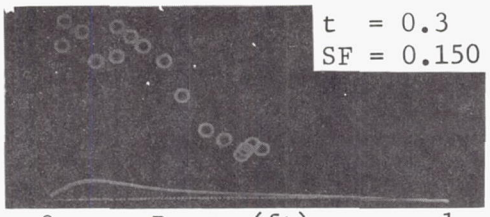
t = 0.3
SF = 0.150
0
Range (ft)
1

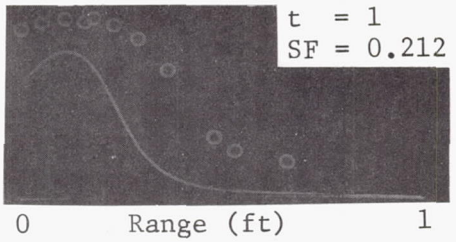
t = 1
SF = 0.212
0
Range (ft)
1

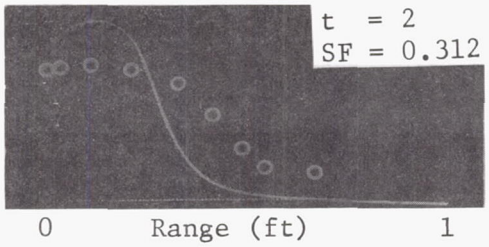
t = 2
SF = 0.312
0
Range (ft)
1

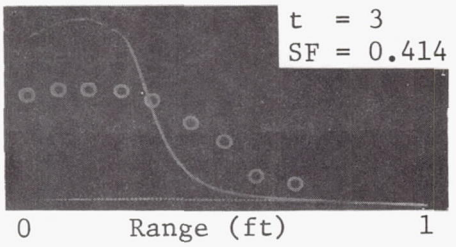
t = 3
SF = 0.414
0
Range (ft)
1

(a)
TEST 2

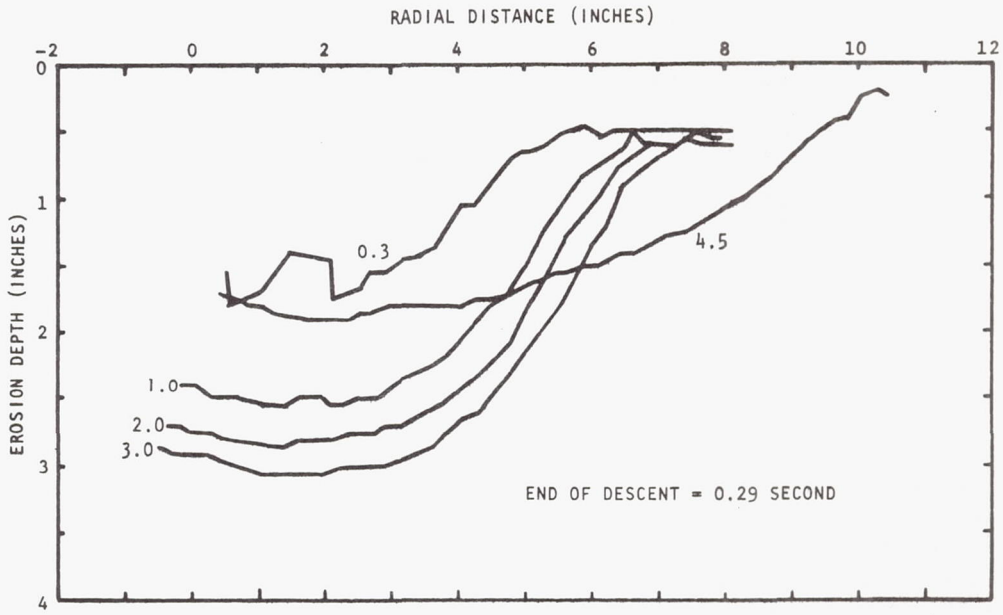

(b)
TEST 2

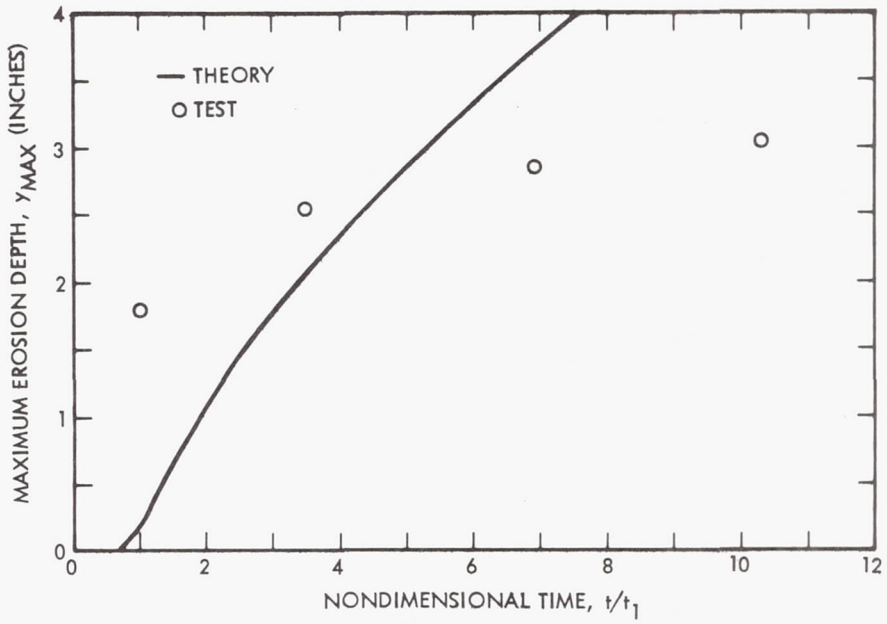

(c)
TEST 2

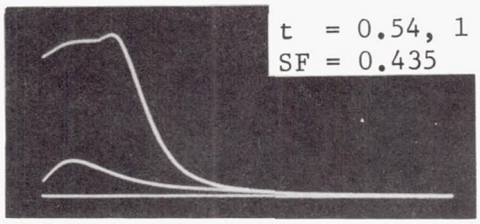
t = 0.54, 1
SF = 0.435
0
Range (ft)
1

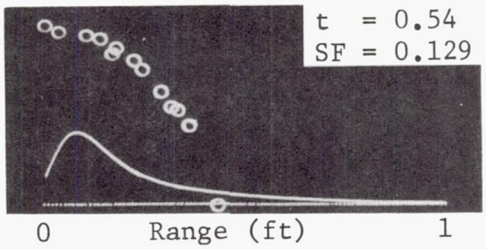
t = 0.54
SF = 0.129
0
Range (ft)
1

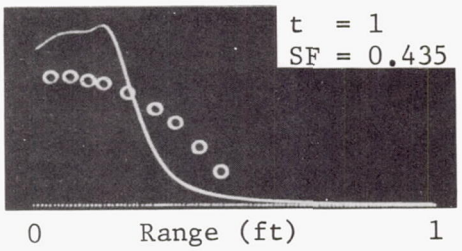
t = 1
SF = 0.435
0
Range (ft)
1

(a)
TEST 3

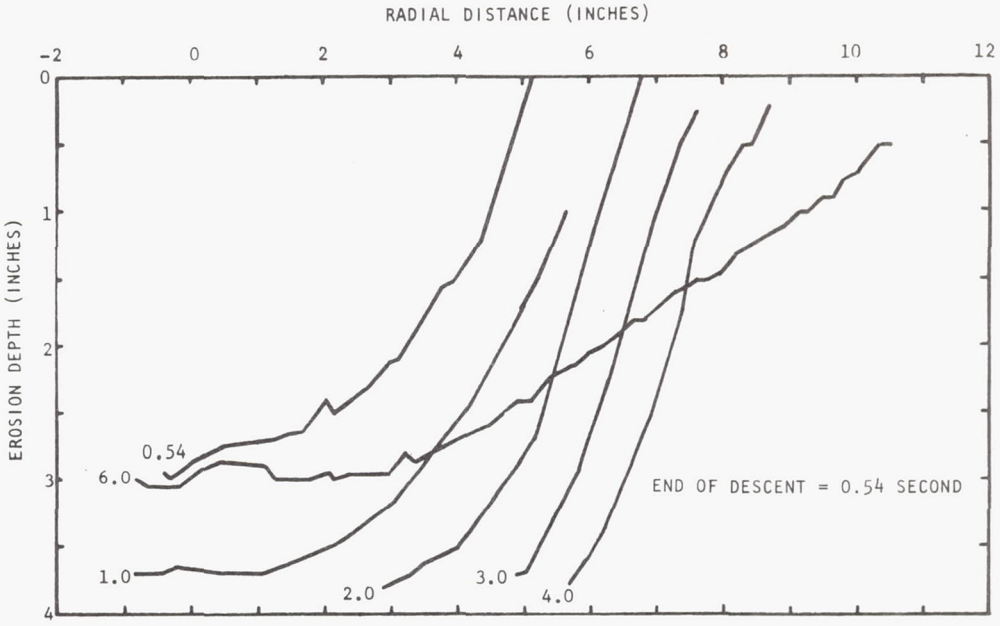

(b)
TEST 3

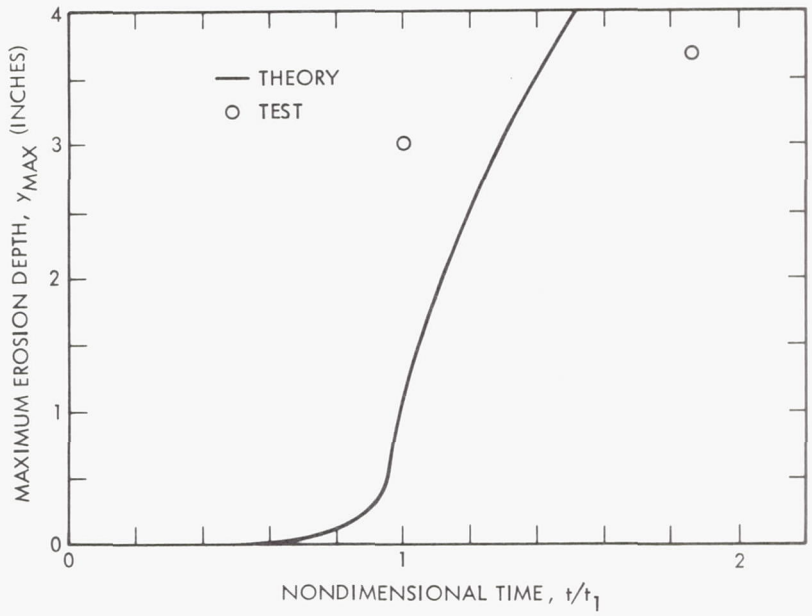

(c)
TEST 3

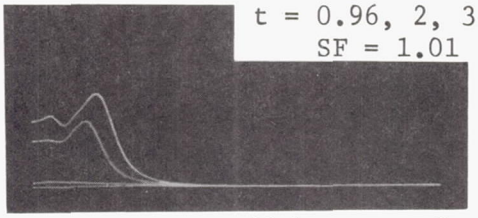

0 Range (ft) 1

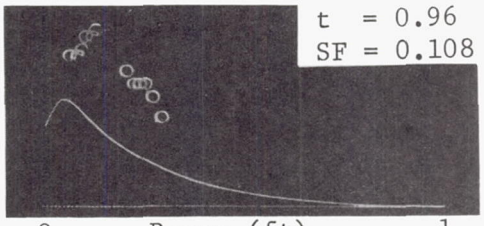

0 Range (ft) 1

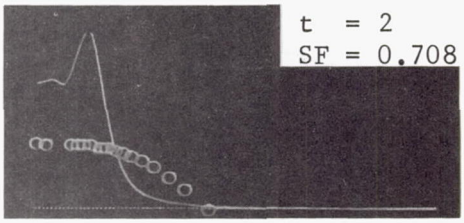

0 Range (ft) 1

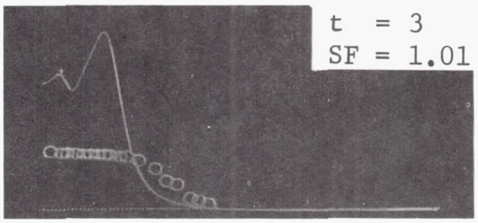

0 Range (ft) 1

(a)
TEST 4

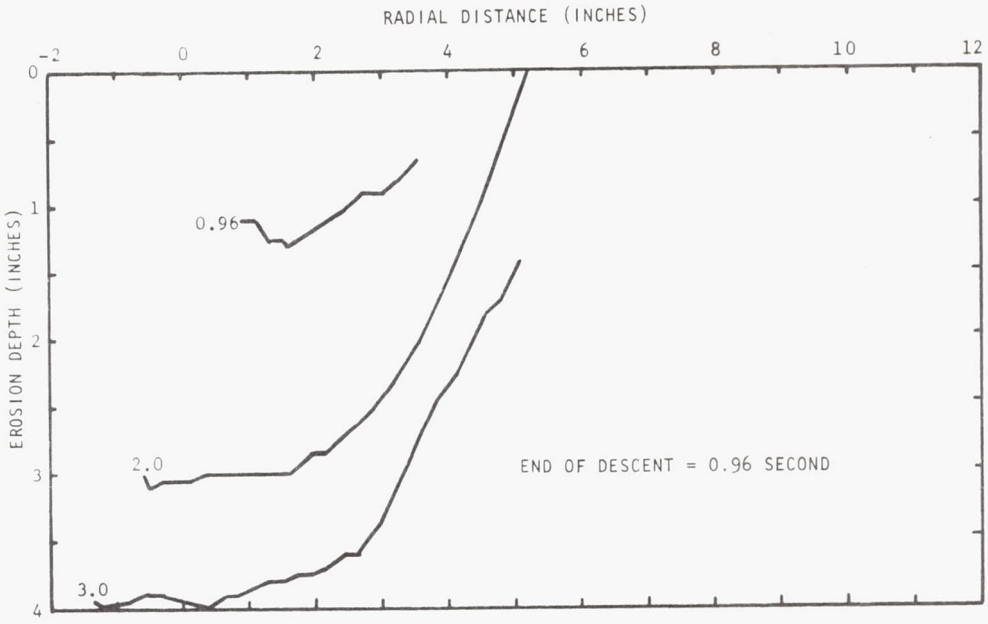

(b)
TEST 4

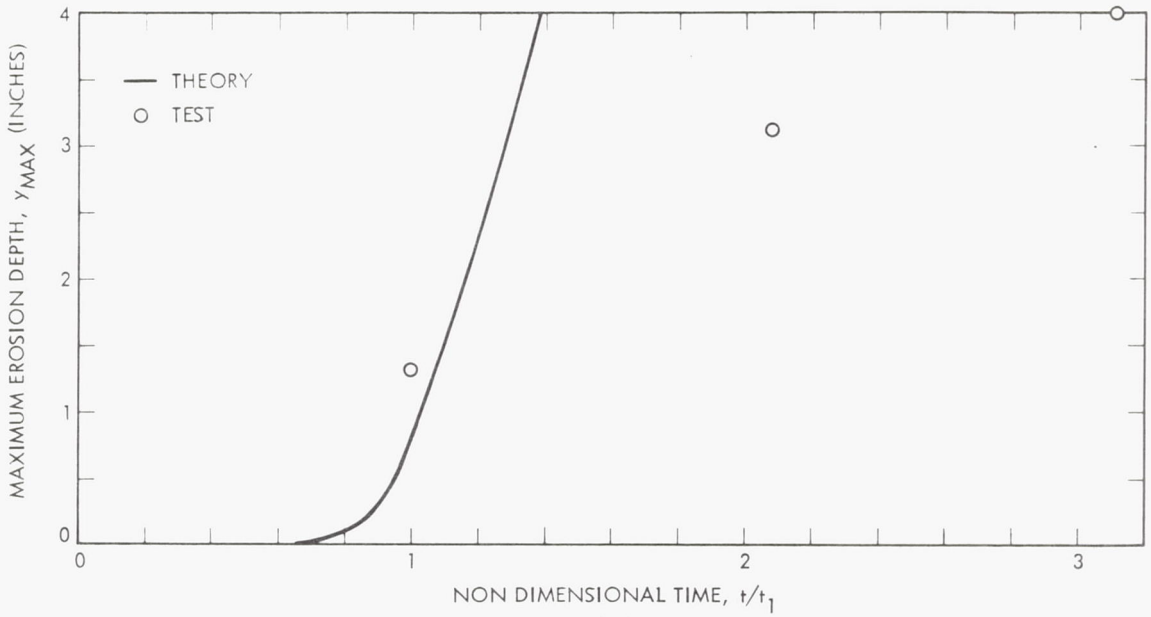

(c)
TEST 4

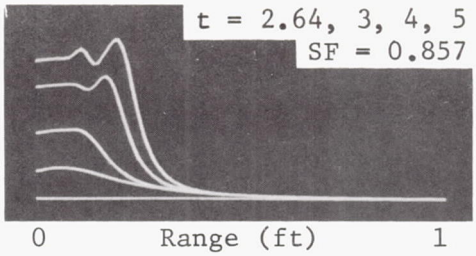
t = 2.64, 3, 4, 5
SF = 0.857
0
Range (ft)
1

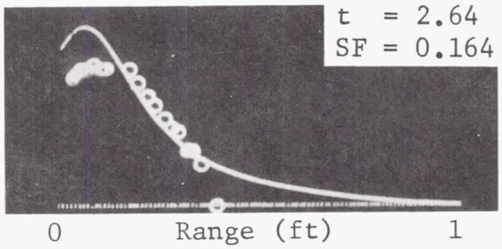
t = 2.64
SF = 0.164
0
Range (ft)
1

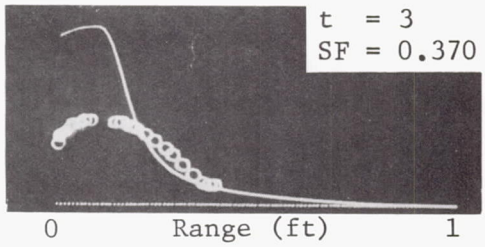
t = 3
SF = 0.370
0
Range (ft)
1

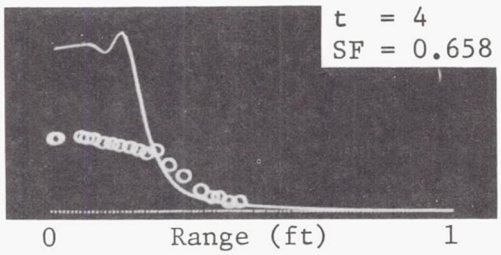
t = 4
SF = 0.658
0
Range (ft)
1

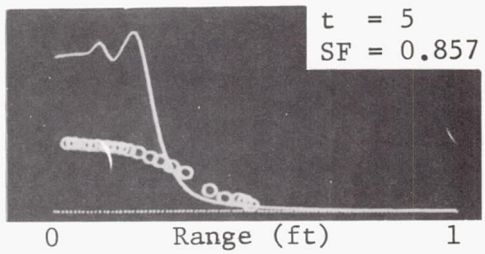
t = 5
SF = 0.857
0
Range (ft)
1

(a)
TEST 5

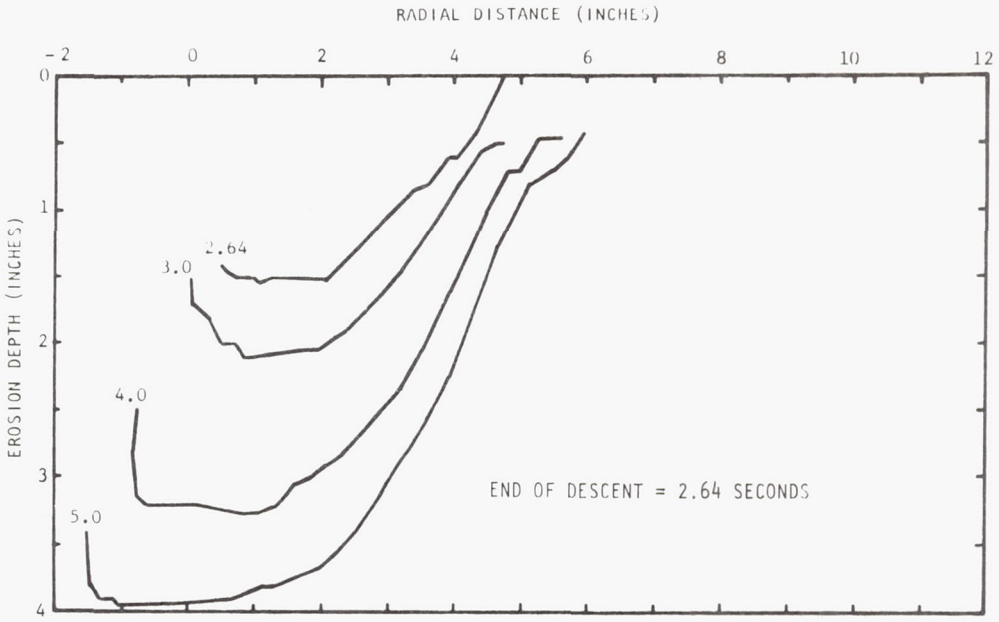

(b)
TEST 5

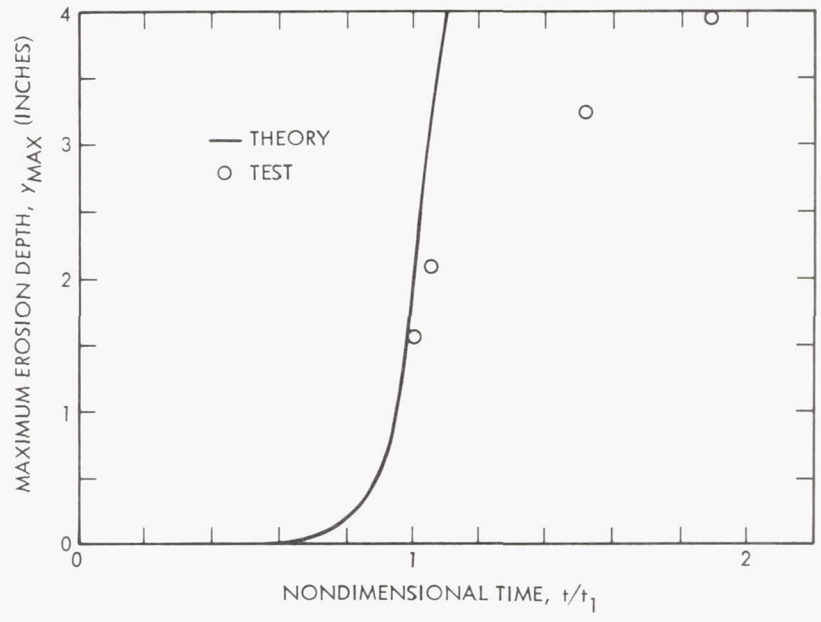

(c)
TEST 5

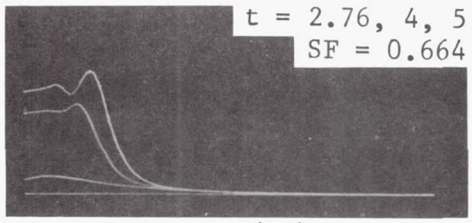
t = 2.76, 4, 5
SF = 0.664
0
Range (ft)
1

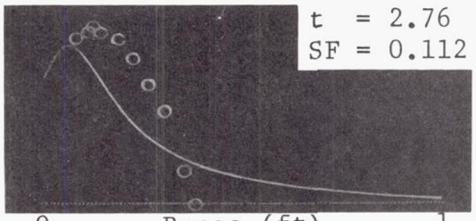
t = 2.76
SF = 0.112
0
Range (ft)
1

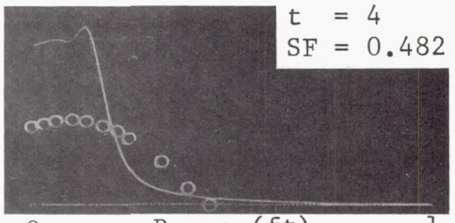
t = 4
SF = 0.482
0
Range (ft)
1

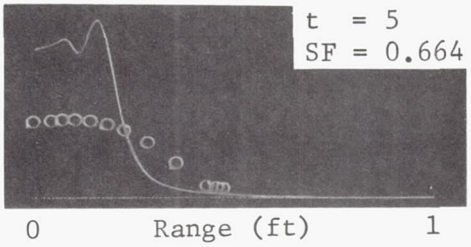
t = 5
SF = 0.664
0
Range (ft)
1

(a)
TEST 6

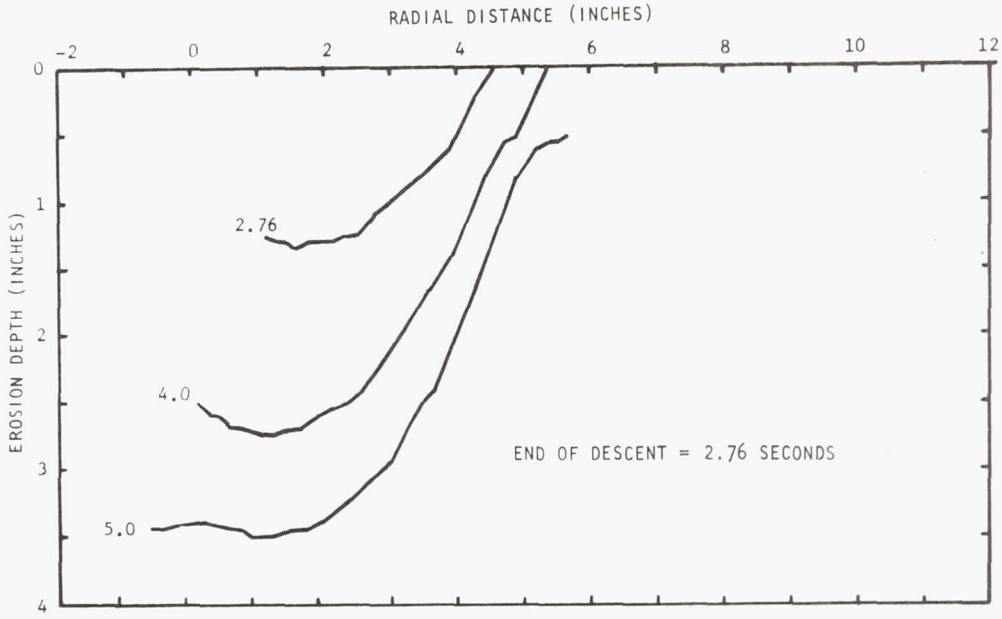

(b)
TEST 6

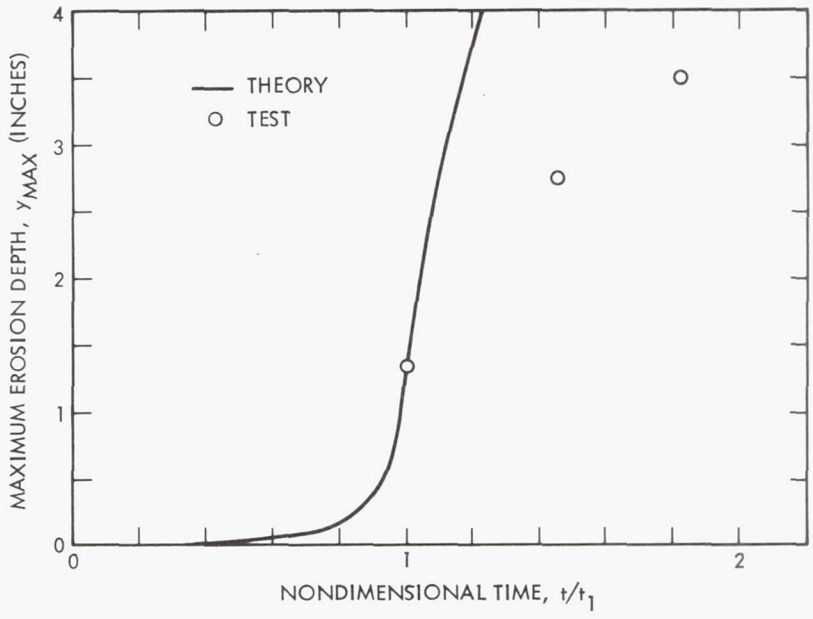

(c)
TEST 6

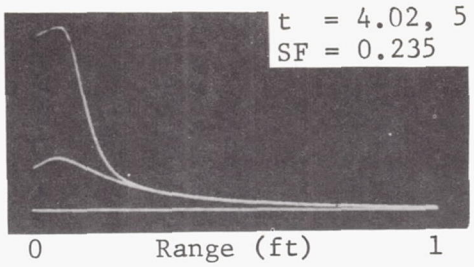
t = 4.02, 5
SF = 0.235
0
Range (ft)
1

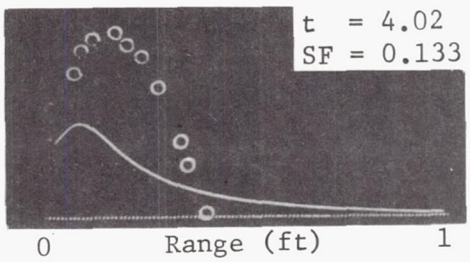
t = 4.02
SF = 0.133
0
Range (ft)
1

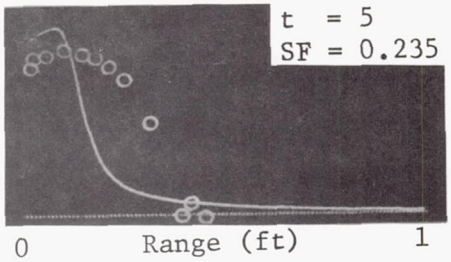
t = 5
SF = 0.235
0
Range (ft)
1

(a)
TEST 7

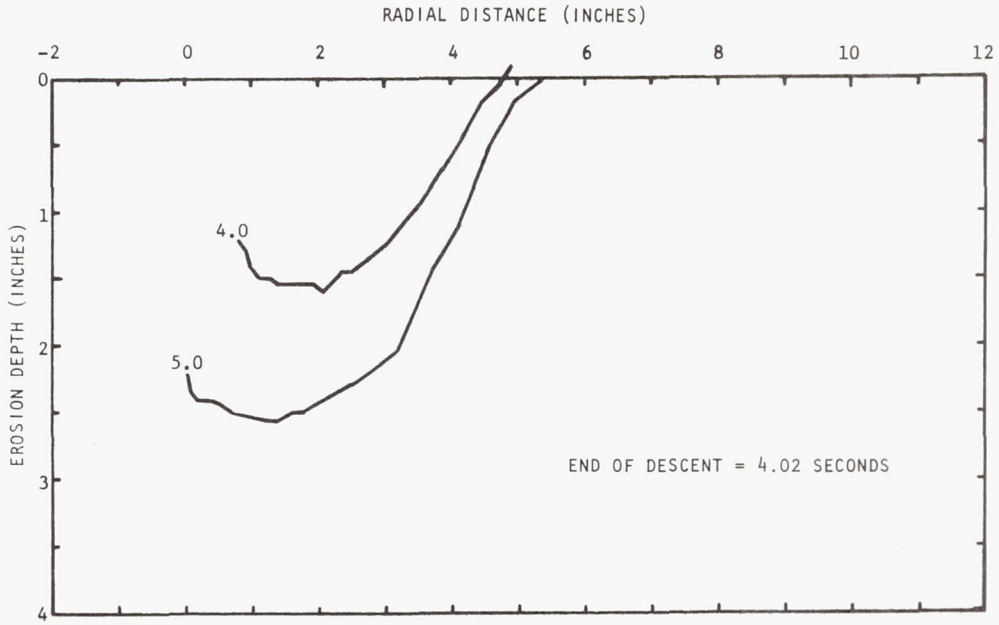

(b)
TEST 7

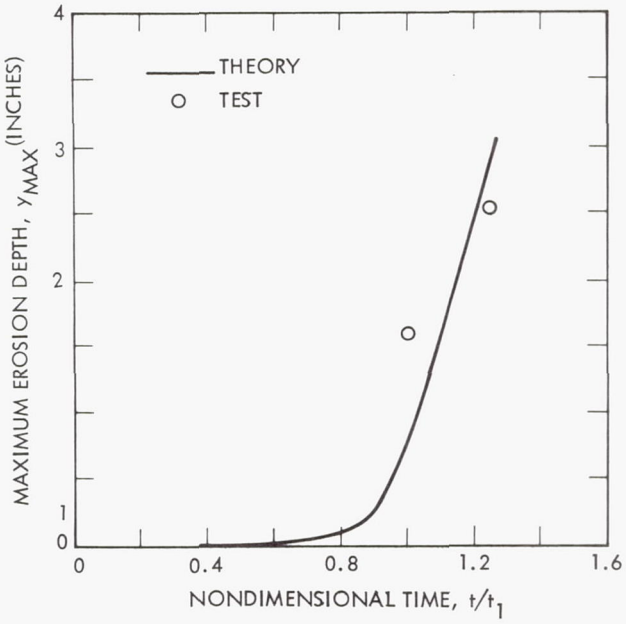

(c)
TEST 7

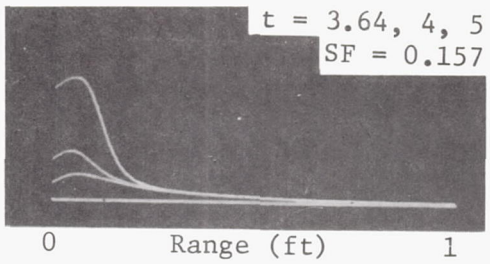
t = 3.64, 4, 5
SF = 0.157
0
Range (ft)
1

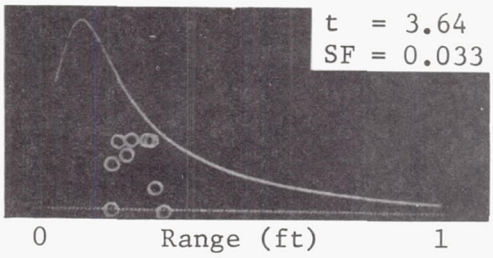
t = 3.64
SF = 0.033
0
Range (ft)
1

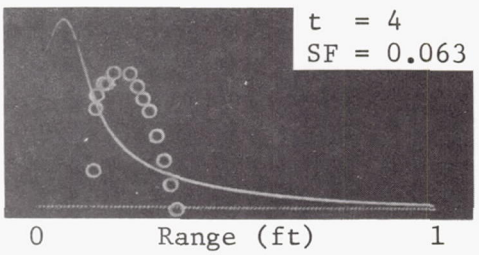
t = 4
SF = 0.063
0
Range (ft)
1

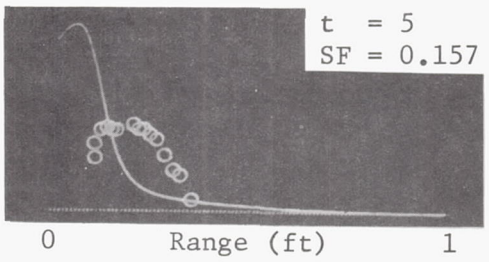
t = 5
SF = 0.157
0
Range (ft)
1

(a)
TEST 8

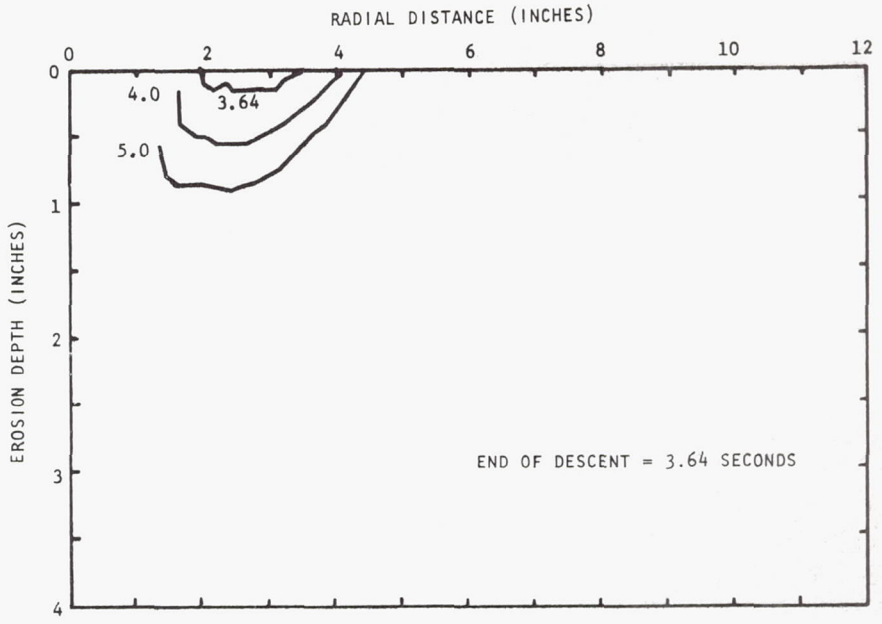

(b)
TEST 8

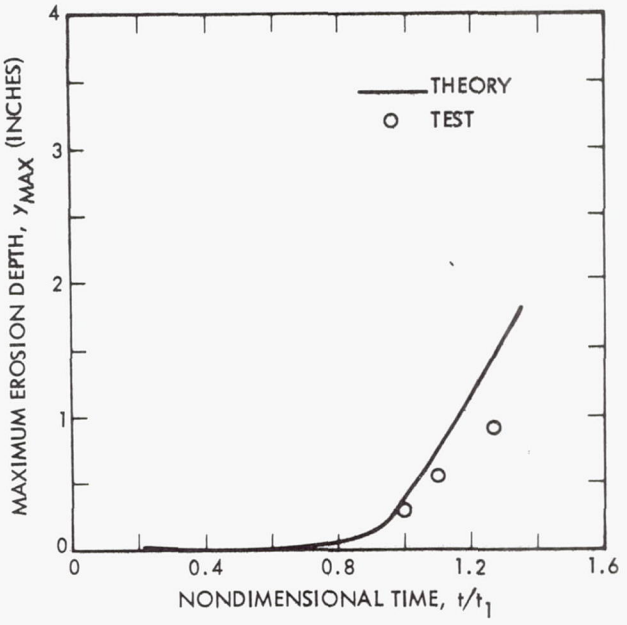

(c)
TEST 8

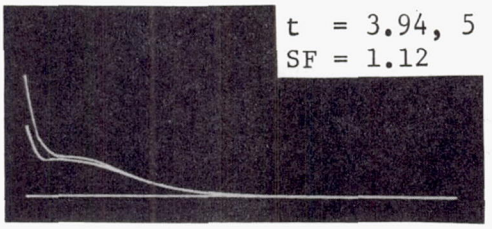
t = 3.94, 5
SF = 1.12
0
Range (ft)
1

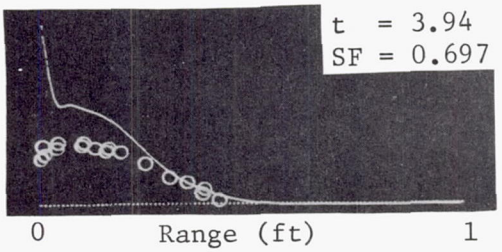
t = 3.94
SF = 0.697
0
Range (ft)
1

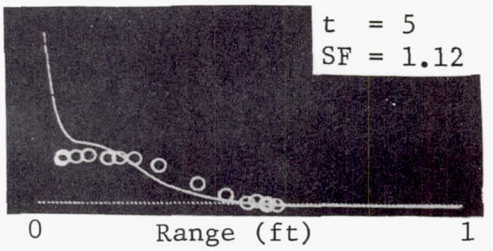
t = 5
SF = 1.12
0
Range (ft)
1

(a)
TEST 9

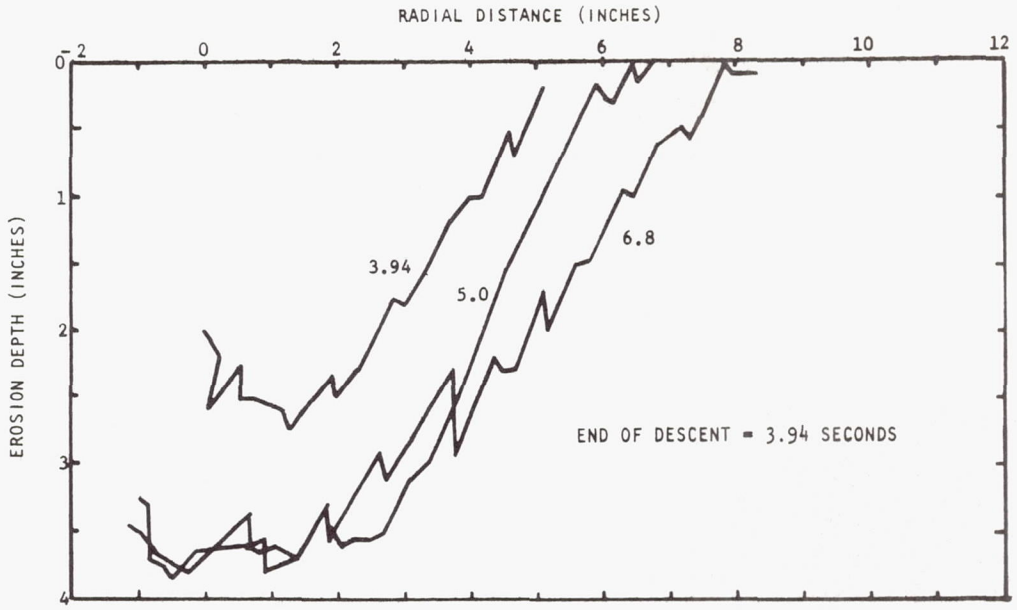

(b)
TEST 9

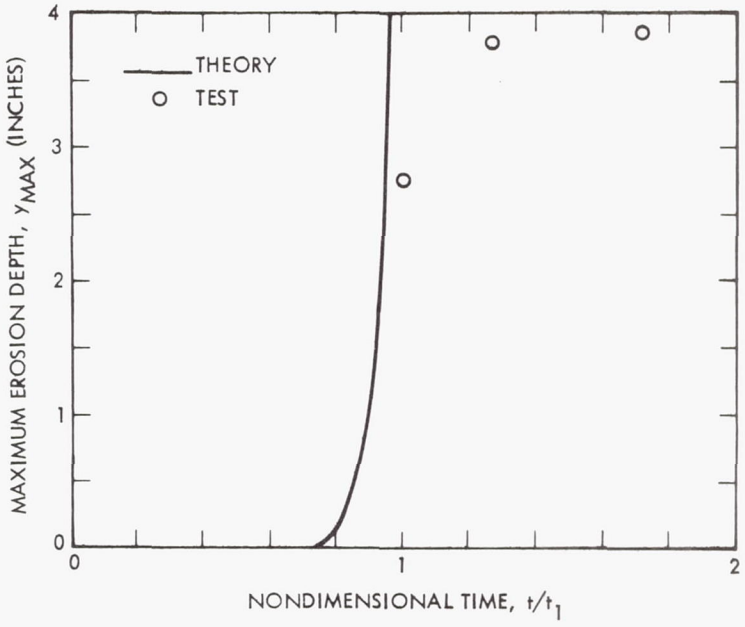

(c)
TEST 9

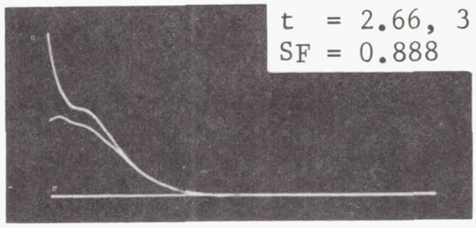
t = 2.66, 3
SF = 0.888
0
Range (ft)
1

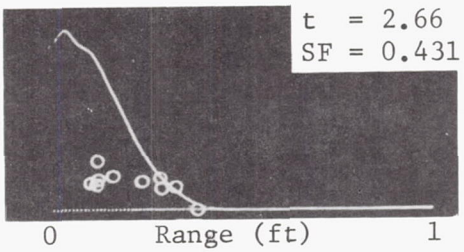
t = 2.66
SF = 0.431
0
Range (ft)
1

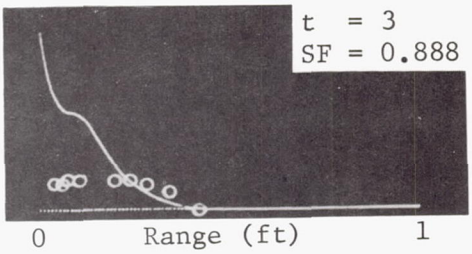
t = 3
SF = 0.888
0
Range (ft)
1

(a)
TEST 10

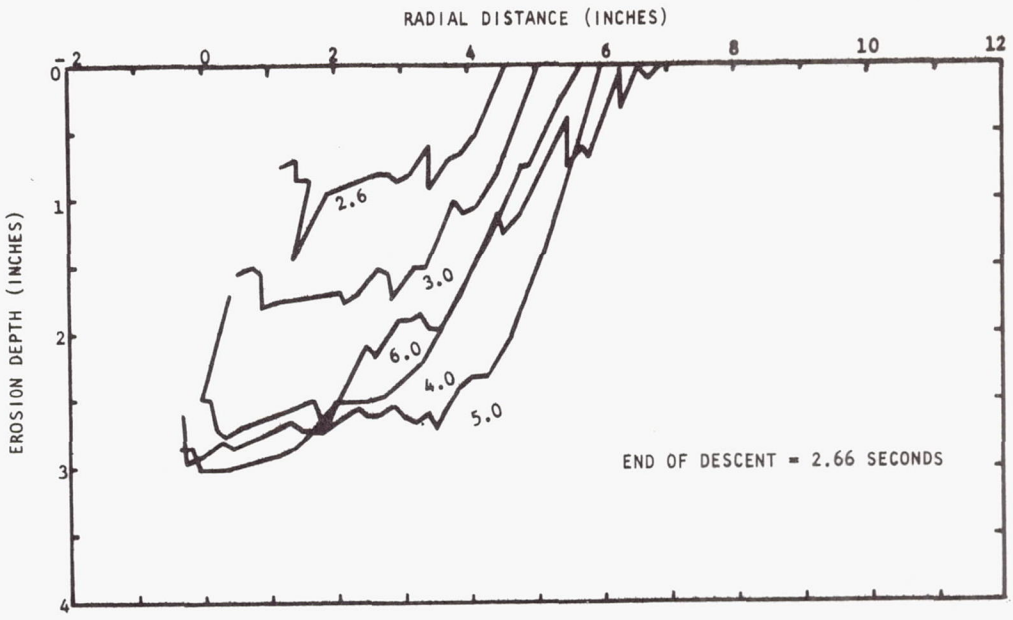

(b)
TEST 10

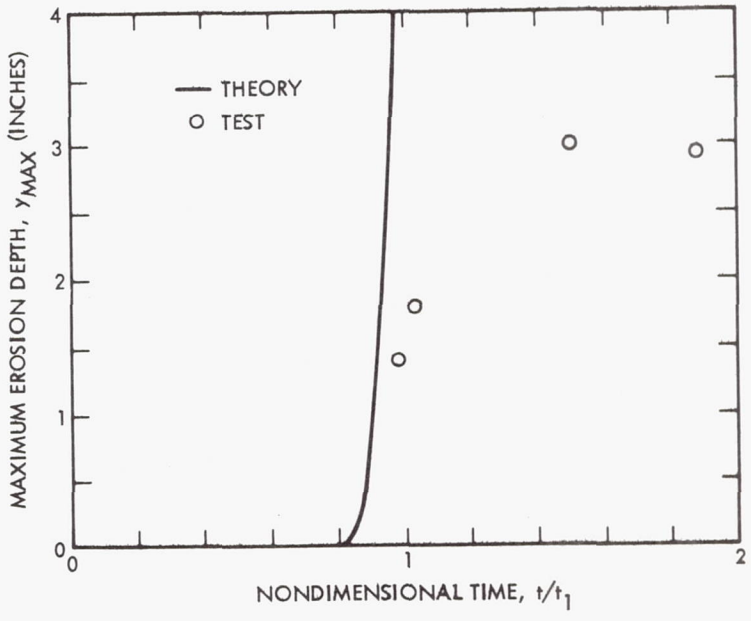

(c)
TEST 10

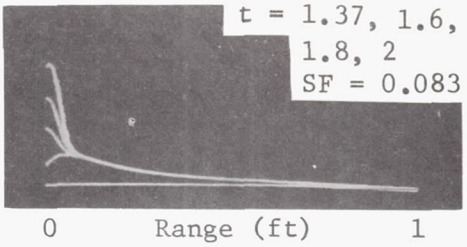
t = 1.37, 1.6,
1.8, 2
SF = 0.083
0
Range (ft)
1

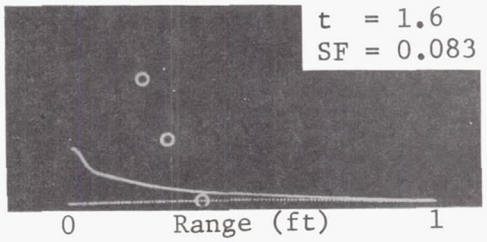
t = 1.6
SF = 0.083
0
Range (ft)
1

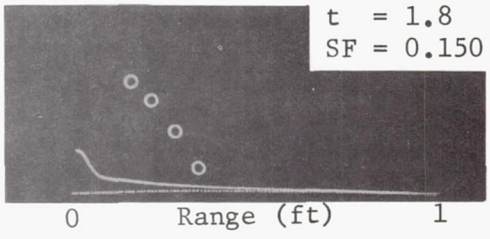
t = 1.8
SF = 0.150
0
Range (ft)
1

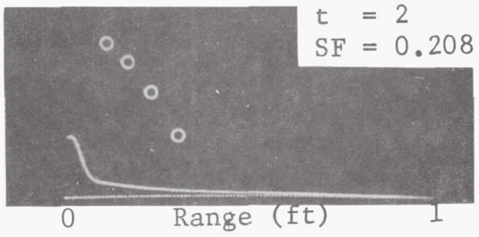
t = 2
SF = 0.208
0
Range (ft)
1

(a)
TEST 15

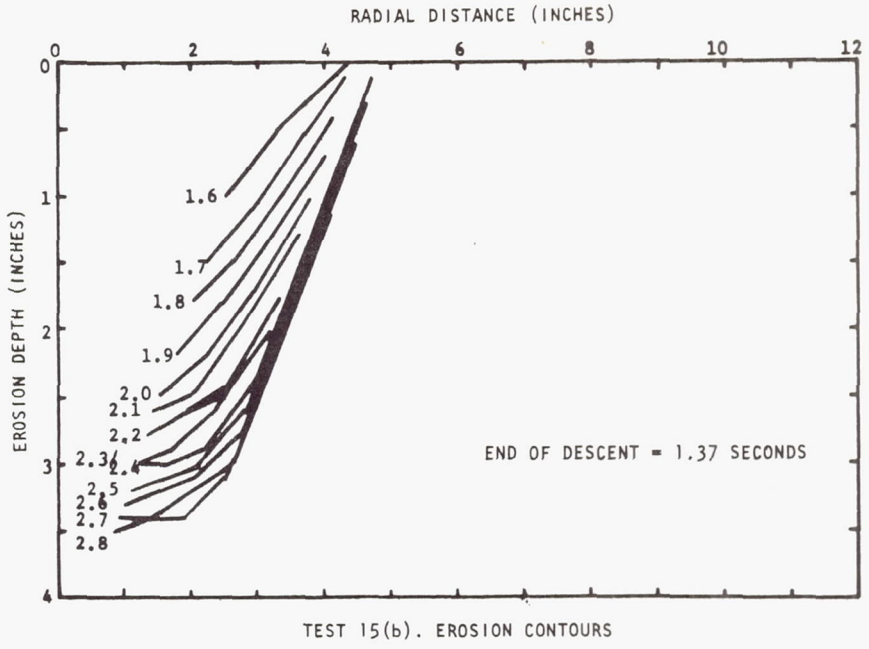

(b)
TEST 15

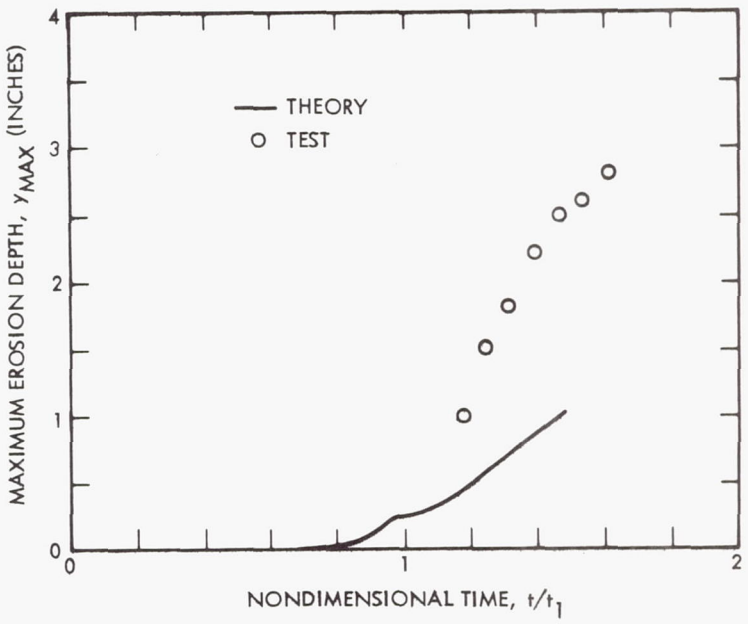

(c)
TEST 15

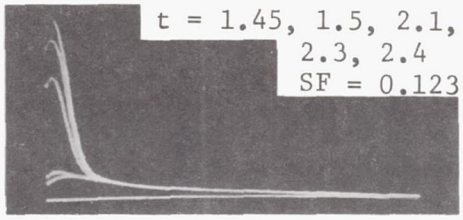
t = 1.45, 1.5, 2.1,
2.3, 2.4
SF = 0.123
0
Range (ft)
1

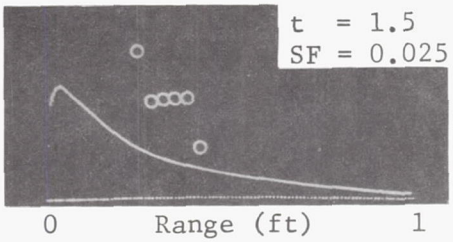
t = 1.5
SF = 0.025
0
Range (ft)
1

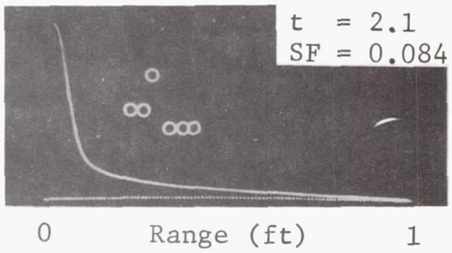
t = 2.1
SF = 0.084
0
Range (ft)
1

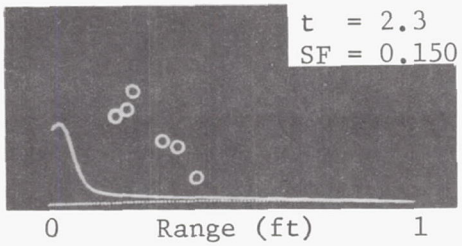
t = 2.3
SF = 0.150
0
Range (ft)
1

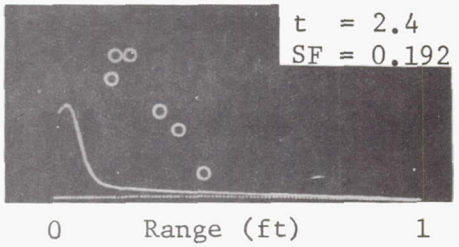
t = 2.4
SF = 0.192
0
Range (ft)
1

(a)
TEST 16

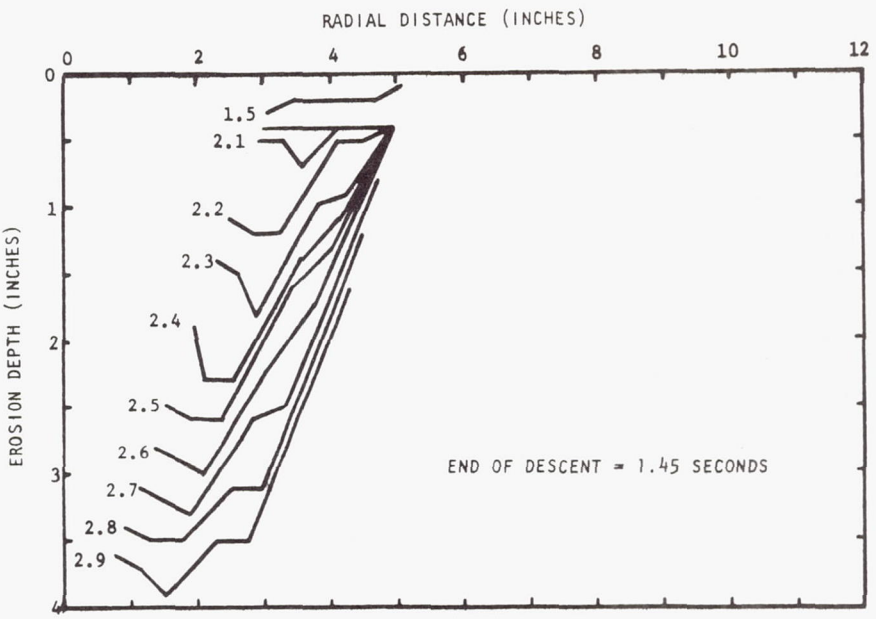

(b)
TEST 16

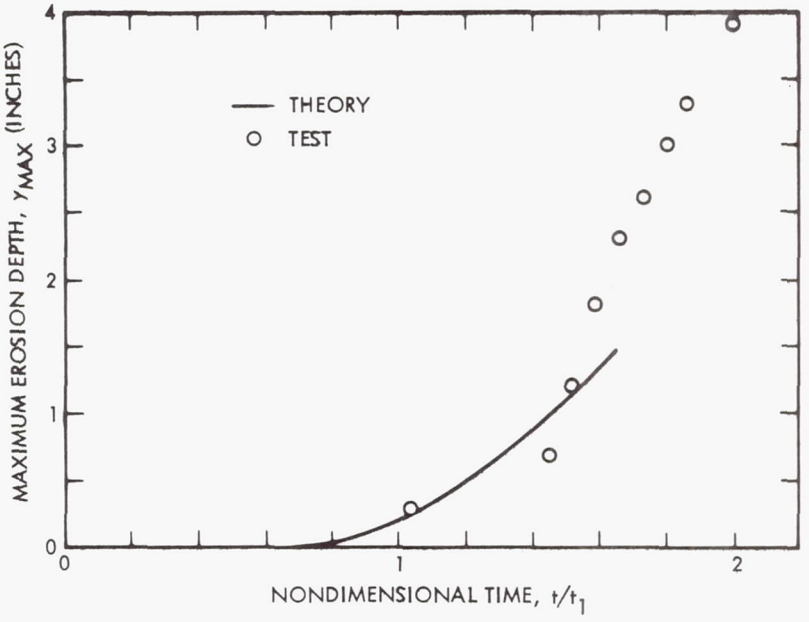

(c)
TEST 16

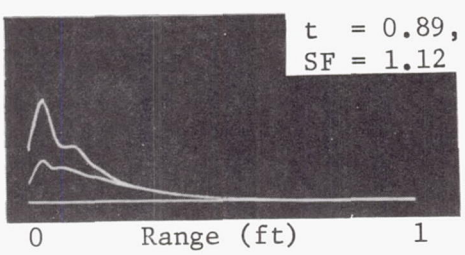

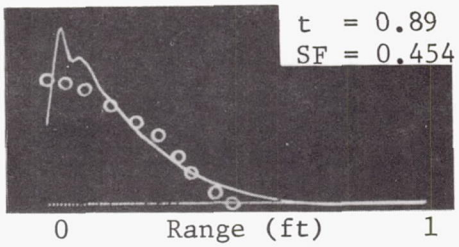

(a)
TEST 19

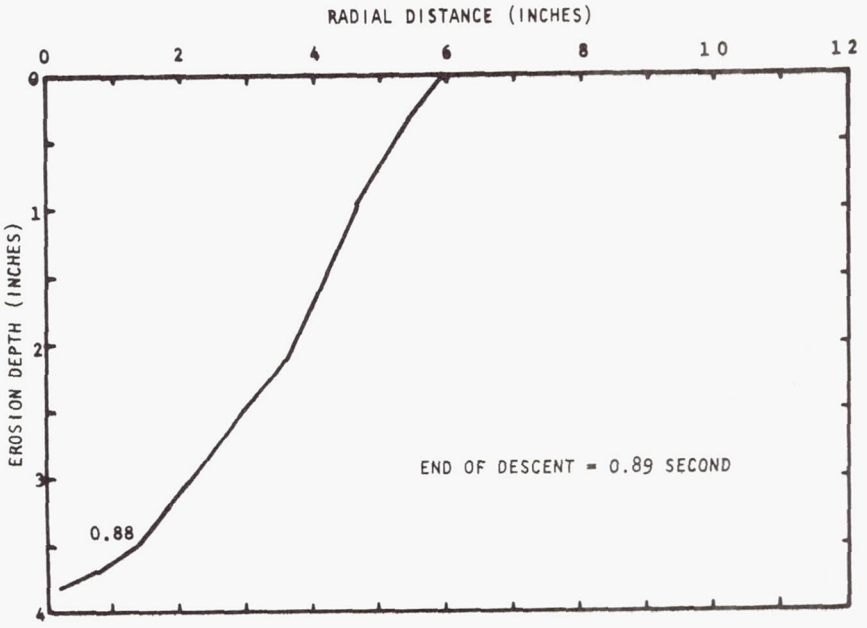

(b)
TEST 19

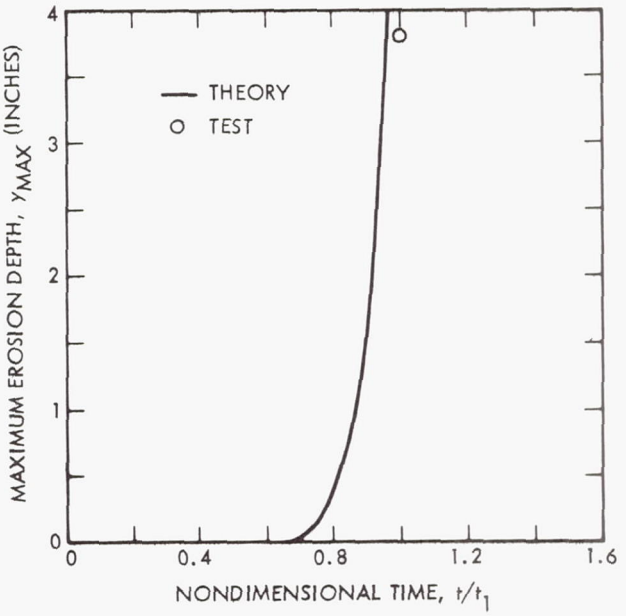

(c)
TEST 19

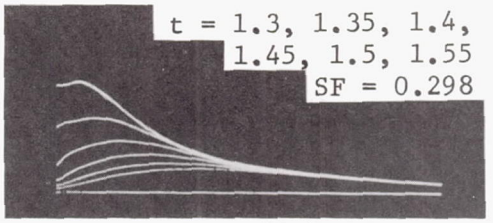

0 Range (ft) 1

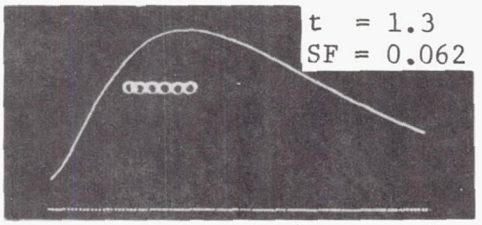

0 Range (ft) 1

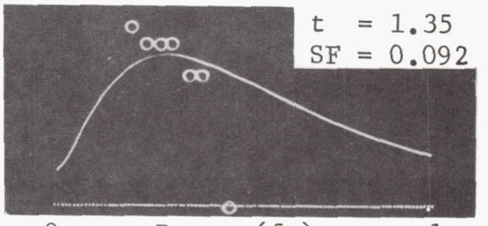

0 Range (ft) 1

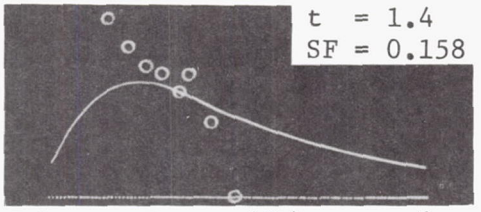

0 Range (ft) 1

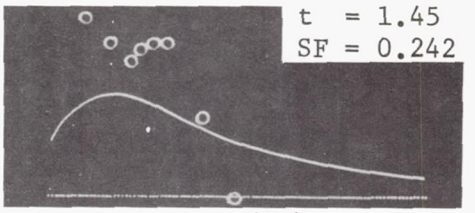

0 Range (ft) 1

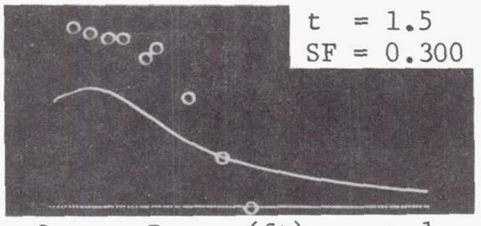

0 Range (ft) 1

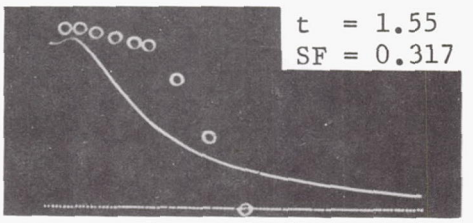

0 Range (ft) 1

(a)
TEST 24

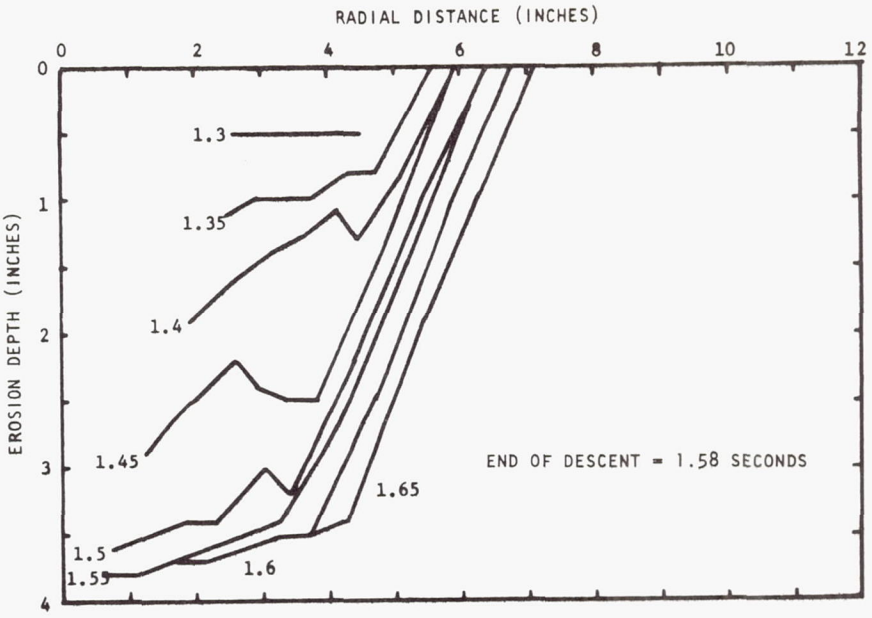

(b)
TEST 24

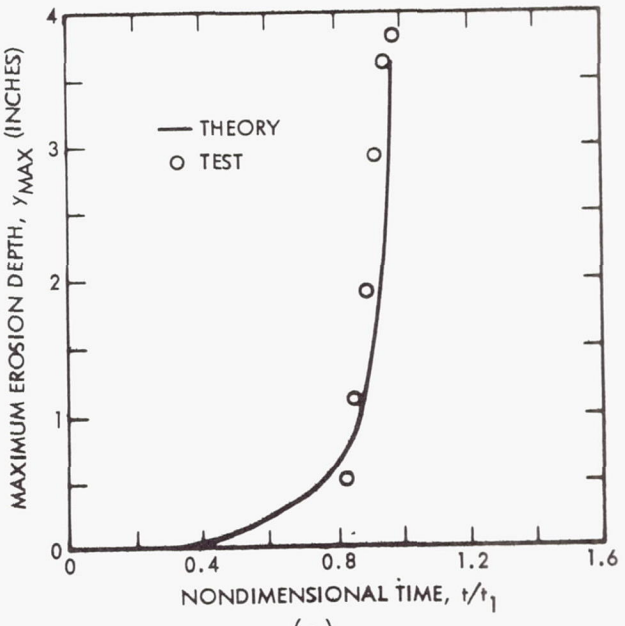

(c)
TEST 24

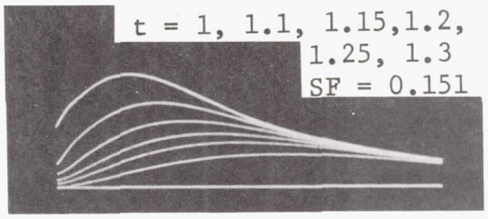

0 Range (ft) 1

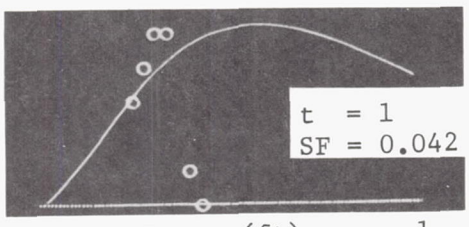

0 Range (ft) 1

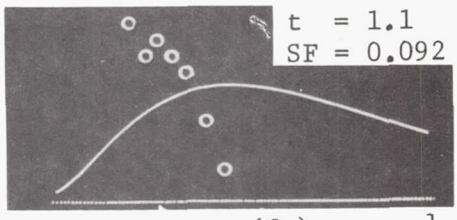

0 Range (ft) 1

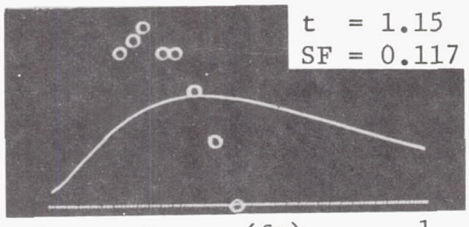

0 Range (ft) 1

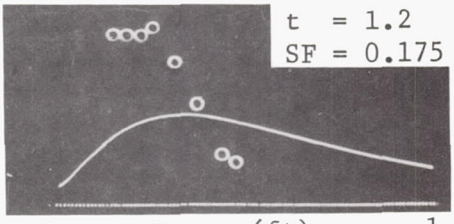

0 Range (ft) 1

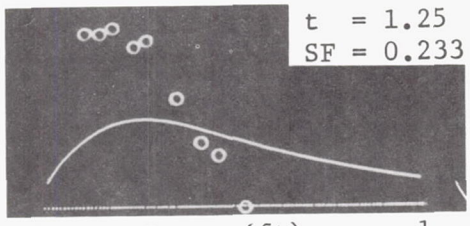

0 Range (ft) 1

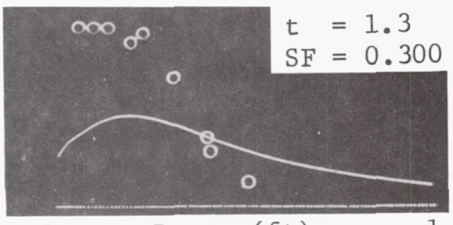

0 Range (ft) 1

(a)
TEST 25

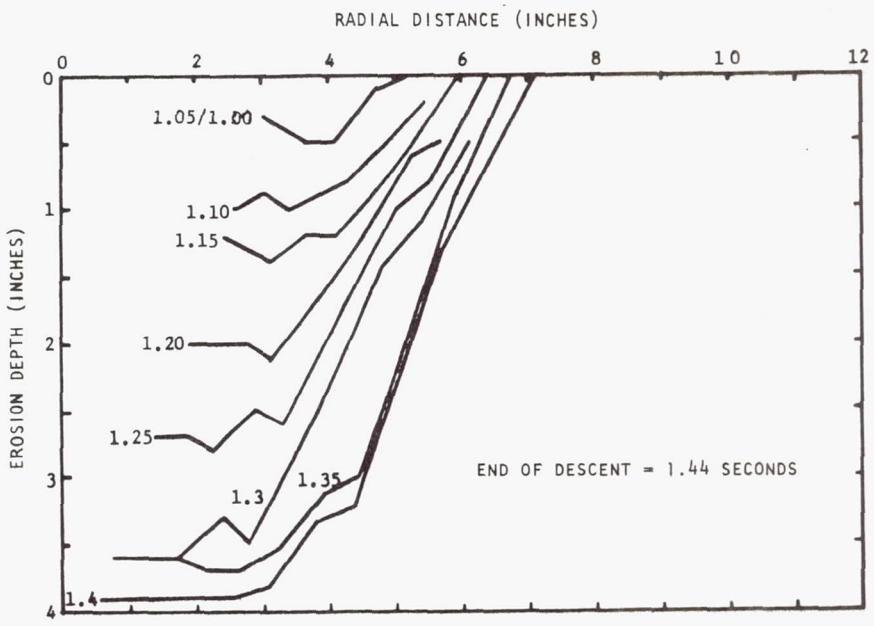

(b)
TEST 25

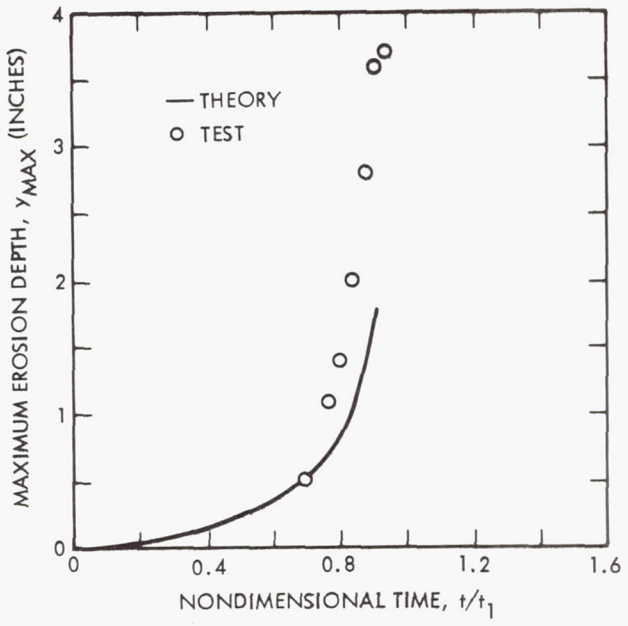

(c)
TEST 25

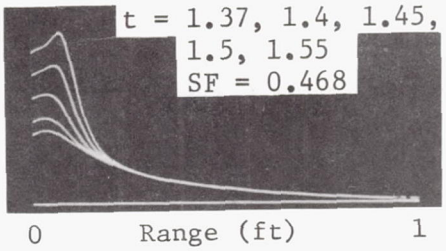
t = 1.37, 1.4, 1.45,
1.5, 1.55
SF = 0.468
0
Range (ft)
1

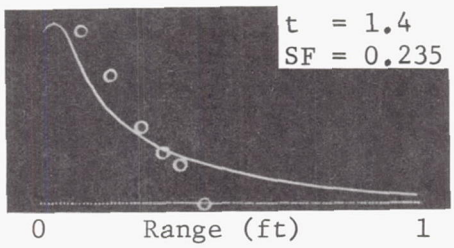
t = 1.4
SF = 0.235
0
Range (ft)
1

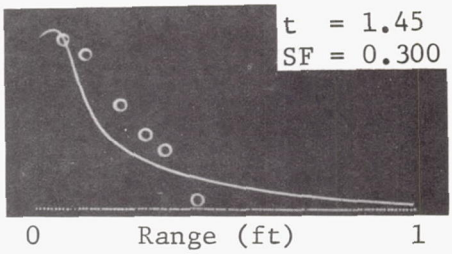
t = 1.45
SF = 0.300
0
Range (ft)
1

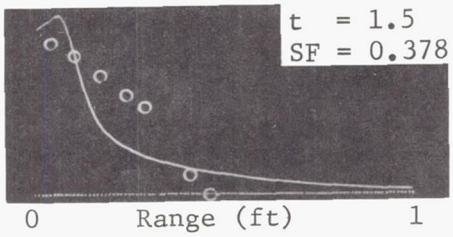
t = 1.5
SF = 0.378
0
Range (ft)
1

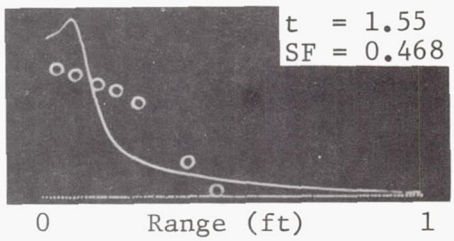
t = 1.55
SF = 0.468
0
Range (ft)
1

(a)
TEST 26

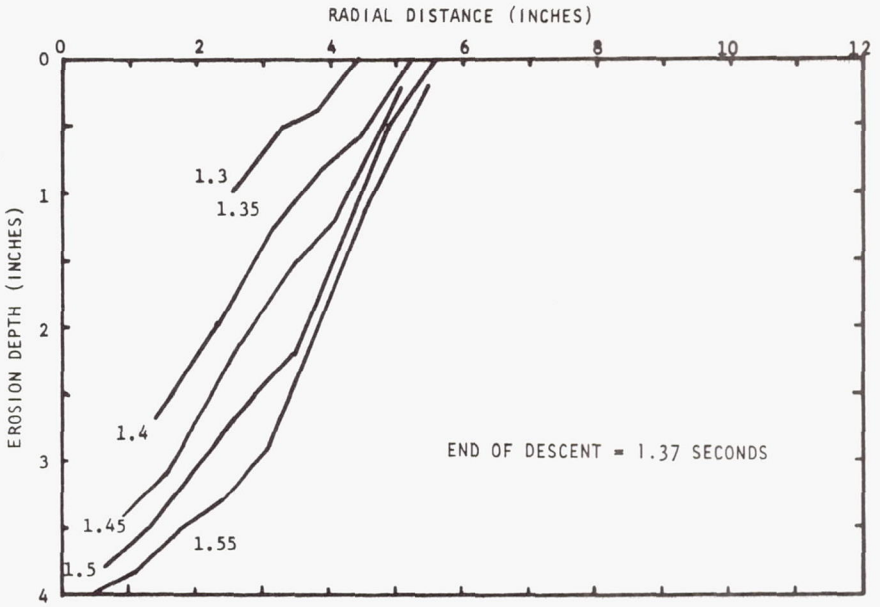

(b)
TEST 26

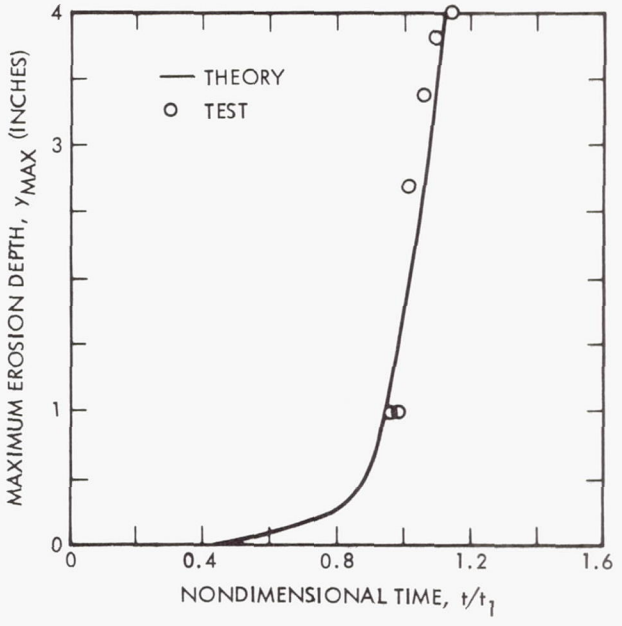

(c)
TEST 26

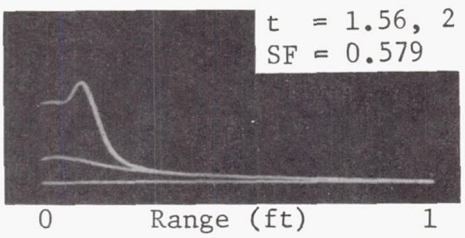

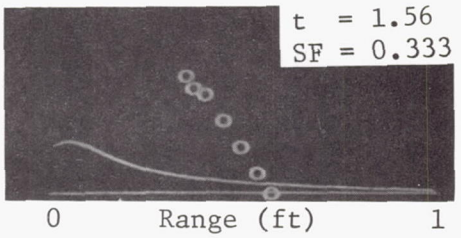

(a)
TEST 28

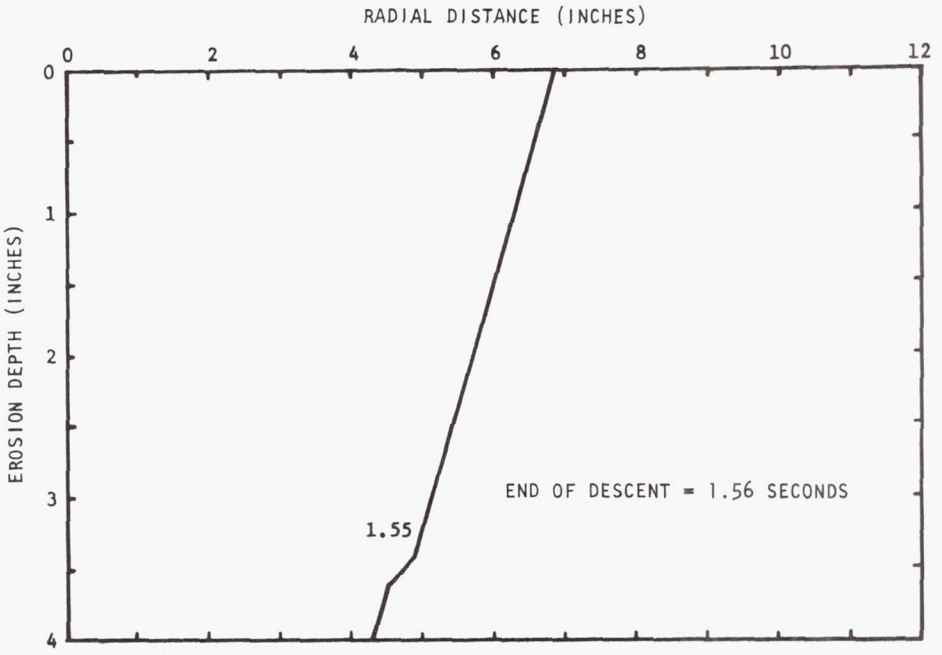

(b)
TEST 28

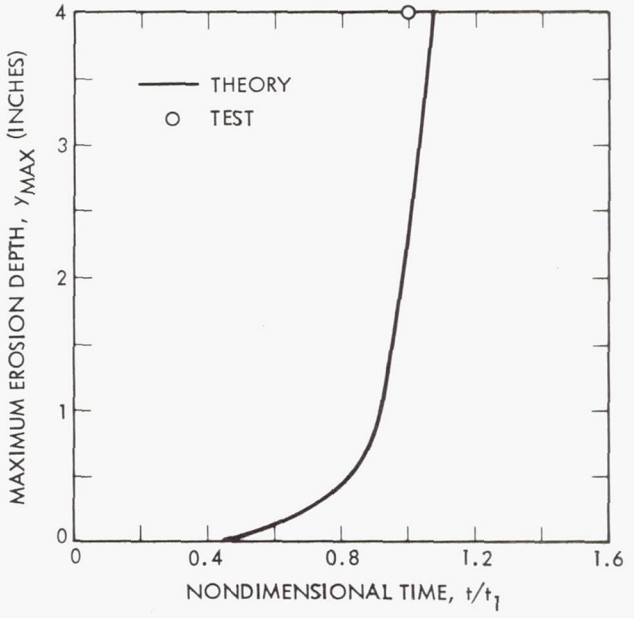

(c)
TEST 28

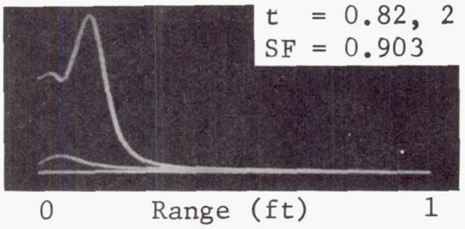

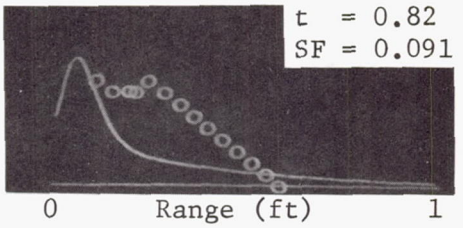

(a)
TEST 29

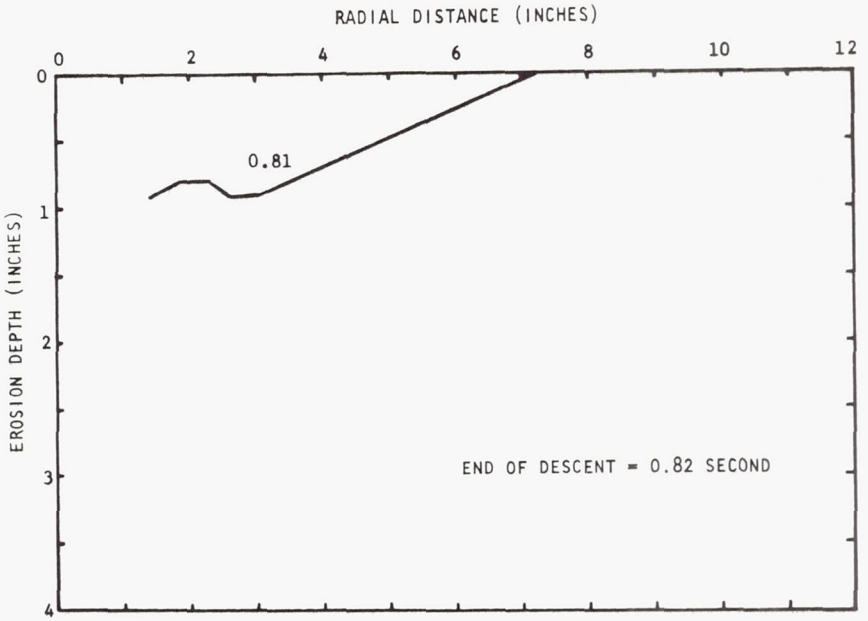

(b)
TEST 29

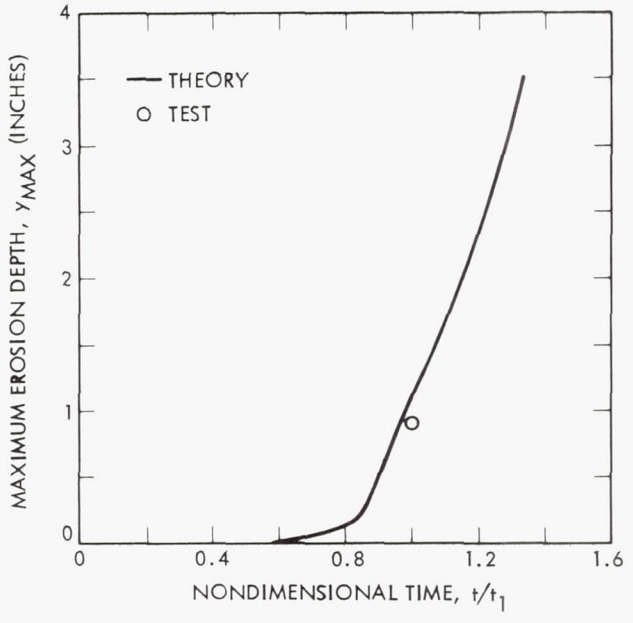

(c)
TEST 29

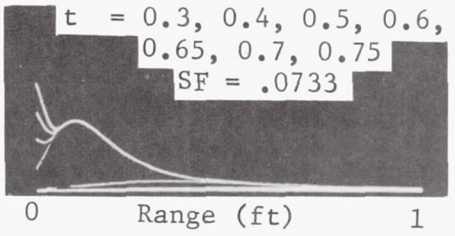
t = 0.3, 0.4, 0.5, 0.6,
0.65, 0.7, 0.75
SF = .0733
0
Range (ft)
1

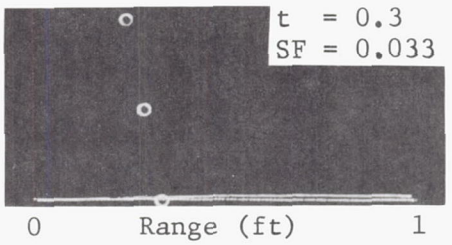
t = 0.3
SF = 0.033
0
Range (ft)
1

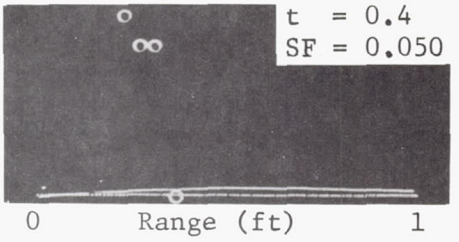
t = 0.4
SF = 0.050
0
Range (ft)
1

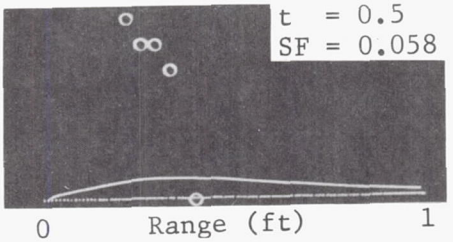
t = 0.5
SF = 0.058
0
Range (ft)
1

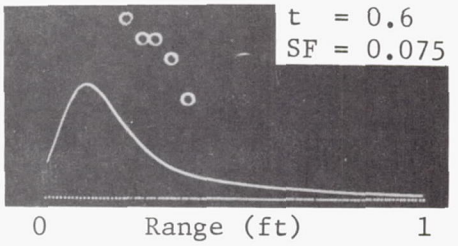
t = 0.6
SF = 0.075
0
Range (ft)
1

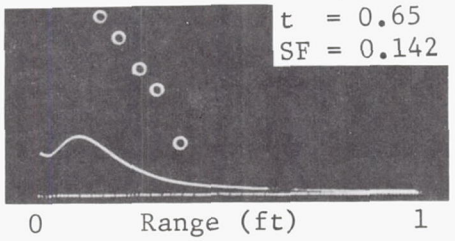
t = 0.65
SF = 0.142
0
Range (ft)
1

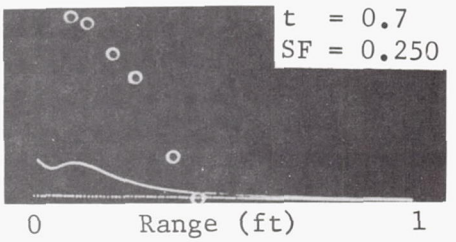
t = 0.7
SF = 0.250
0
Range (ft)
1

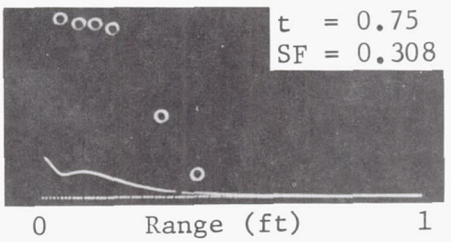
t = 0.75
SF = 0.308
0
Range (ft)
1

(a)
TEST 31

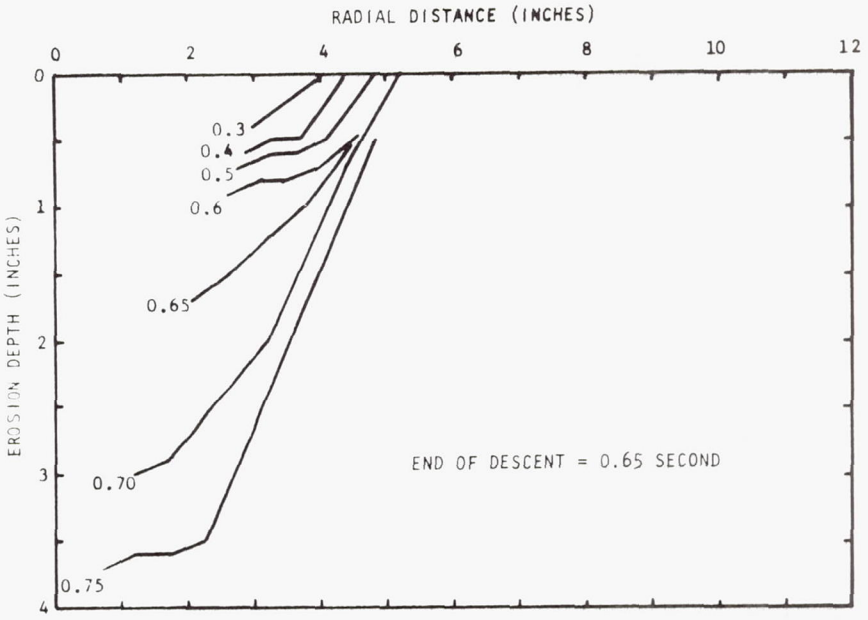

(b)
TEST 31

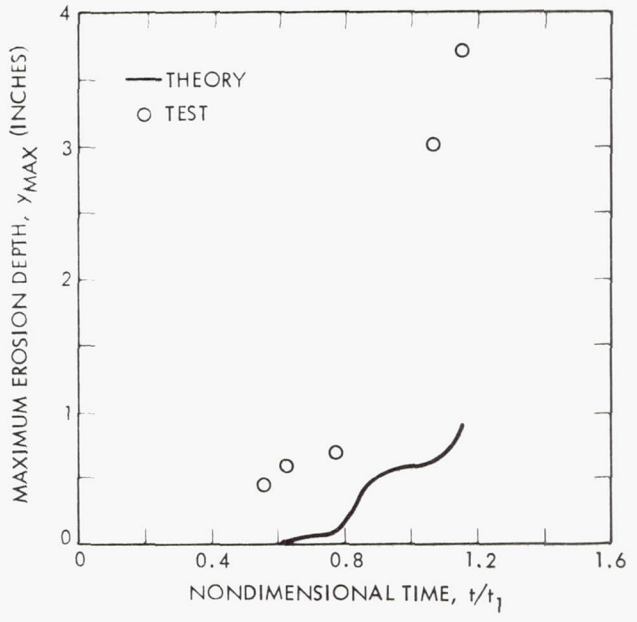

(c)
TEST 31

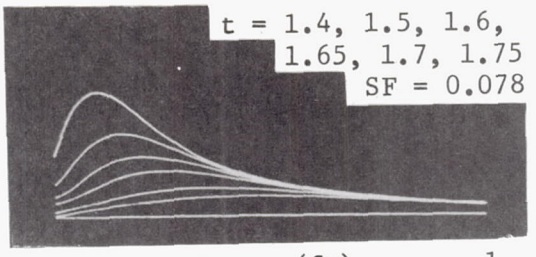
t = 1.4, 1.5, 1.6,
1.65, 1.7, 1.75
SF = 0.078
0
Range (ft)
1

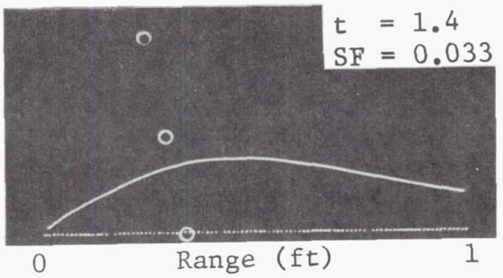
t = 1.4
SF = 0.033
0
Range (ft)
1

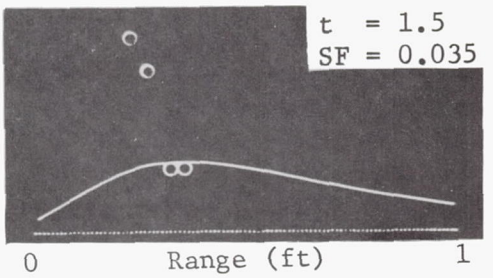
t = 1.5
SF = 0.035
0
Range (ft)
1

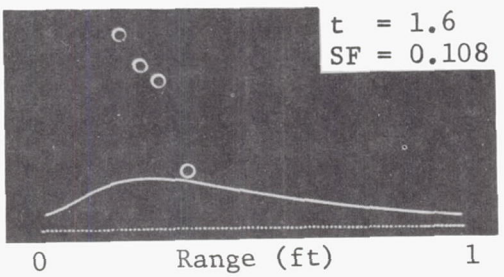
t = 1.6
SF = 0.108
0
Range (ft)
1

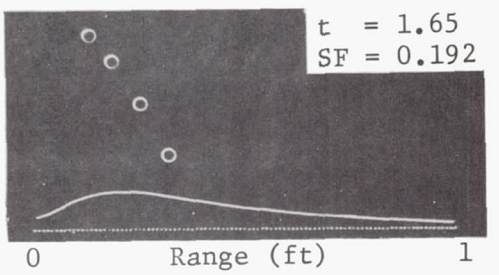
t = 1.65
SF = 0.192
0
Range (ft)
1

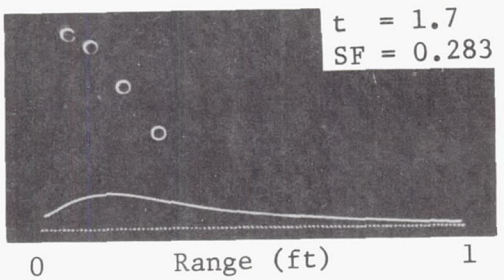
t = 1.7
SF = 0.283
0
Range (ft)
1

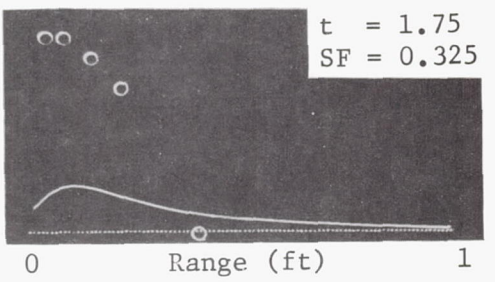
t = 1.75
SF = 0.325
0
Range (ft)
1

(a)
TEST 32

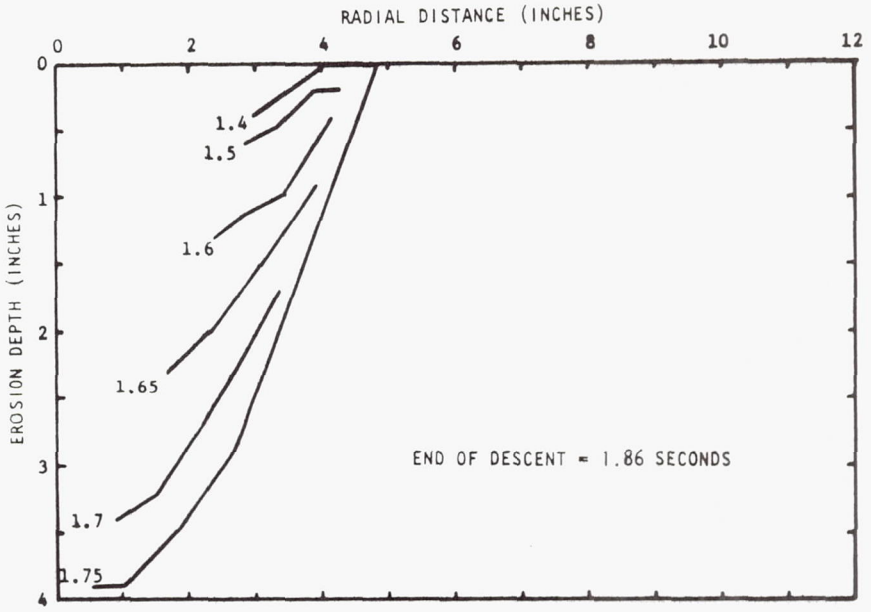

(b)
TEST 32

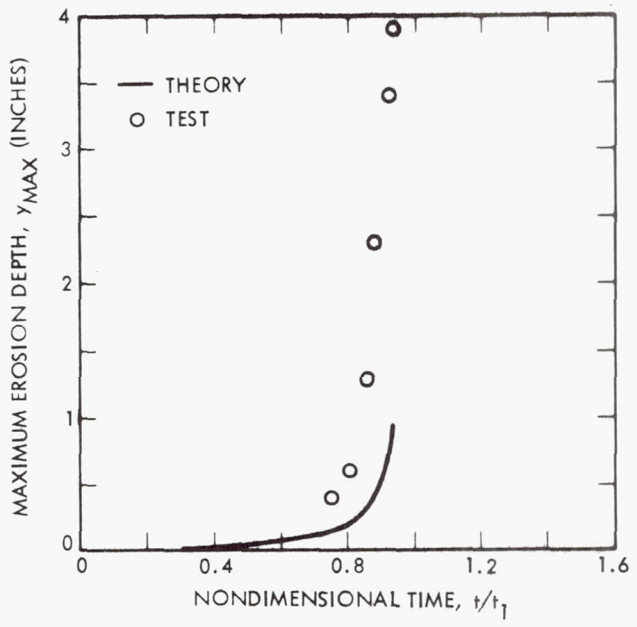

(c)
TEST 32

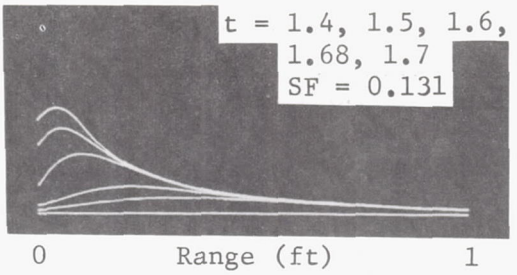
t = 1.4, 1.5, 1.6,
1.68, 1.7
SF = 0.131
0
Range (ft)
1

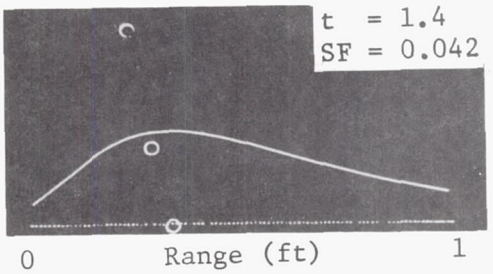
t = 1.4
SF = 0.042
0
Range (ft)
1

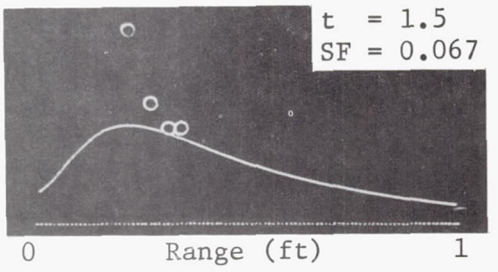
t = 1.5
SF = 0.067
0
Range (ft)
1

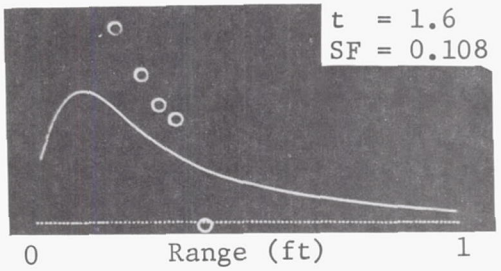
t = 1.6
SF = 0.108
0
Range (ft)
1

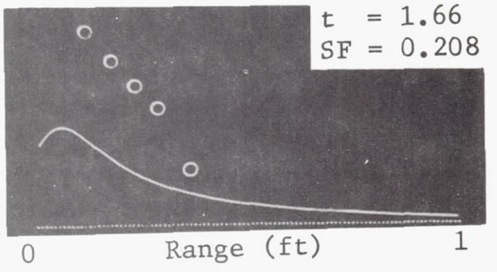
t = 1.66
SF = 0.208
0
Range (ft)
1

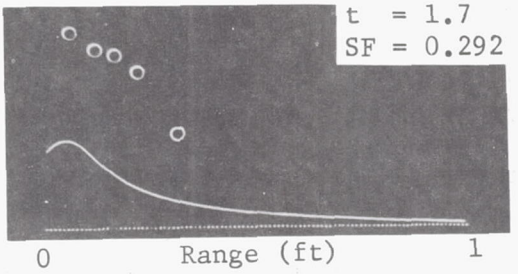
t = 1.7
SF = 0.292
0
Range (ft)
1

(a)

TEST 35

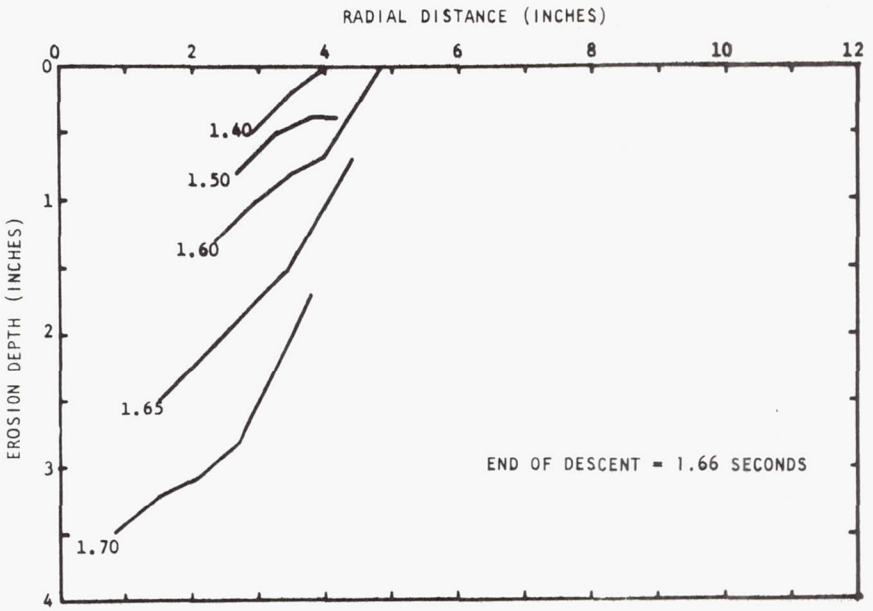

(b)
TEST 35

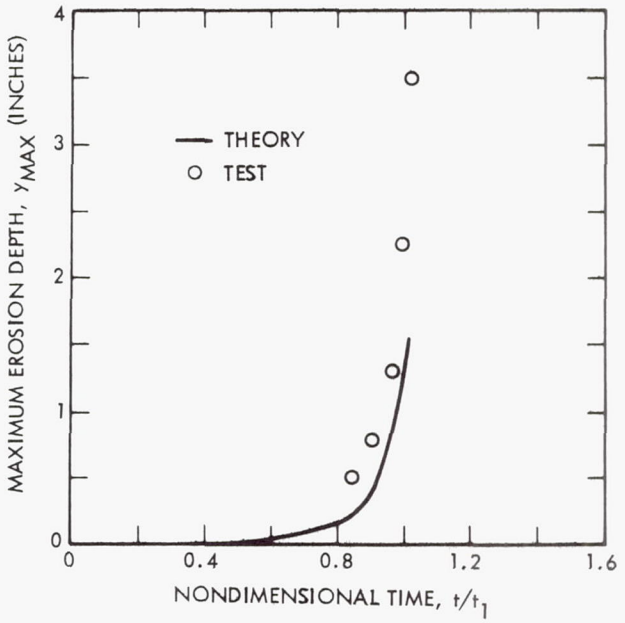

(c)
TEST 35

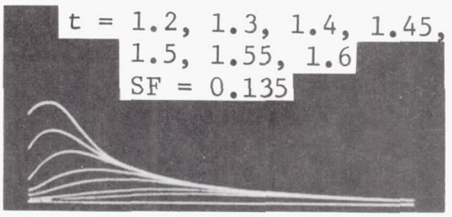

0 Range (ft) 1

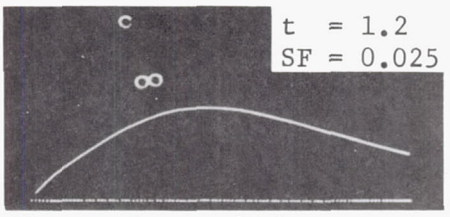

0 Range (ft) 1

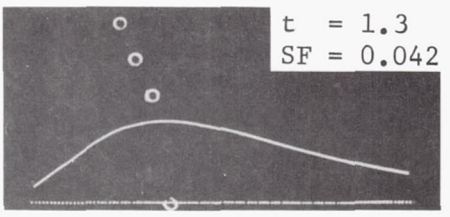

0 Range (ft) 1

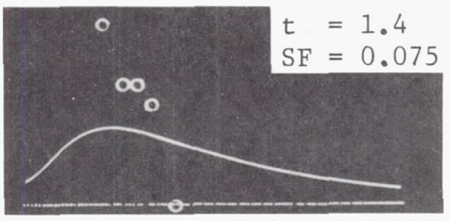

0 Range (ft) 1

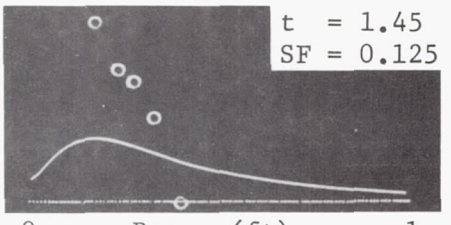

0 Range (ft) 1

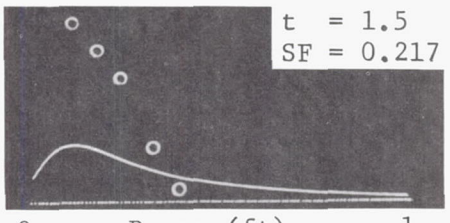

0 Range (ft) 1

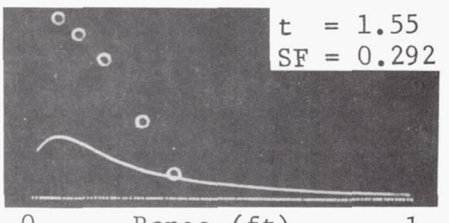

0 Range (ft) 1

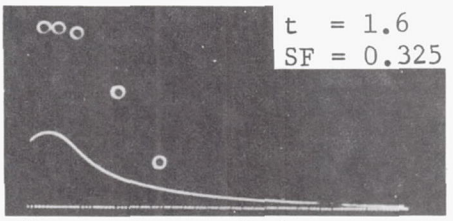

0 Range (ft) 1

(a)
TEST 37

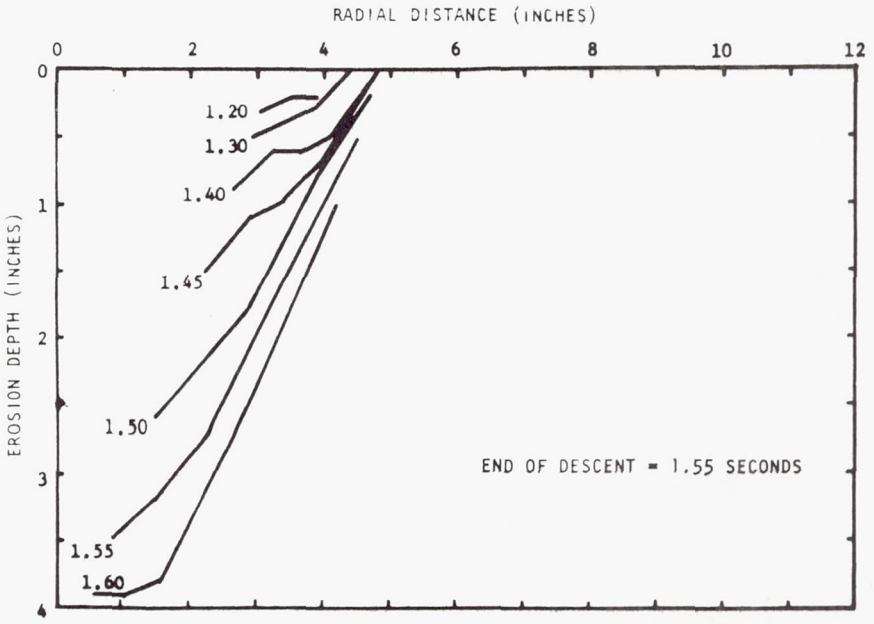

(b)
TEST 37

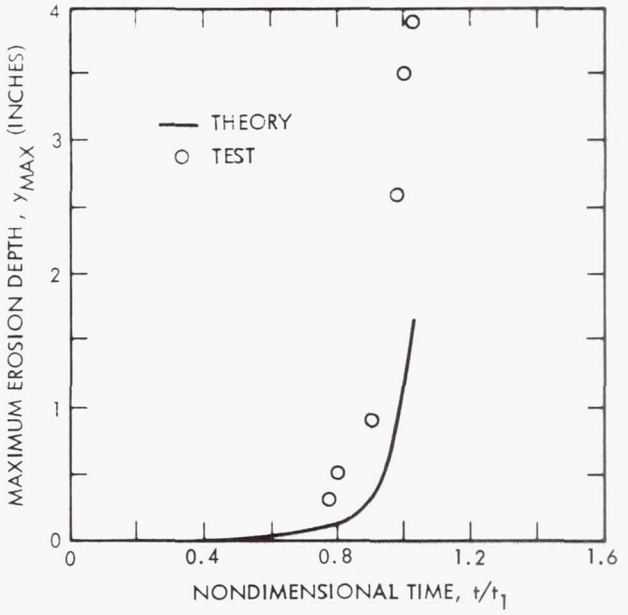

(c)
TEST 37

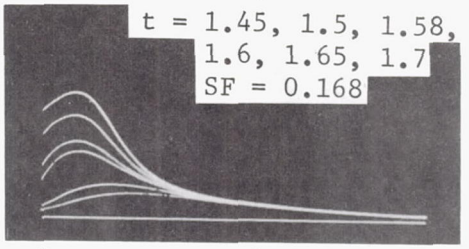
t = 1.45, 1.5, 1.58,
1.6, 1.65, 1.7
SF = 0.168
0
Range (ft)
1

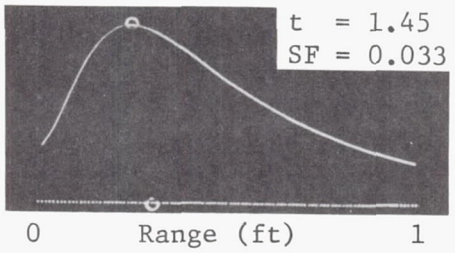
t = 1.45
SF = 0.033
0
Range (ft)
1

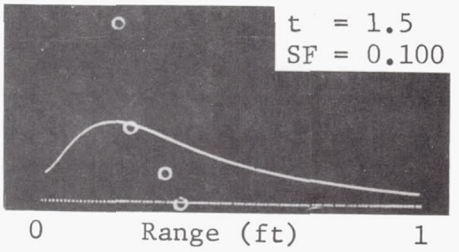
t = 1.5
SF = 0.100
0
Range (ft)
1

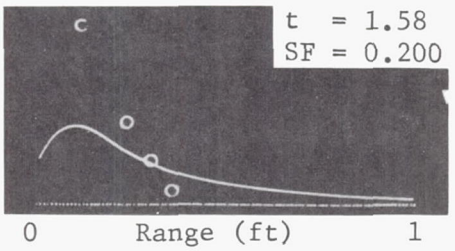
t = 1.58
SF = 0.200
0
Range (ft)
1

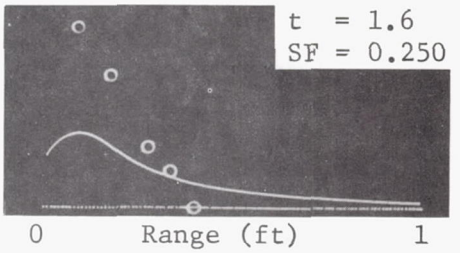
t = 1.6
SF = 0.250
0
Range (ft)
1

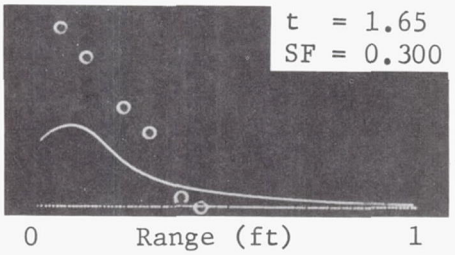
t = 1.65
SF = 0.300
0
Range (ft)
1

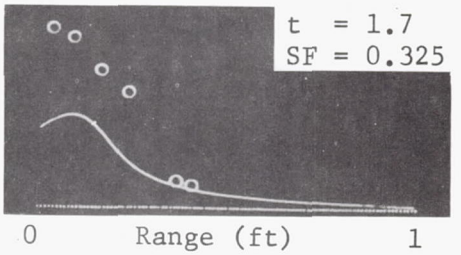
t = 1.7
SF = 0.325
0
Range (ft)
1

(a)
TEST 38

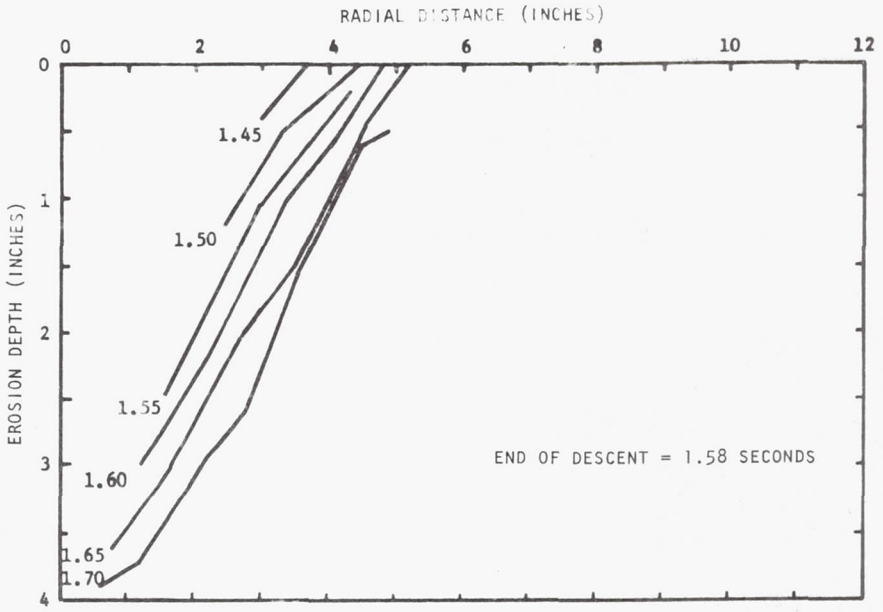

(b)
TEST 38

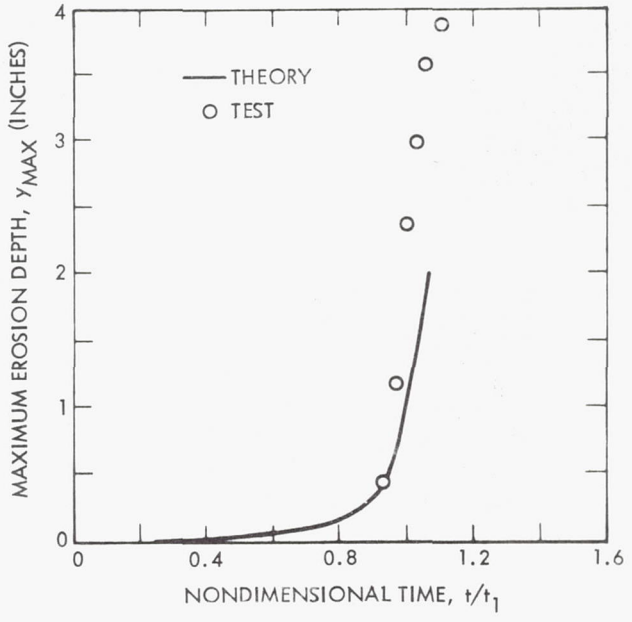

(c)
TEST 38

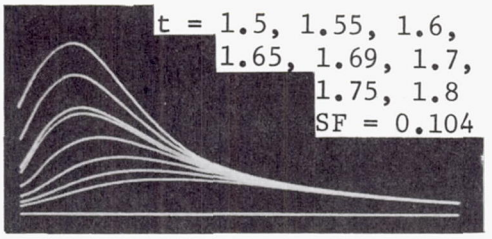

0 Range (ft) 1

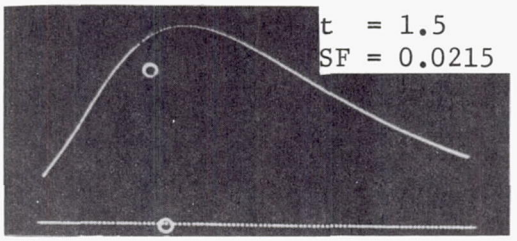

0 Range (ft) 1

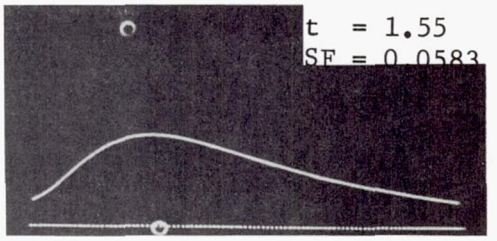

0 Range (ft) 1

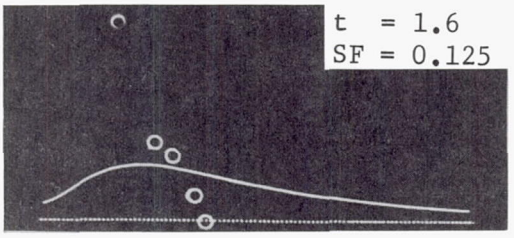

0 Range (ft) 1

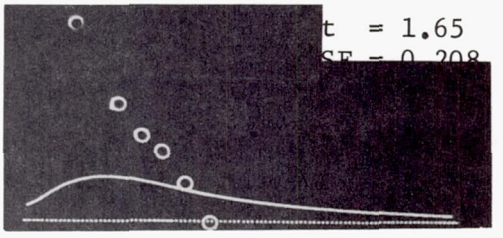

0 Range (ft) 1

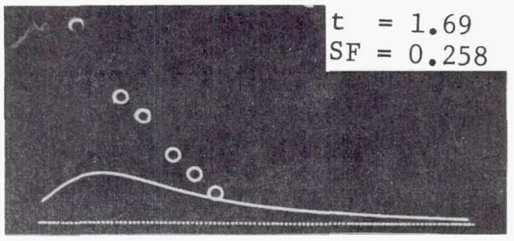

0 Range (ft) 1

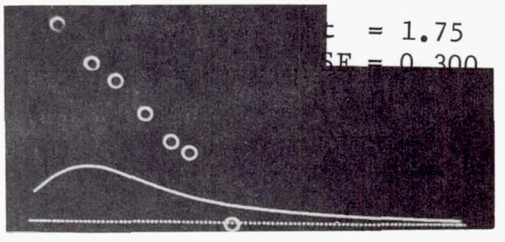

0 Range (ft) 1

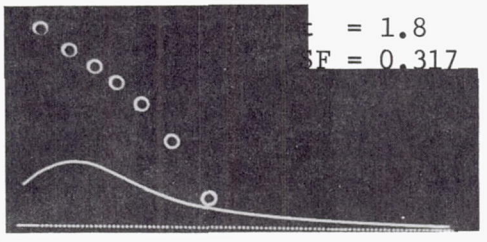

0 Range (ft) 1

(a)
TEST 39

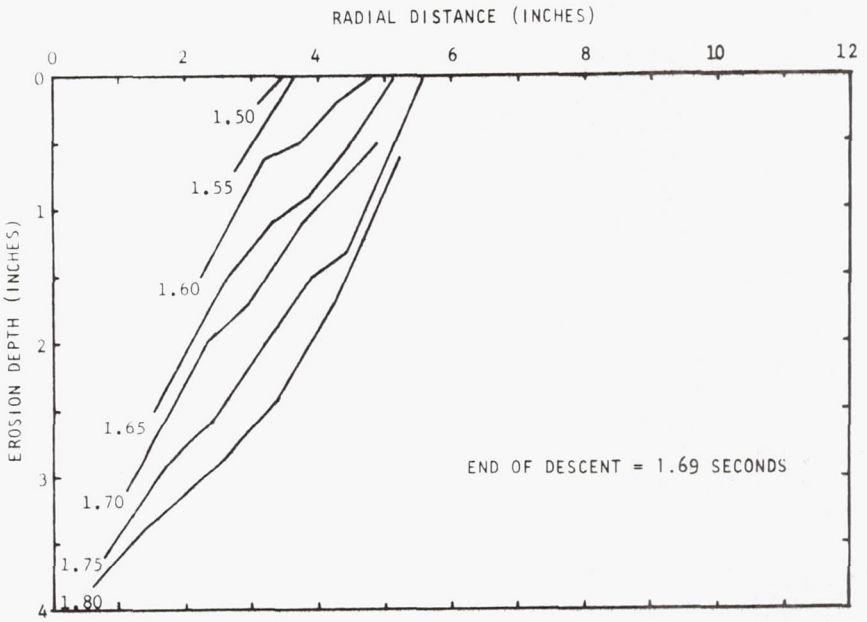

(b)
TEST 39

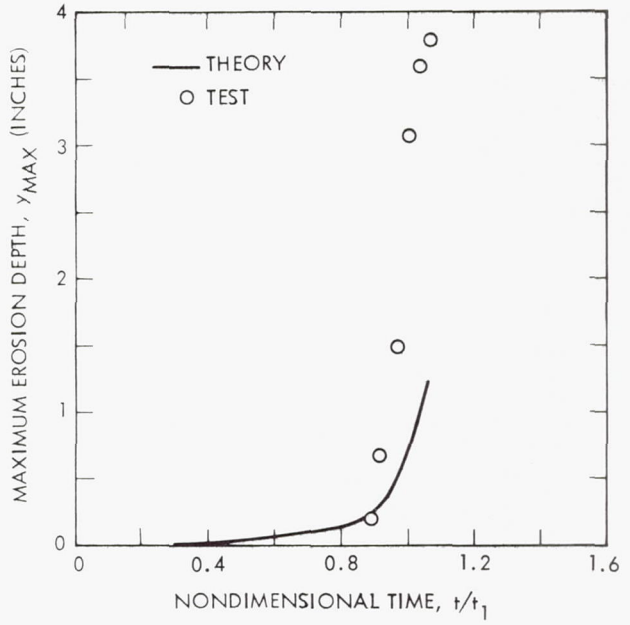

(c)
TEST 39

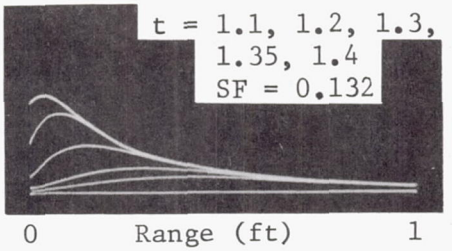
t = 1.1, 1.2, 1.3,
1.35, 1.4
SF = 0.132
0
Range (ft)
1

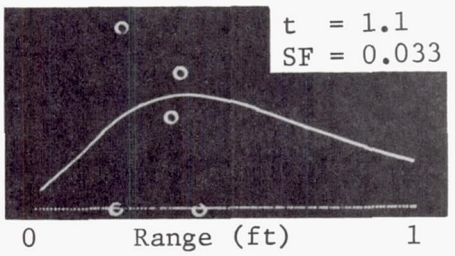
t = 1.1
SF = 0.033
0
Range (ft)
1

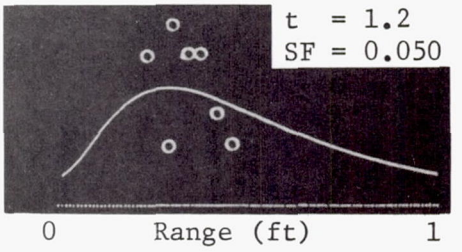
t = 1.2
SF = 0.050
0
Range (ft)
1

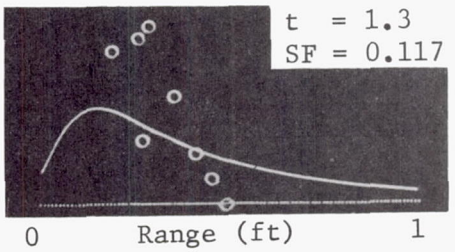
t = 1.3
SF = 0.117
0
Range (ft)
1

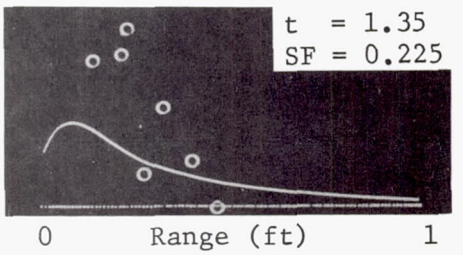
t = 1.35
SF = 0.225
0
Range (ft)
1

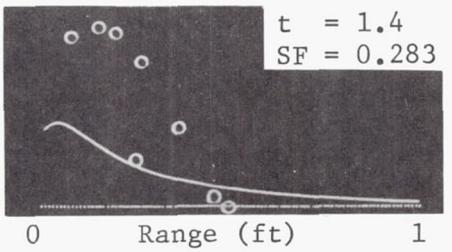
t = 1.4
SF = 0.283
0
Range (ft)
1

(a)
TEST 46

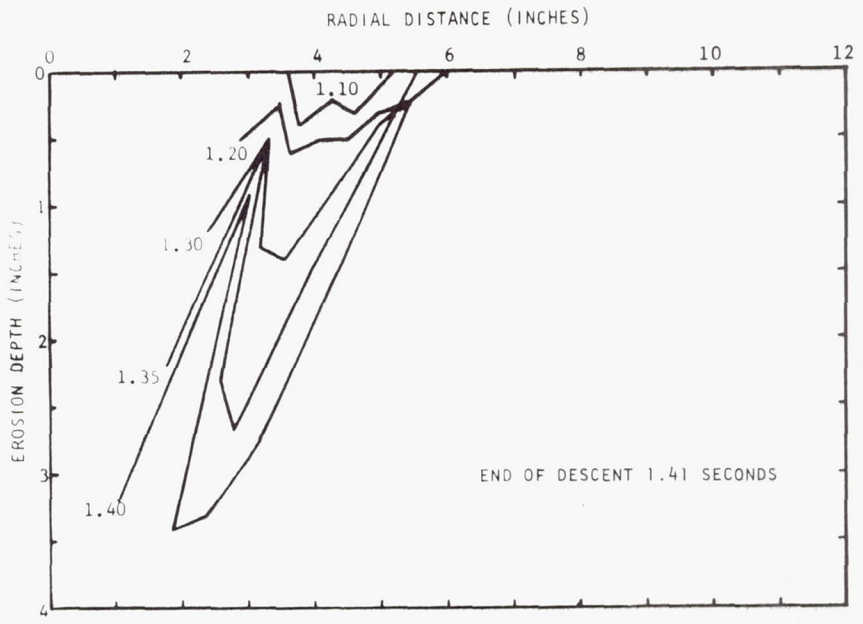

(b)
TEST 46

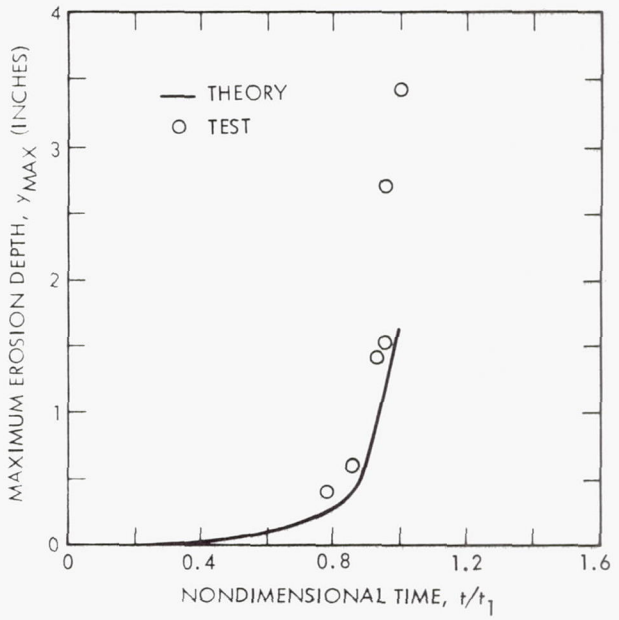

(c)
TEST 46

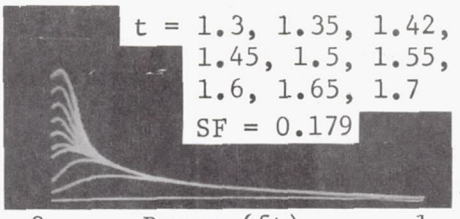
t = 1.3, 1.35, 1.42,
1.45, 1.5, 1.55,
1.6, 1.65, 1.7
SF = 0.179
0
Range (ft)
1

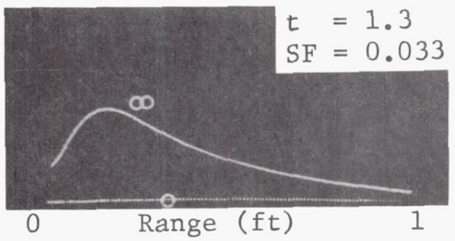
t = 1.3
SF = 0.033
0
Range (ft)
1

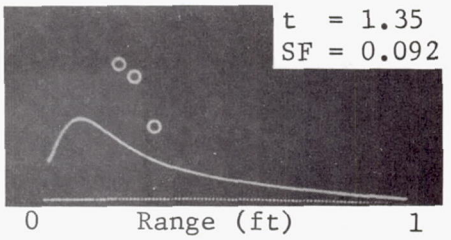
t = 1.35
SF = 0.092
0
Range (ft)
1

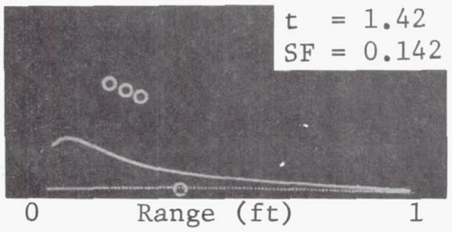
t = 1.42
SF = 0.142
0
Range (ft)
1

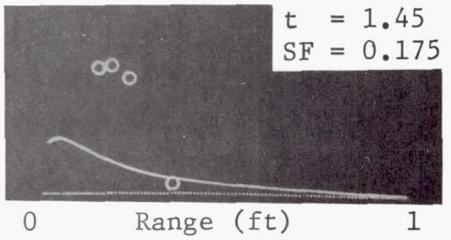
t = 1.45
SF = 0.175
0
Range (ft)
1

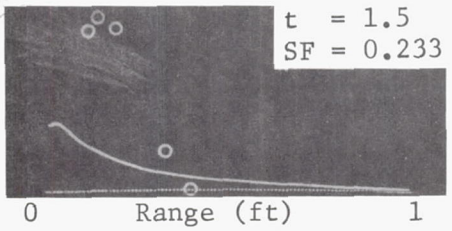
t = 1.5
SF = 0.233
0
Range (ft)
1

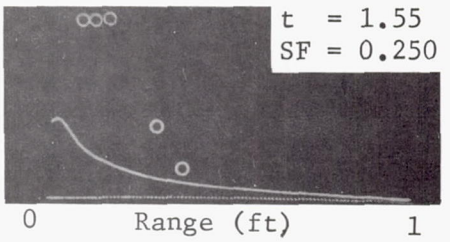
t = 1.55
SF = 0.250
0
Range (ft)
1

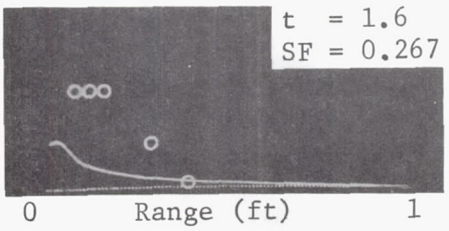
t = 1.6
SF = 0.267
0
Range (ft)
1

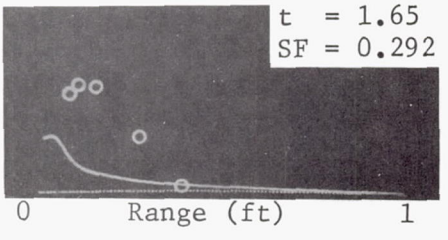
t = 1.65
SF = 0.292
0
Range (ft)
1

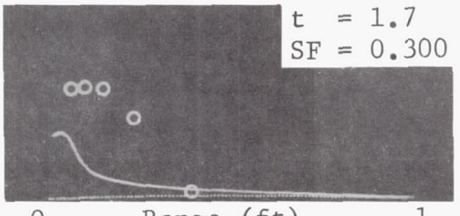
t = 1.7
SF = 0.300
0
Range (ft)
1

(a)
TEST 47

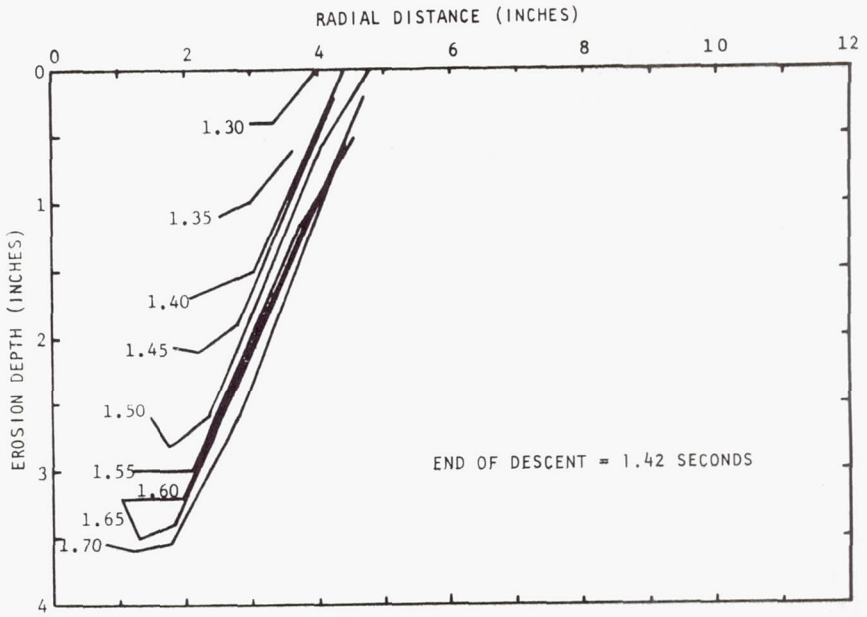

(b)
TEST 47

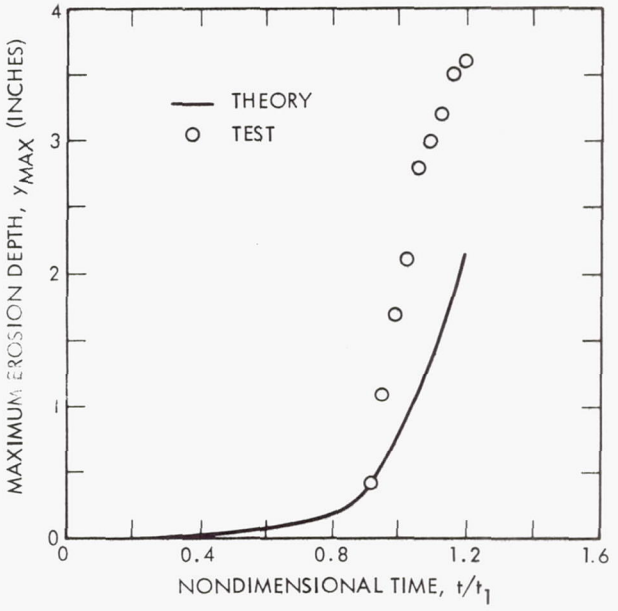

(c)
TEST 47

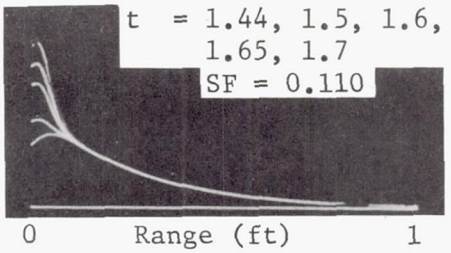
t = 1.44, 1.5, 1.6,
1.65, 1.7
SF = 0.110
0
Range (ft)
1

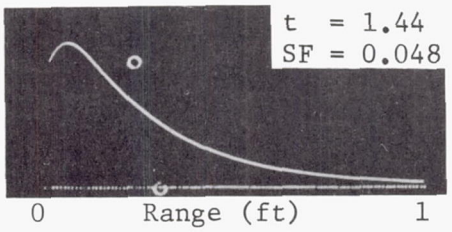
t = 1.44
SF = 0.048
0
Range (ft)
1

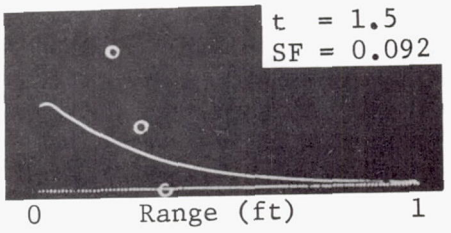
t = 1.5
SF = 0.092
0
Range (ft)
1

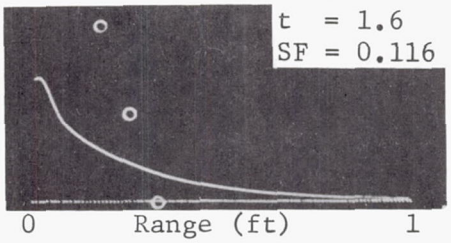
t = 1.6
SF = 0.116
0
Range (ft)
1

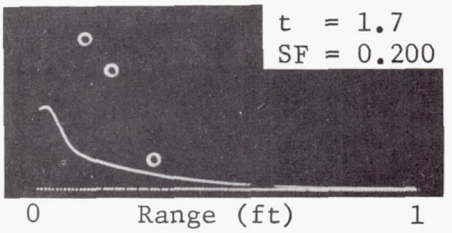
t = 1.7
SF = 0.200
0
Range (ft)
1

(a)
TEST 48

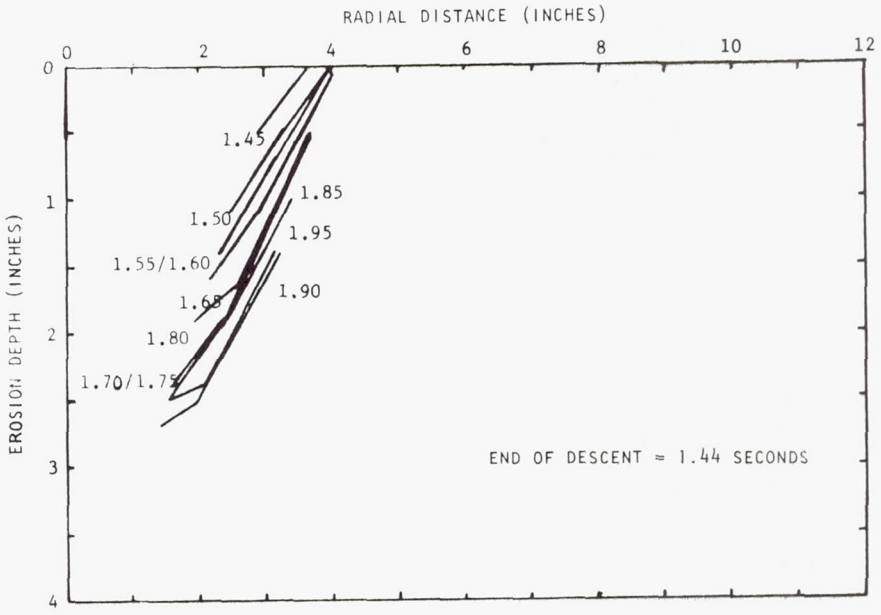

(b)
TEST 48

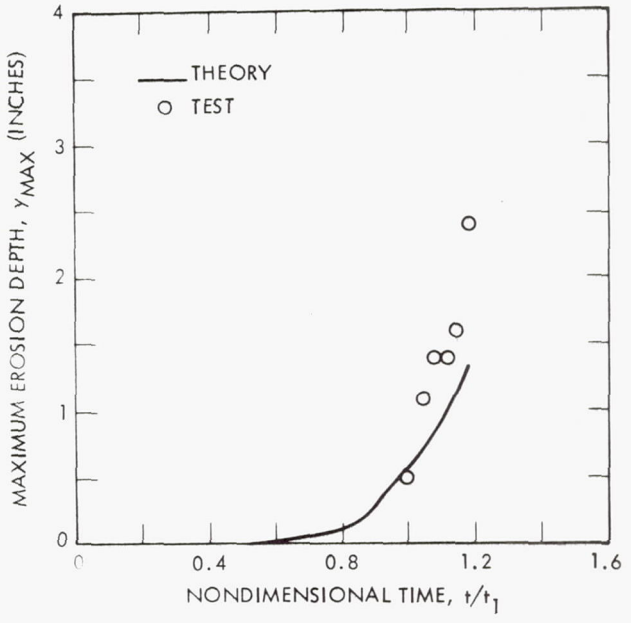

(c)
TEST 48

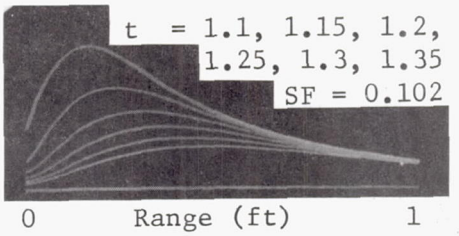
t = 1.1, 1.15, 1.2,
1.25, 1.3, 1.35
SF = 0.102
0
Range (ft)
1

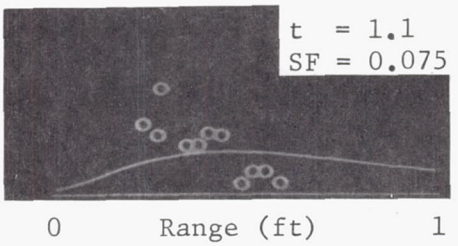
t = 1.1
SF = 0.075
0
Range (ft)
1

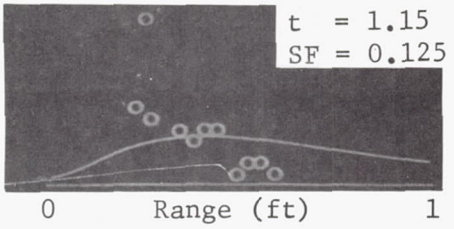
t = 1.15
SF = 0.125
0
Range (ft)
1

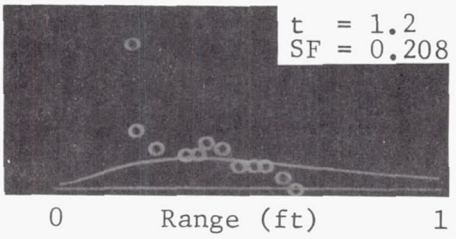
t = 1.2
SF = 0.208
0
Range (ft)
1

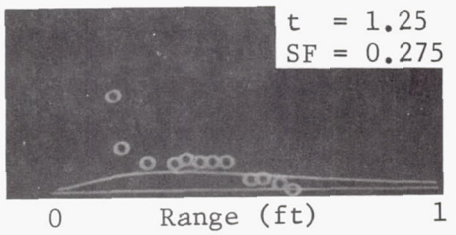
t = 1.25
SF = 0.275
0
Range (ft)
1

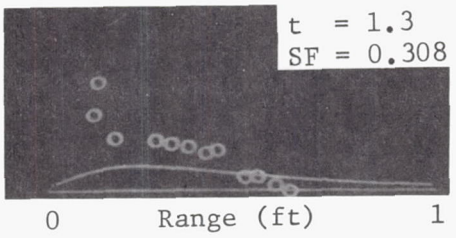
t = 1.3
SF = 0.308
0
Range (ft)
1

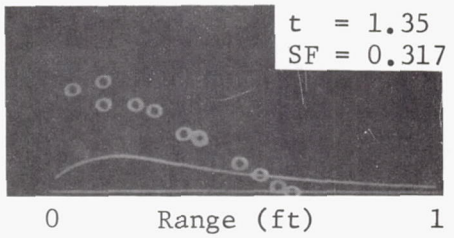
t = 1.35
SF = 0.317
0
Range (ft)
1

(a)
TEST 49

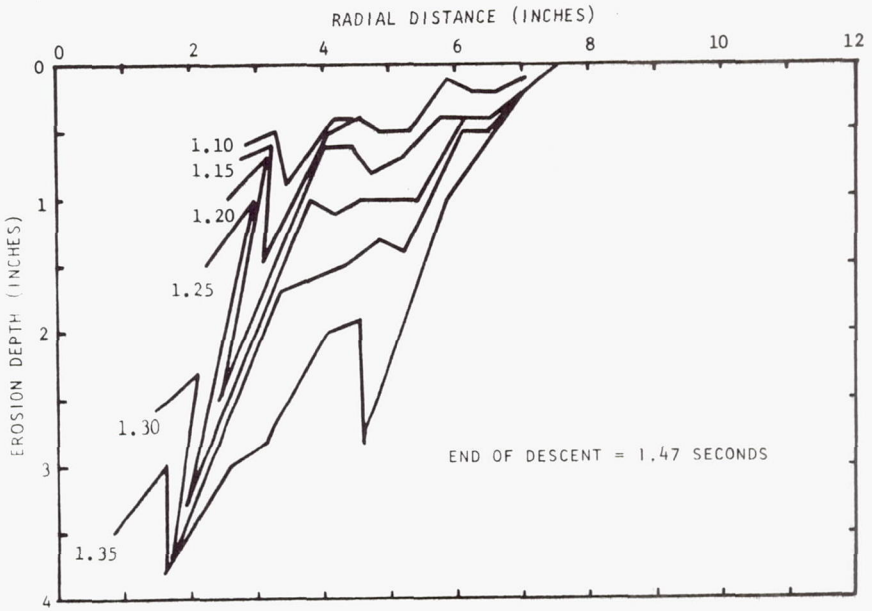

(b)
TEST 49

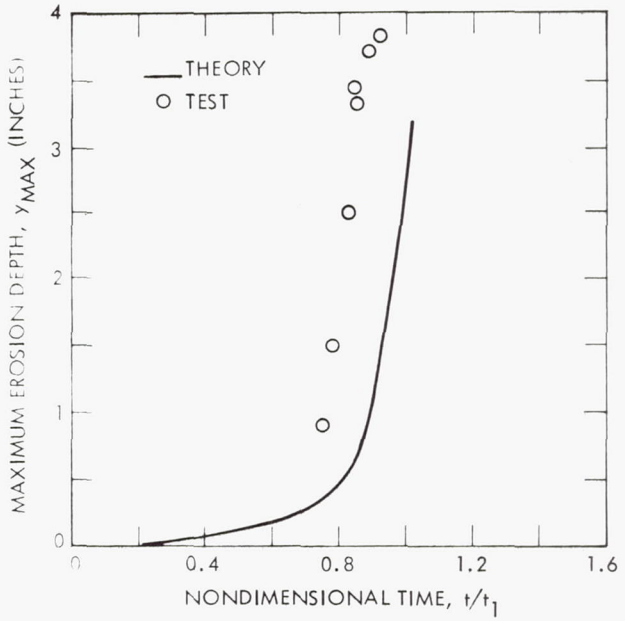

(c)
TEST 49

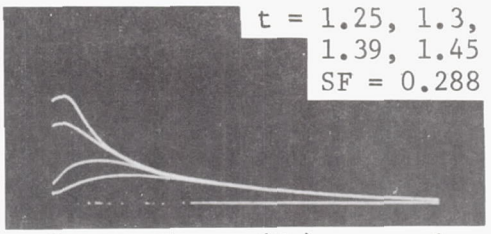
t = 1.25, 1.3,
1.39, 1.45
SF = 0.288
0
Range (ft)
1

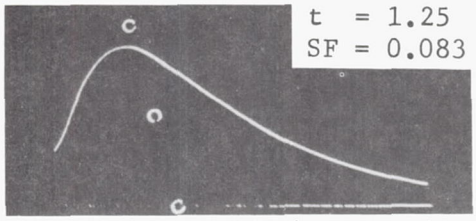
t = 1.25
SF = 0.083
0
Range (ft)
1

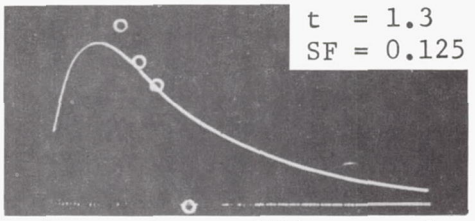
t = 1.3
SF = 0.125
0
Range (ft)
1

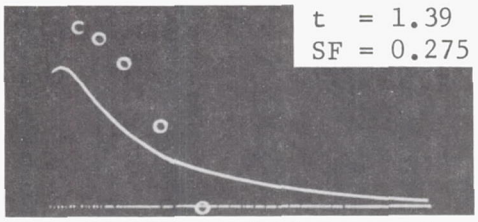
t = 1.39
SF = 0.275
0
Range (ft)
1

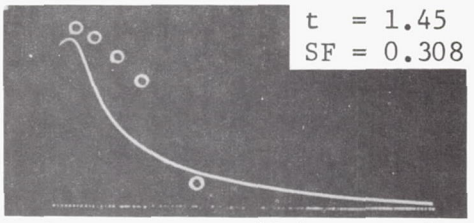
t = 1.45
SF = 0.308
0
Range (ft)
1

(a)
TEST 51

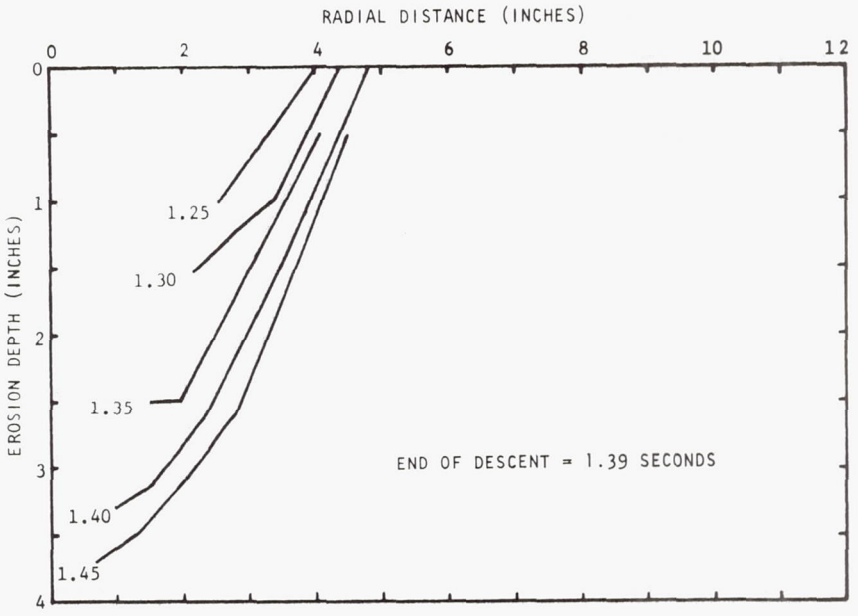

(b)
TEST 51

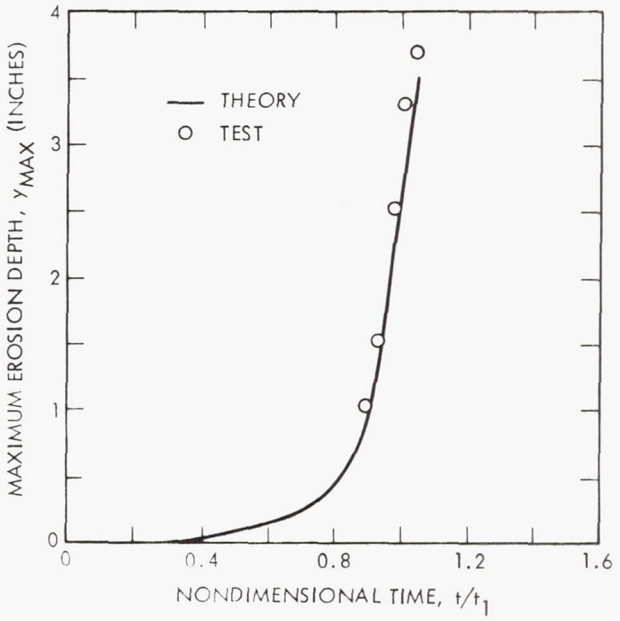

(c)
TEST 51

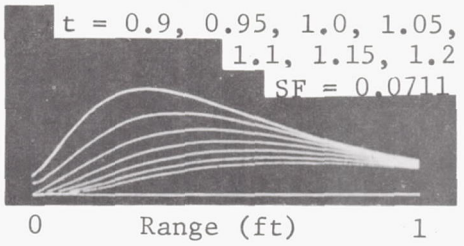
t = 0.9, 0.95, 1.0, 1.05,
1.1, 1.15, 1.2
SF = 0.0711
0
Range (ft)
1

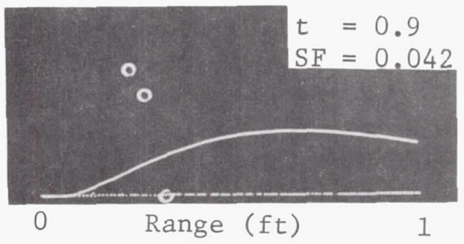
t = 0.9
SF = 0.042
0
Range (ft)
1

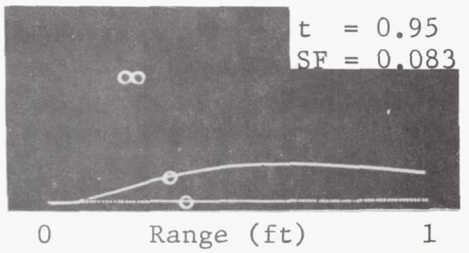
t = 0.95
SF = 0.083
0
Range (ft)
1

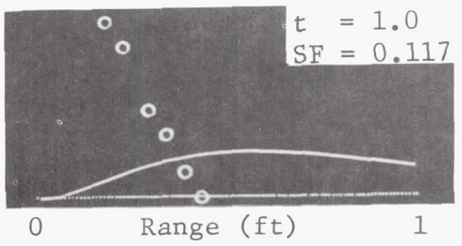
t = 1.0
SF = 0.117
0
Range (ft)
1

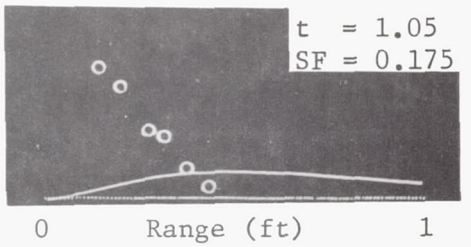
t = 1.05
SF = 0.175
0
Range (ft)
1

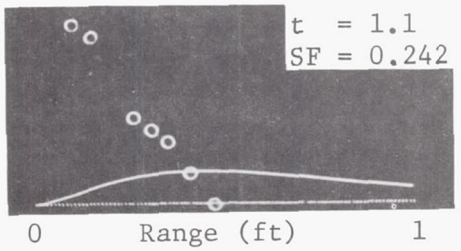
t = 1.1
SF = 0.242
0
Range (ft)
1

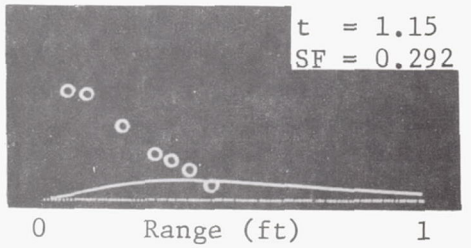
t = 1.15
SF = 0.292
0
Range (ft)
1

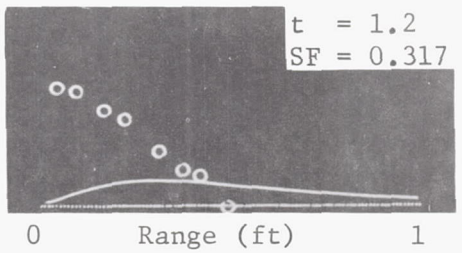
t = 1.2
SF = 0.317
0
Range (ft)
1

(a)
TEST 52

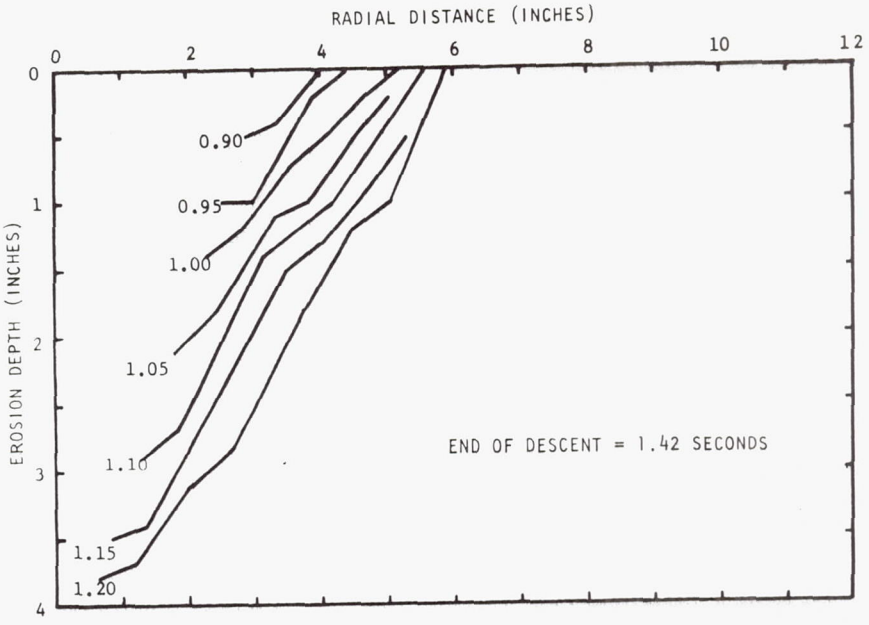

(b)
TEST 52

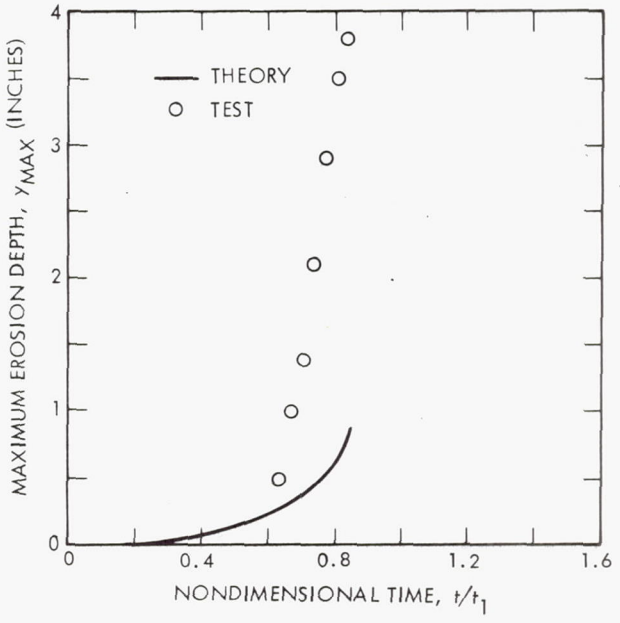

(c)
TEST 52

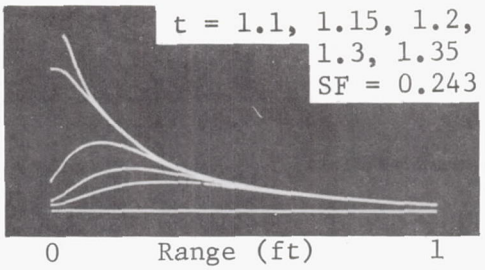
t = 1.1, 1.15, 1.2,
1.3, 1.35
SF = 0.243
0
Range (ft)
1

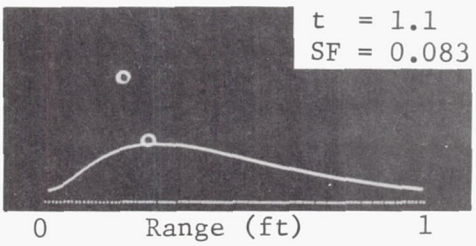
t = 1.1
SF = 0.083
0
Range (ft)
1

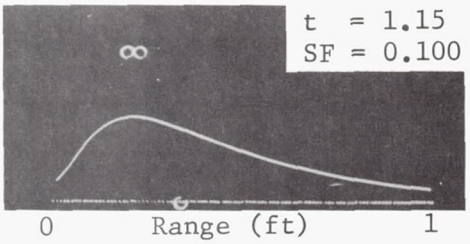
t = 1.15
SF = 0.100
0
Range (ft)
1

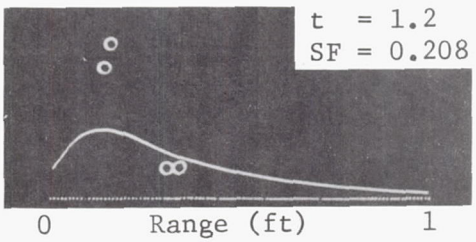
t = 1.2
SF = 0.208
0
Range (ft)
1

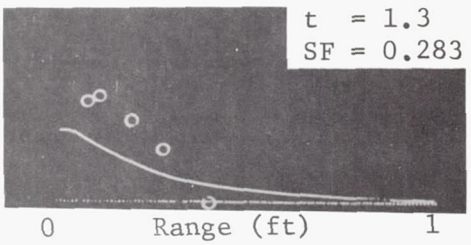
t = 1.3
SF = 0.283
0
Range (ft)
1

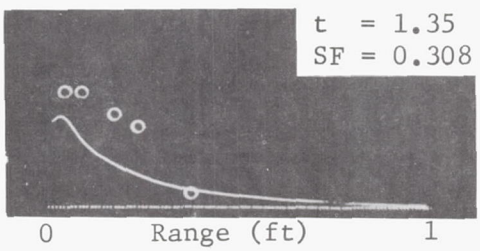
t = 1.35
SF = 0.308
0
Range (ft)
1

(a)
TEST 54

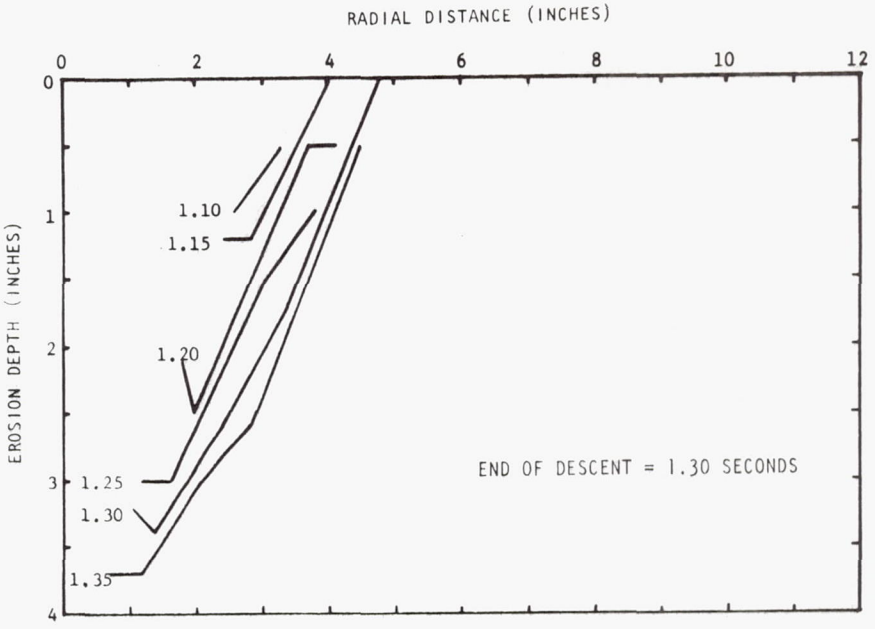

(b)
TEST 54

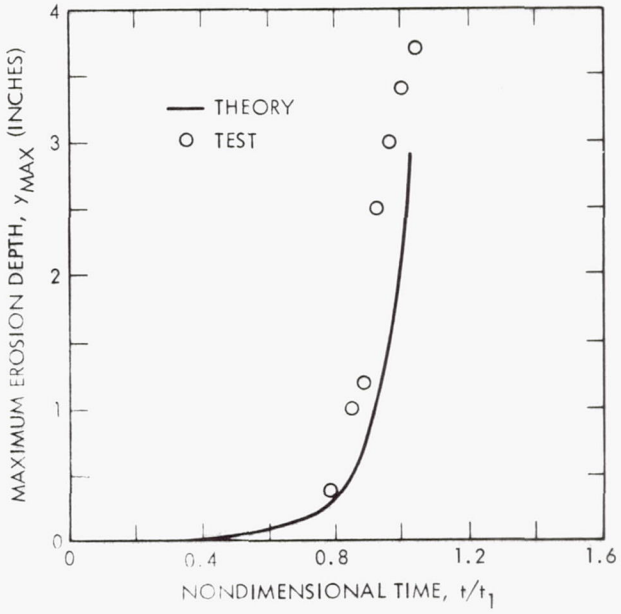

(c)
TEST 54

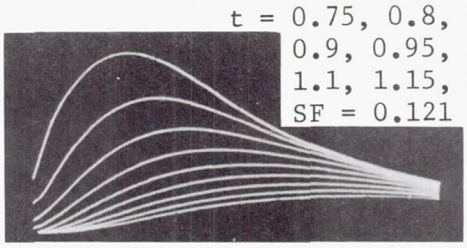
t = 0.75, 0.8, 0.85,
0.9, 0.95, 1, 1.05,
1.1, 1.15, 1.2
SF = 0.121
0
Range (ft)
1

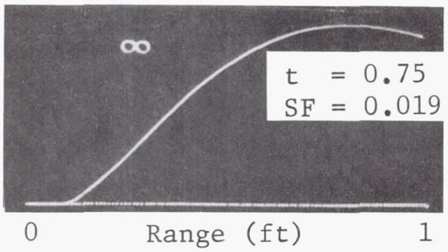
t = 0.75
SF = 0.019
0
Range (ft)
1

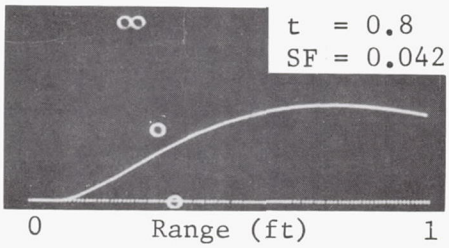
t = 0.8
SF = 0.042
0
Range (ft)
1

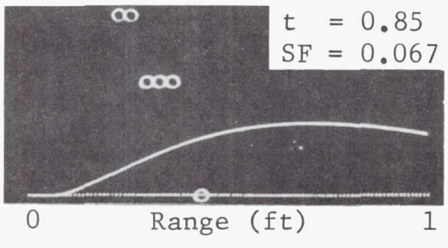
t = 0.85
SF = 0.067
0
Range (ft)
1

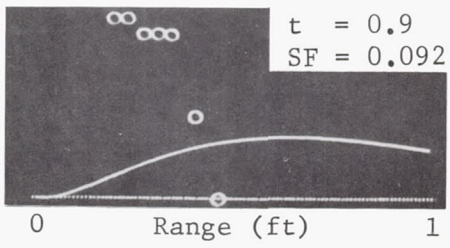
t = 0.9
SF = 0.092
0
Range (ft)
1

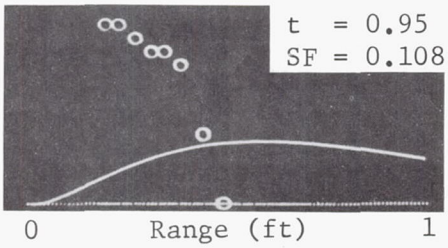
t = 0.95
SF = 0.108
0
Range (ft)
1

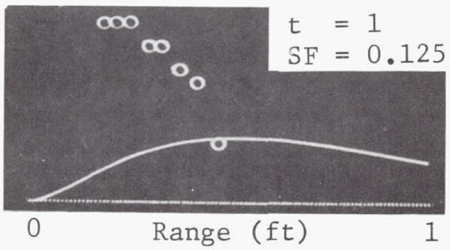
t = 1
SF = 0.125
0
Range (ft)
1

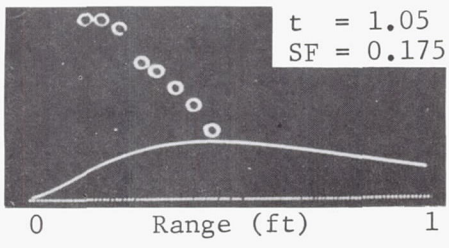
t = 1.05
SF = 0.175
0
Range (ft)
1

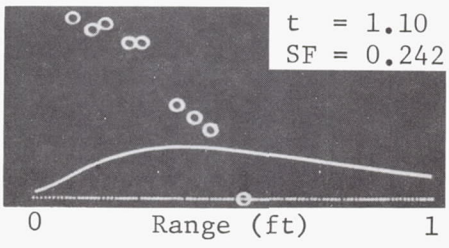
t = 1.10
SF = 0.242
0
Range (ft)
1

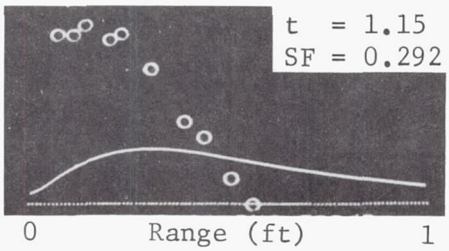
t = 1.15
SF = 0.292
0
Range (ft)
1

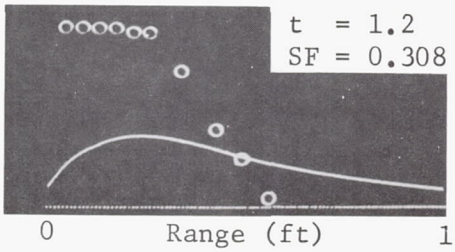
t = 1.2
SF = 0.308
0
Range (ft)
1

(a)
TEST 55

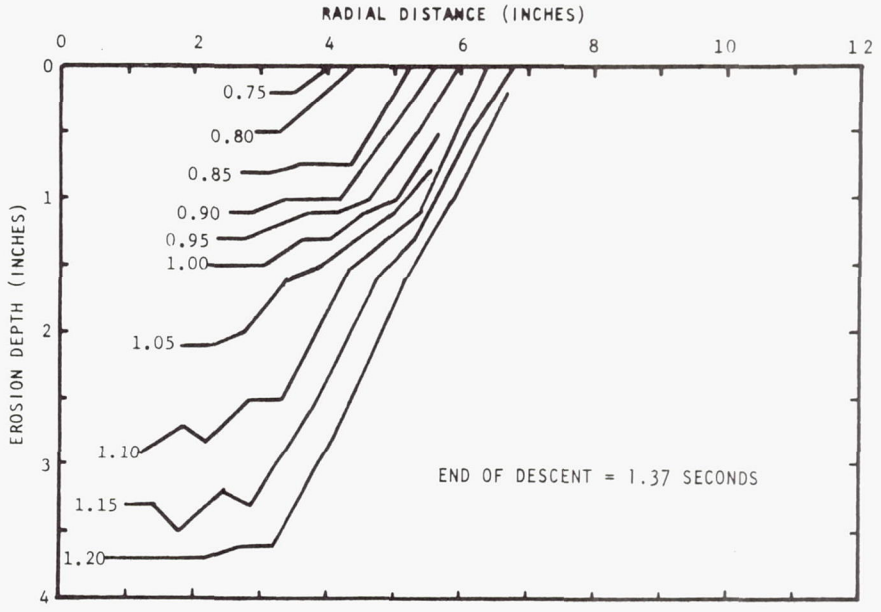

(b)
TEST 55

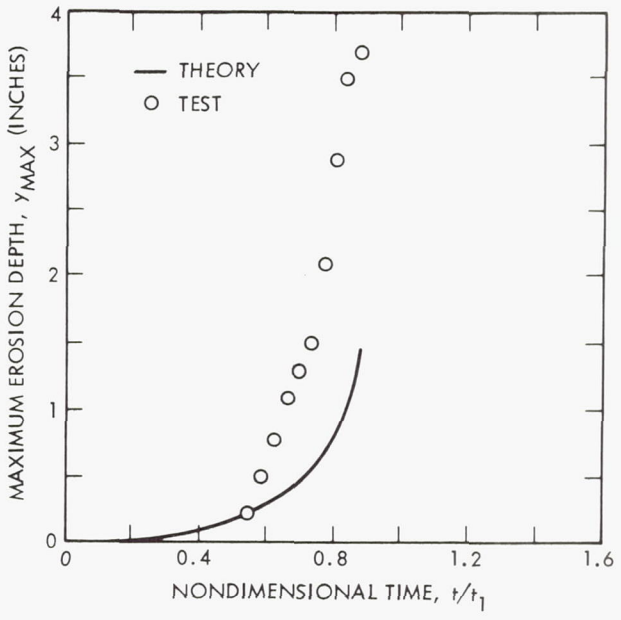

(c)
TEST 55

APPENDIX D

FRICTION COEFFICIENT INVESTIGATIONS

Included in this appendix are two memoranda concerned with investigations of the friction coefficient C_f which were conducted at the beginning of this work. These investigations were motivated as a result of earlier erosion computations made using Roberts' theory which showed that a constant value of C_f did not predict erosion as observed during tests.

It was reasoned that if Roberts' formulation provides an acceptable description of the first-order effects of soil erosion, then test data can be used to determine the spatial and time variation of C_f required to bring Roberts' theory into agreement with test results. Four tests (5, 10, 39 and 55) were arbitrarily selected for these C_f computations. The philosophy of this procedure was to use these results to determine whether C_f was essentially constant, and if so, to determine a representative value; or if C_f varied, to determine the type of variation. Then from these results, a procedure would be proposed and followed in the theoretical erosion computations for each of the 32 tests.

The first memorandum (68-3343.5-49) displayed the variation of C_f averaged over time at each radial station; and the variation of C_f averaged over the radial stations at each time. Also displayed were the corresponding standard deviations. The resultant average values of C_f over all time and radial stations considered were 0.854, 3.41, 1.30 and 1.47 for Tests 5, 10, 39 and 55, respectively. The C_f values ranged from about 0 to 12. As a result of these calculations, it was concluded that C_f was not constant and a representative value for use in the subsequent erosion calculations did not appear to exist.

The second memorandum (68.3340.4-23) investigated the possible correlation of the individual C_f values at each radial station and time with Reynolds number. A plot of these C_f values against particle Reynolds

number suggested an approximate correlation did exist in that C_f did decrease with increasing Reynolds number. Even though there was considerable scatter in the data, the C_f values tended to follow the trend of drag coefficients measured on spheres. On the basis of these investigations, it was decided that the value of C_f to be used in the erosion calculations should be determined at each radial position and time on the basis of the local Reynolds number and corresponding coefficient measured on spheres.

Such a procedure is within the framework of the theory advanced by Roberts. Roberts indicated that the friction coefficient C_f and boundary layer thickness both depend on the Reynolds number (R_θ). The length parameter in this Reynolds number is the distance from the stagnation point to the radial station. If the functional relation between the drag coefficient measured on spheres and Reynolds number R_e is represented as $C_f = f(R_e)$, then in the subsequent erosion calculations the friction coefficient was determined by the equation

$$C_f = f(R_\theta)$$

Roberts' formulation contains a term denoted by "a" which represents the velocity imparted to a soil particle to the velocity of the gas where the particle enters the gas stream. The particle is assumed to be accelerated by viscous and pressure drag forces. The expression derived by Roberts for "a" contains a pressure drag coefficient which he denotes as C_D. Roberts also introduces the particle Reynolds number R_D in which the length parameter is taken as the particle diameter. The particle drag coefficient used in the erosion calculations were made dependent on the particle Reynolds number. (It should be mentioned that in the determination of the C_f values presented in the memorandum C_D was assumed constant and equal to 2. However, even if C_D was made dependent on Reynolds number, the computed values of C_f would fall within the same scatter band.)

In the erosion calculations the value of C_D was computed from the formula

$$C_D = f(R_D)$$

The experimentally determined drag coefficient on spheres presented in Figure 1.5 of Reference 14 is reproduced here in Figure D1. This same curve is superimposed in Figure 1 of memorandum 68-3340.4-23 included in this appendix.

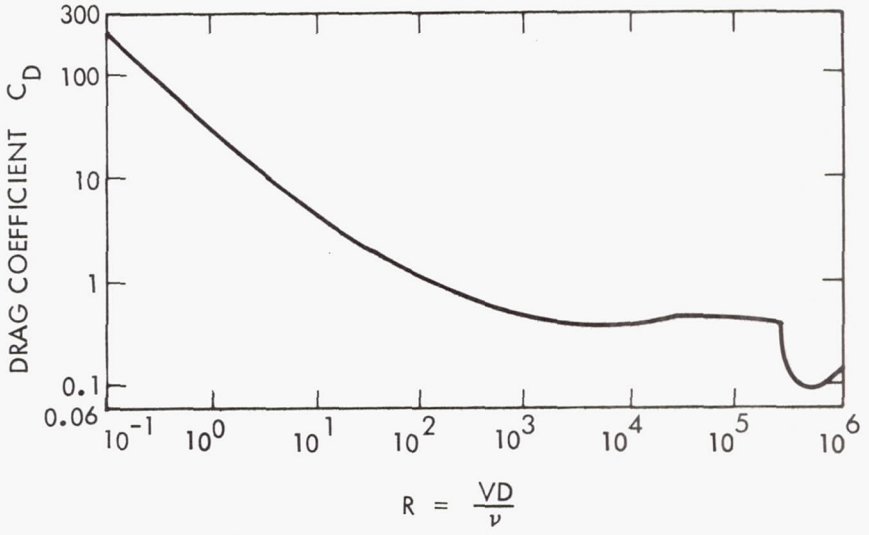

Figure D1. Drag Coefficient for Spheres as a Function of the Reynolds Number (Taken from Figure 1.5 of Reference 14)

TRW
SYSTEMS GROUP

INTEROFFICE CORRESPONDENCE 68-3343.5-49

TO: File CC: See Distribution DATE: 23 May 1968

Approved: R. E. Hutton REH.

SUBJECT: Friction Coefficients Calculated From Erosion Profiles Using Roberts' Theory

FROM: J. C. McMunn JCM
BLDG. R1 MAIL STA. 1032 EXT. 68535

References:

1. "The Action of a Hypersonic Jet on a Dusty Surface," L. Roberts, Presented at the 31st Annual Meeting of the Institute of Aerospace Sciences. January 1963.

2. "Scaled LEM Jet Erosion Tests," N. S. Land and H.F. Scholl, NASA Langley Working Paper 252, July 1966.

3. "Further Scaled LM Jet Erosion Tests." N.S. Land and H.F. Scholl, NASA Langley Working Paper 455.

4. Unpublished Erosion Profiles Supplied by N. S. Land, Langley Research Center.

Introduction

This memo presents friction coefficients calculated from three glass bead erosion profiles and one gravel profile according to Roberts' erosion theory (Reference 1). The erosion test data was obtained by lowering a supersonic gas jet over a bed of particles and measuring erosion profiles using x-ray techniques. These data are presented in References 2, 3, and 4. The friction coefficient was calculated from these data for several times and at each time over radial stations. These values were used to compute averages and standard deviations. First, we present Roberts' formulation and the method used to compute friction coefficients and then present the results.

Discussion

Roberts' formulation states the rate of soil erosion caused by retrorocket gas impingement is given by

$$\frac{1}{2} a u \sigma c \cos\beta \frac{\partial y}{\partial t} = C_f q - \tau^* \qquad (1)$$

where

$$\tau^* = \sigma c D g \left[\text{Cos}\beta \tan\alpha - \text{Sin}\beta \right] + \tau_{coh} \qquad (2)$$

and "a" is a momentum factor, u the gas radial velocity, σ the soil particle mass density, c the packing constant, β the surface slope, y the erosion depth, t time, C_f the friction coefficient, q the dynamic pressure, D particle diameter. g the gravitational acceleration, α the soil friction angle and τ_{coh} the soil cohesion stress.

Roberts states that C_f is essentially constant and equal to 0.2. If test data is used, Equation (1) can be solved to determine the values of C_f at each radial station and time to agree with the observed erosion rate. For such calculations (1) is solved for C_f to obtain

$$C_f(r,t) = \frac{\frac{1}{2} a u \sigma c \text{Cos}\beta \frac{\partial y}{\partial t} + \tau^*}{q} \qquad (3)$$

By taking a range of times and radial stations, and the measured erosion profiles at each time instant, Equation (3) gives the corresponding C_f value at each of these times and radial stations. These values can then be used to determine the average values and standard deviations of C_f. If these data indicate a significant variation of C_f, attempts can be made to correlate C_f with Reynolds number or other system parameters.

Results

Data from four tests were used to determine C_f. The erosion profiles are presented in Appendix A and the input parameters along with computer printout of the C_f computations are presented in Appendix B. All input values are presented in Appendix B. All input values are model dimensions. The dashed lines in the profile curves are either "faired in" data or extended profiles.

Computations were made to determine the required value of $C_f(r,t)$ necessary to match the observed erosion rates. Then average values and standard deviations were formed over radial stations at a given time and over time at each radial station. Finally a grand average and standard deviation was calculated for each test.

Figures 1-4 present the variation of average friction coefficient and standard deviation at each time and over radial stations for each test. The plots indicate that for both gravel and glass beads most average C_f values are greater than 0.2. The grand averages for glass beads were 0.854, 1.30, 1.47 and for gravel 3.41. The standard deviations were of the same magnitude indicating the large spread in C_f values.

FIGURE 1: TEST 5

Variation of Average Friction Coefficient and Standard Deviation with Time and Radial Station (a) averages over radial stations (b) averages over time.

For Test 5, $\overline{C}_f = .854$ $\sigma = 1.06$

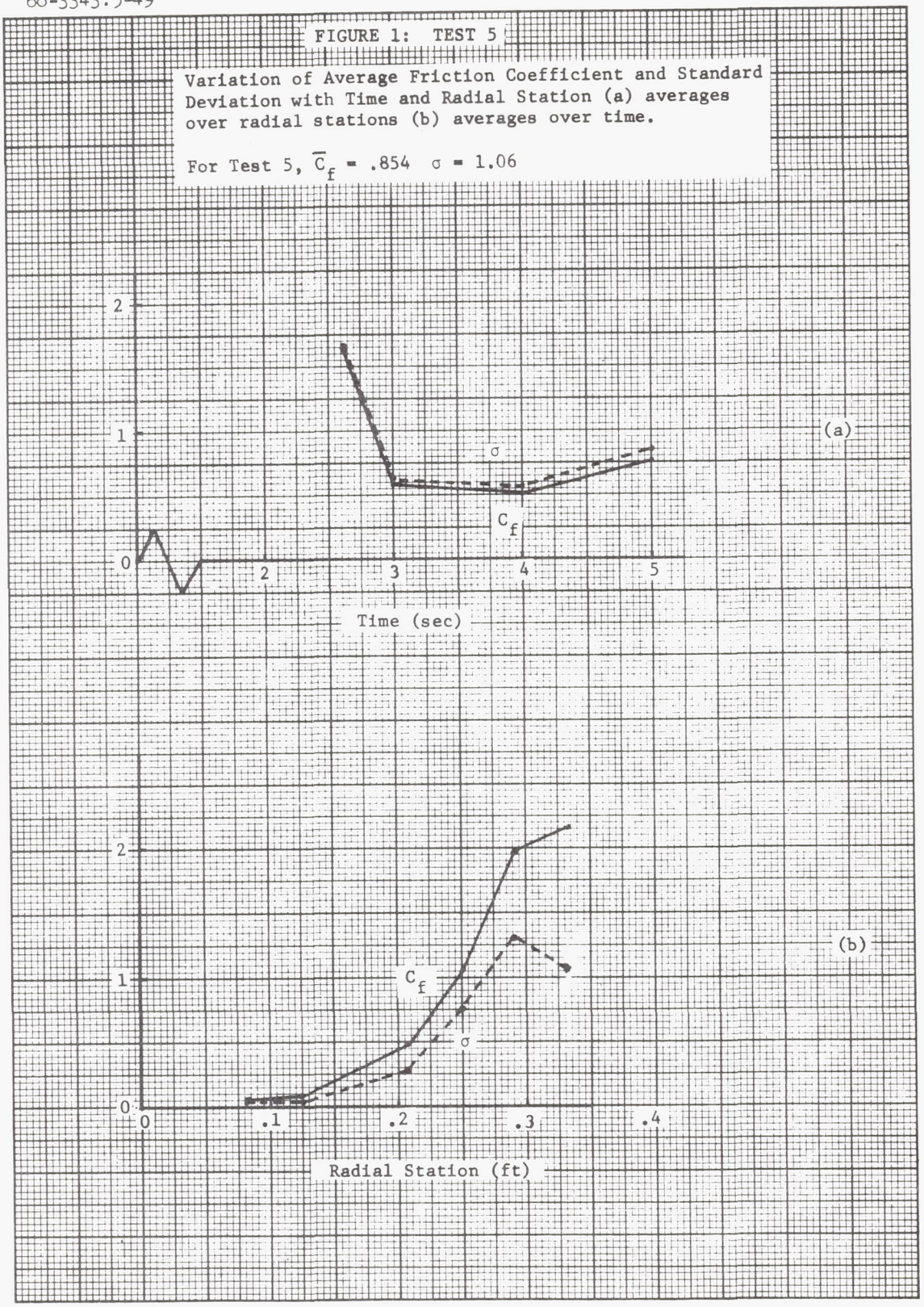

FIGURE 2. TEST 10

Variation of Average Friction Coefficient and Standard Deviation with Time and Radial Station (a) averages over radial stations (b) averages over time.

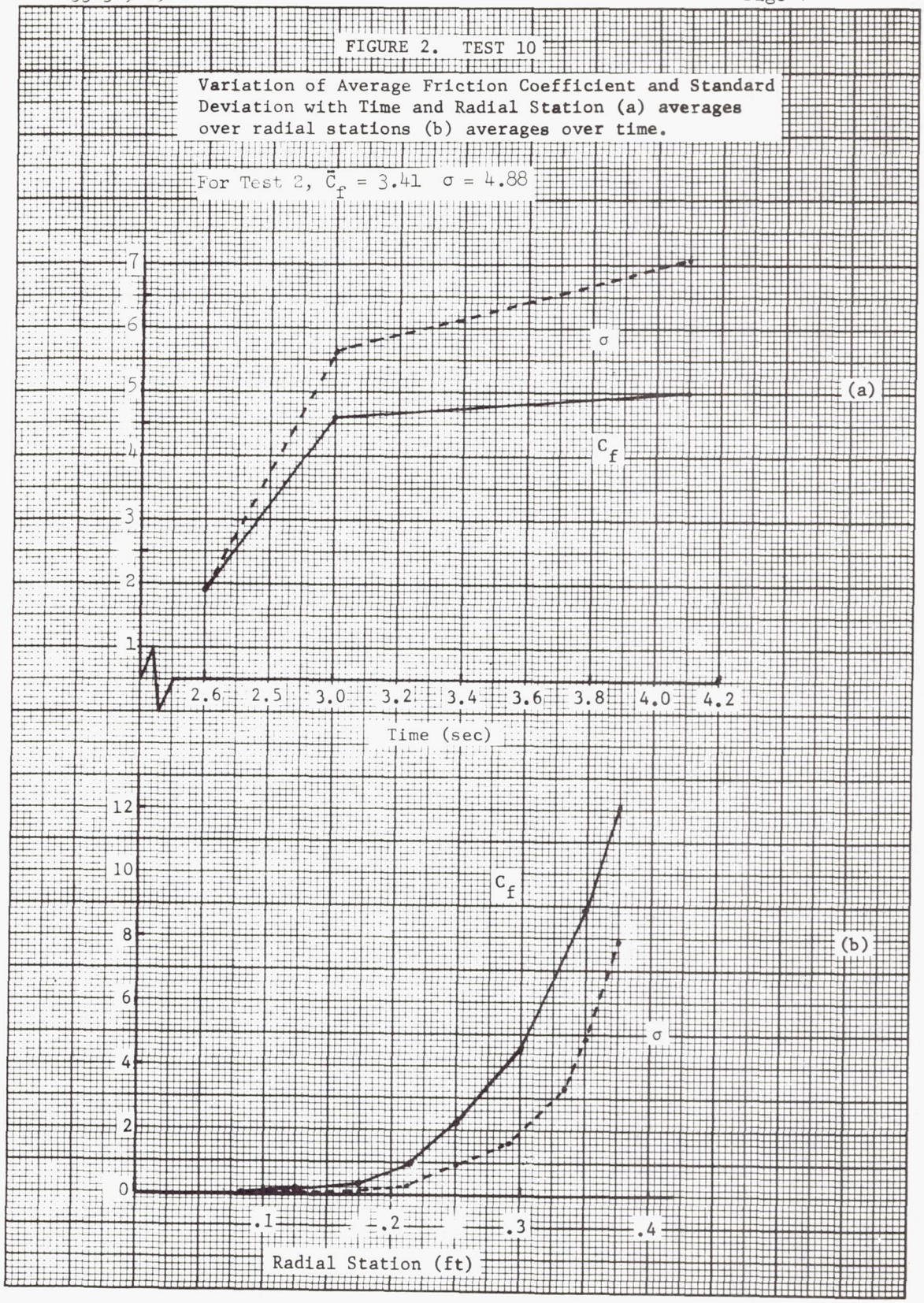

FIGURE 3. TEST 39

Variation of Average Friction Coefficient and Standard Deviation with Time and Radial Station (a) averages over radial stations (b) averages over time.

For Test 39, $\overline{C}_f = 1.30$ $\sigma = 1.14$

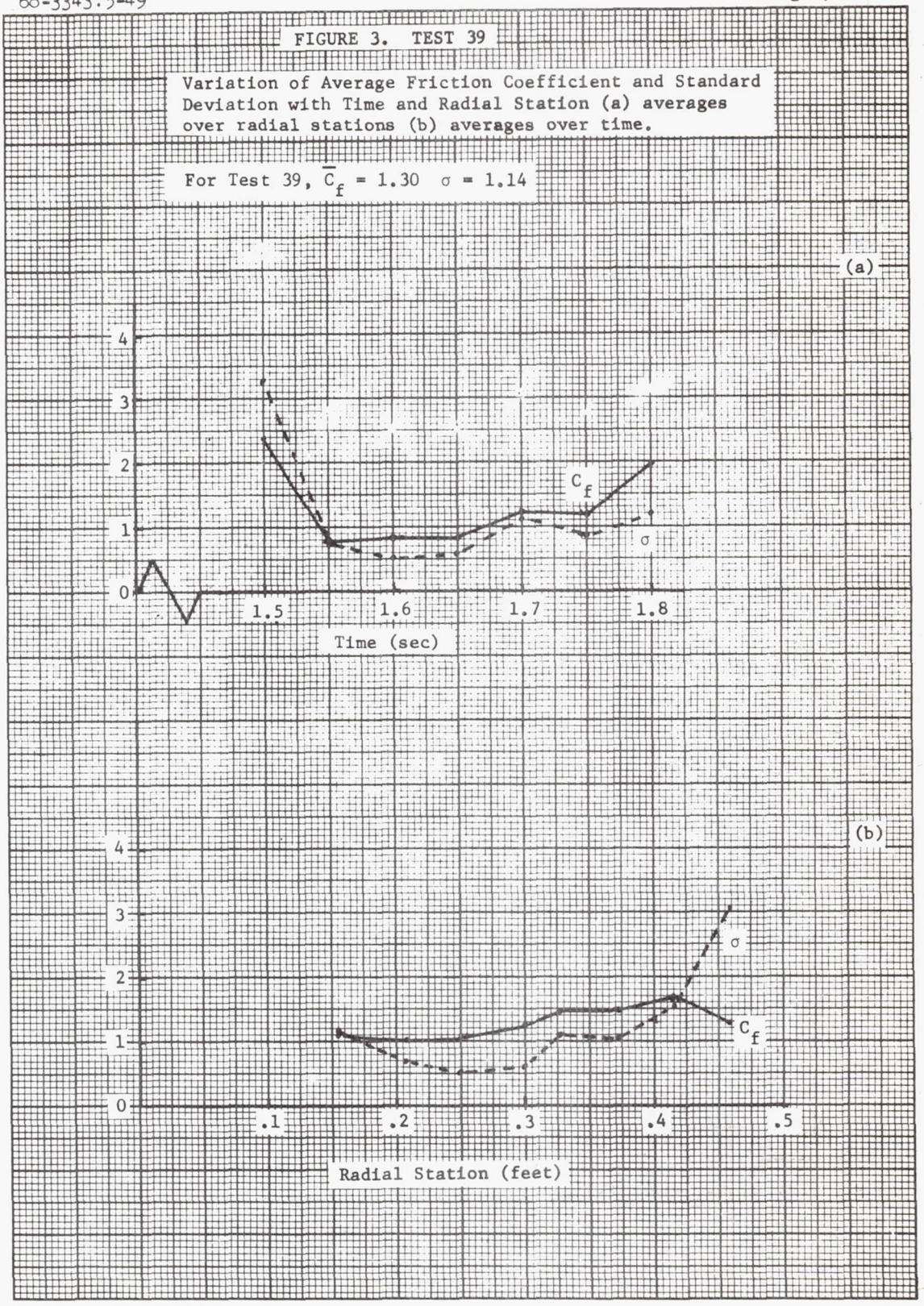

FIGURE 4. TEST 55

Variation of Average Friction Coefficient and Standard Deviation with Time and Radial Station (a) average over radial stations (b) averages over time.

For Test 55, $\overline{C}_f = 1.47$ $\sigma = 1.12$

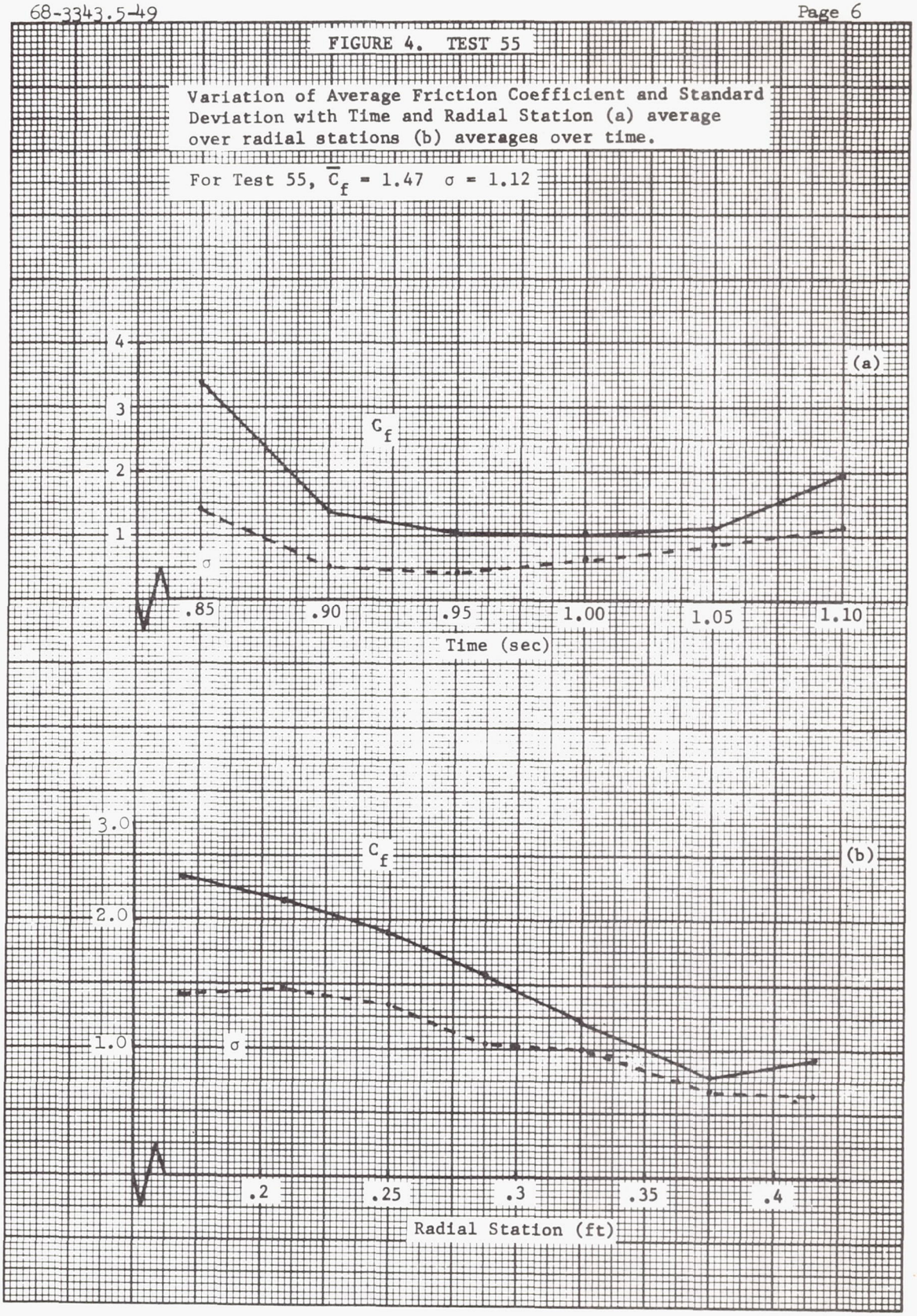

APPENDIX A

In Appendix A we present the erosion profiles for the four test cases. The dashed lines are either "faired in" or extended profiles. Tests 5, 39 and 55 are glass bead data and Test 10 is for gravel.

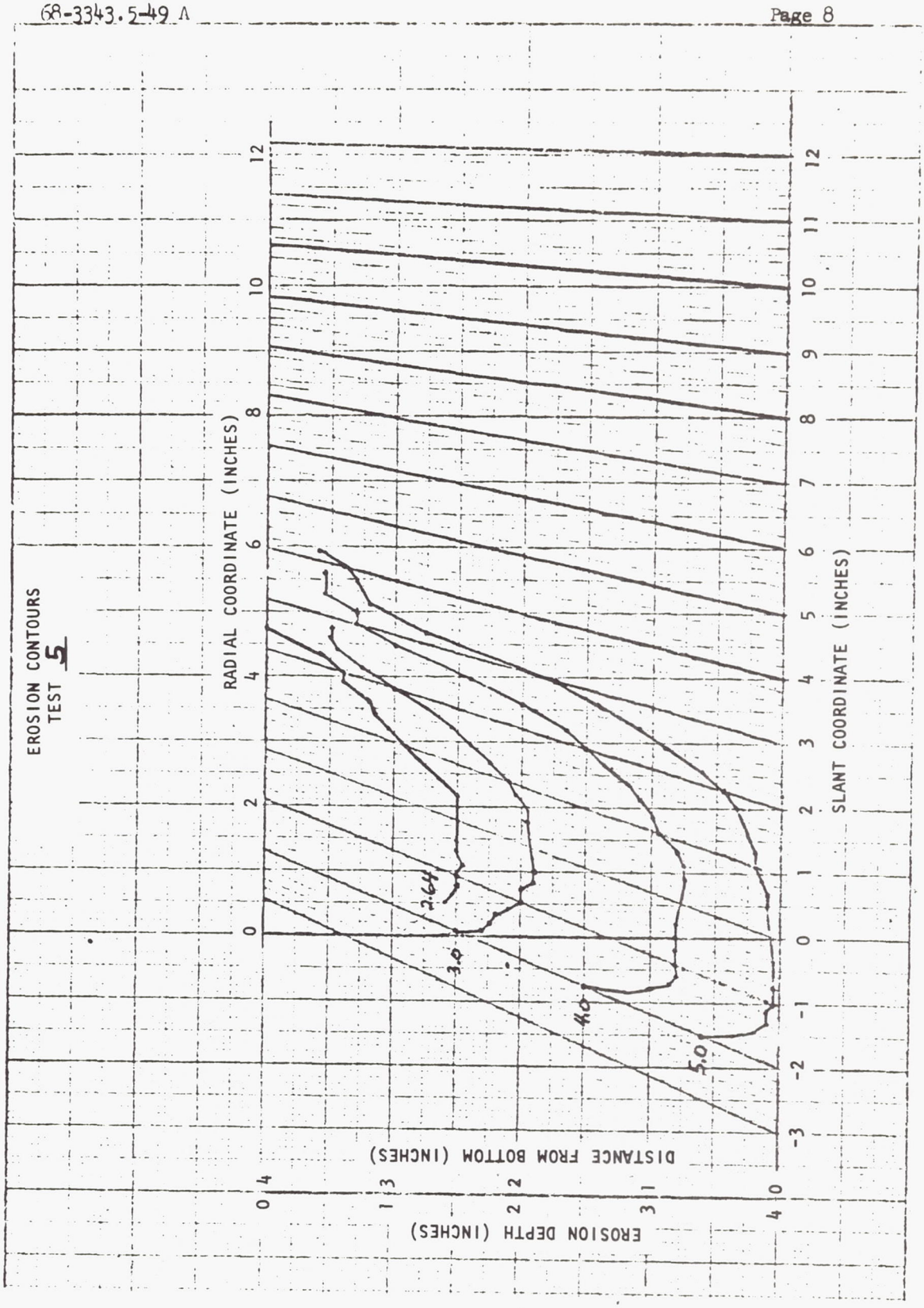
EROSION CONTOURS
TEST 5
RADIAL COORDINATE (INCHES)
SLANT COORDINATE (INCHES)
DISTANCE FROM BOTTOM (INCHES)
EROSION DEPTH (INCHES)
2.64
3.0
4.0
5.0

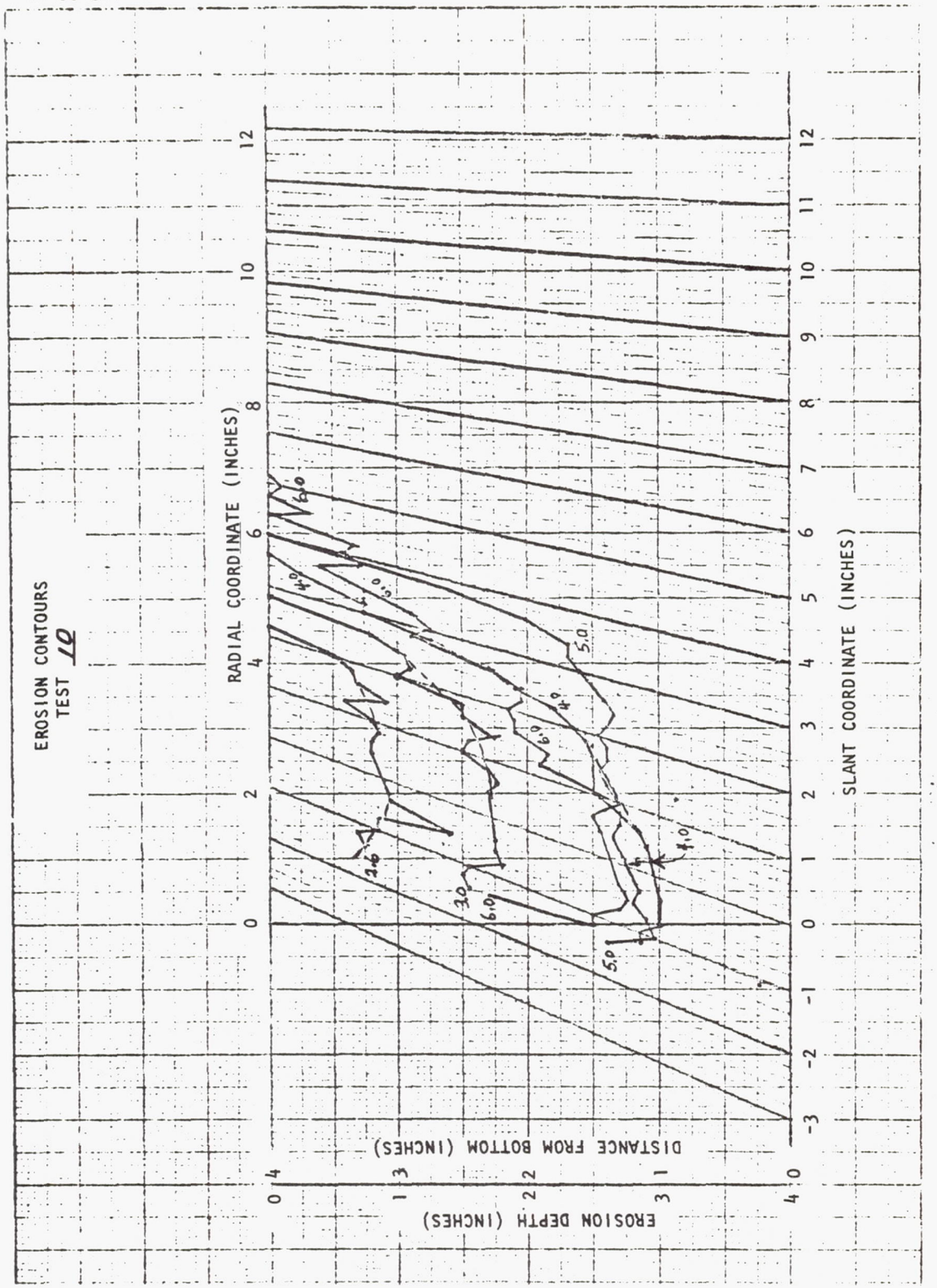
EROSION CONTOURS
TEST 10
RADIAL COORDINATE (INCHES)
SLANT COORDINATE (INCHES)
DISTANCE FROM BOTTOM (INCHES)
EROSION DEPTH (INCHES)
6.0
4.0
4.0
5.0
4.0
6.0
4.0
2.6
3.0
6.0
5.0

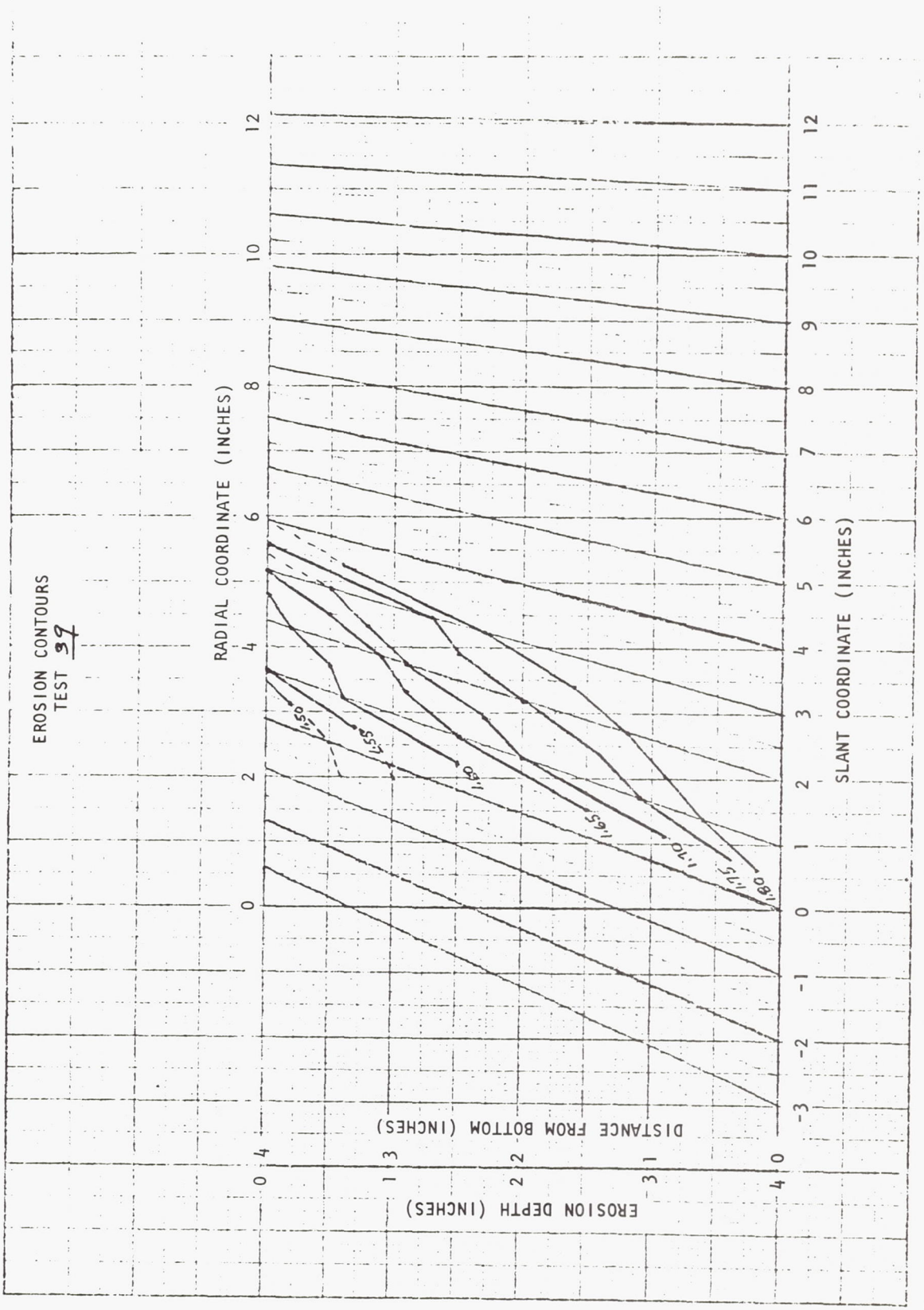
EROSION CONTOURS
TEST 39
RADIAL COORDINATE (INCHES)
SLANT COORDINATE (INCHES)
DISTANCE FROM BOTTOM (INCHES)
EROSION DEPTH (INCHES)
1.50
1.55
1.60
1.65
1.70
1.75
1.80

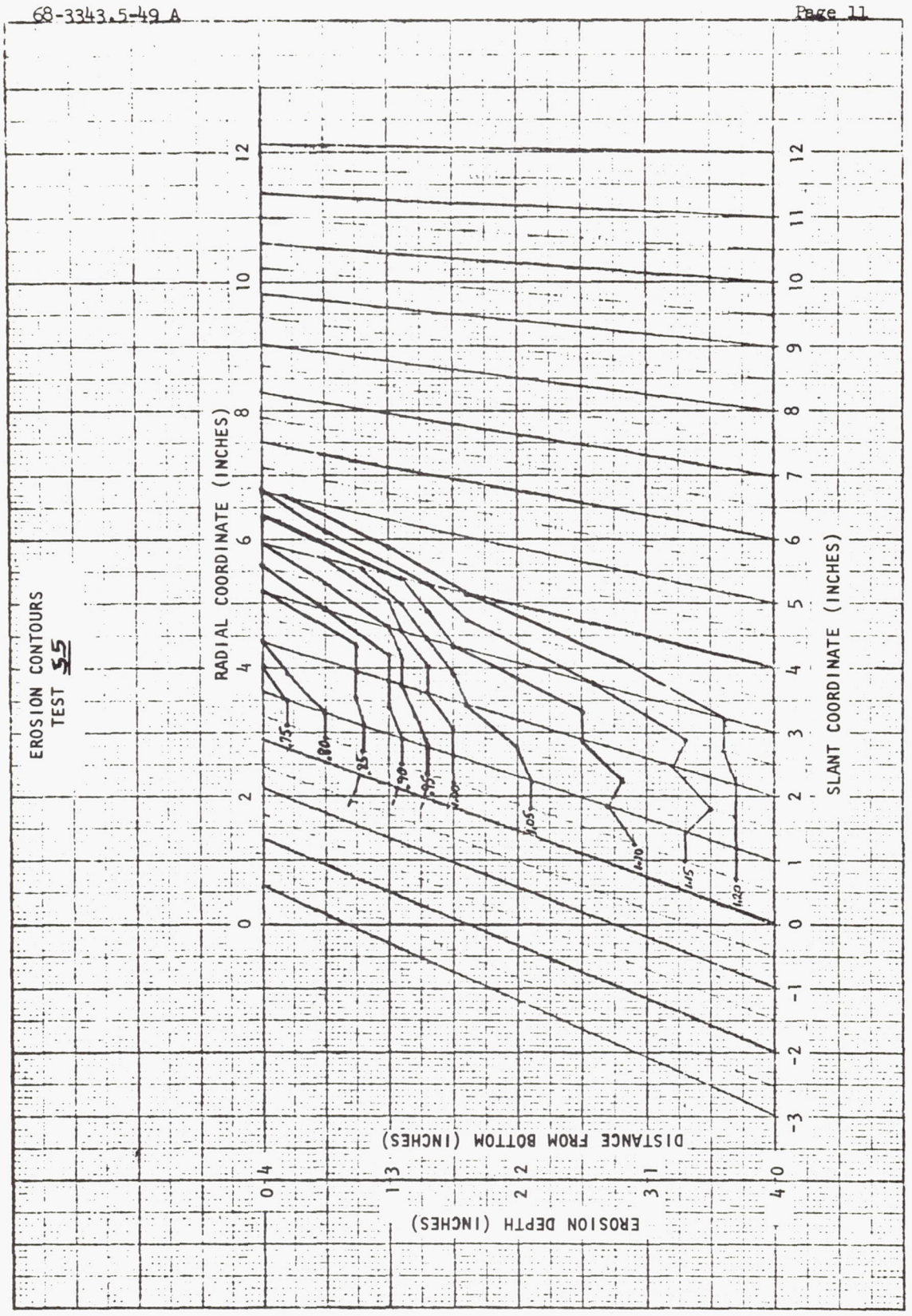
EROSION CONTOURS
TEST 55
RADIAL COORDINATE (INCHES)
SLANT COORDINATE (INCHES)
DISTANCE FROM BOTTOM (INCHES)
EROSION DEPTH (INCHES)
.75
.80
.85
.90
.95
1.00
1.05
1.10
1.15
1.20

APPENDIX B

In this appendix we present the computations of the friction coefficients for Tests 5 and 10 (Reference 2) and Tests 39 and 55 (Reference 3). The input data listed at the top of each table are model dimensions. The friction angle and packing constant for glass was taken as 27 degrees and .575, respectively, and for Test 10 (gravel) the angle was measured from the slumped crater and the packing constant was assumed to be 0.40.

Nozzle heights were computed using time at end of descent (References 2, 3), descent velocity and nozzle height at end of descent. To illustrate the data presented, see e.g., Table B-3. The nozzle heights presented correspond to the seven times shown in the next line. Erosion depths are the depths at each radial station shown above and each of the seven groups of erosion depths correspond to the times shown. For example, at t = 1.55 sec, the nozzle height is .599 and the erosion depth at r = .25 is .043 feet. These input values are used to compute the erosion profile slopes $\frac{\partial y}{\partial r}$ and erosion rates $\frac{\partial y}{\partial t}$ which is presented next, using the same format.

Roberts momentum factor "a" is also printed at the corresponding nozzle height at each time. The matrix of C_f values is presented next, each of the seven groups represent one time and radial stations read across to the right. For example, C_f = 3.72153 is at t = 1.5 and r = .167 and C_f = 2.62118 is for t = 1.5 at r = .208. Next we present the test grand average and standard deviation and then averages and standard deviations over radial stations and times using the same format.

Table B-1: Computation of Friction Coefficients

Test 5

TEST NØ = 5
NØZ RAD = .1108 FT MACH NØ = 2.68
CHAM TEMP = 507 DEG R CHAM VISC = 3.90000 E-7 LB SEC/SQ FT
CHAM PRESS= .6 PSI GAS CØNS = 12430 SQ FT/SQ SEC DEG R
DRAG CØEFF= 2 HEAT RATIØ= 1.67
SØIL DENS = 4.85 SLUG/CU FT GRAV = 32.2 FT/SQ SEC
PART DIA = .0042 FT ØR = 1280.49 MICRØNS
CØHESIØN = 0 PSF
PACK CØNS = .575 FRICT ANG = 27 DEG
DESCEN VEL= 1.11 FT/SEC

NØZZLE HEIGHTS ,FEET

.133	.133	.133	.133

TIME ,SEC

2.64	3	4	5

RAD STATIØNS ,FEET

.083	.125	.167	.208	.25
.291	.333			

ERØSIØN DEPTHS ,FEET

.125	.125	.125	.108	.087
.069	.05			
.175	.173	.169	.153	.132
.104	.071			
.271	.271	.246	.227	.204
.163	.129			
.319	.314	.304	.284	.254
.221	.179			

Table B-1: Computation of Friction Coefficients
Test 5 (Continued)

EROSION PROFILE SLOPES

0	0	-.10241	-.228916	-.23494
-.222892	-.452381			
-.047619	-3.57143 E-2	-.120482	-.222892	-.295181
-.36747	-.785714			
0	-.14881	-.26506	-.253012	-.385542
-.451807	-.809524			
-.119048	-8.92857 E-2	-.180723	-.301205	-.379518
-.451807	-1.			

EROSION RATES ,FT/SEC

.138889	.133333	.122222	.125	.125
9.72222 E-2	5.83333 E-2			
5.36765 E-2	5.36765 E-2	4.44853 E-2	.04375	4.30147 E-2
3.45588 E-2	2.90441 E-2			
.036	.03525	.03375	.03275	.0305
.02925	.027			
.048	.043	.058	.057	.05
.058	.05			

VALUES OF NON ZERO C SUB F= 28

MOMENTUM FACTORS AT EACH NOZ HEIGHT

6.31838 E-3	6.31838 E-3	6.31838 E-3	6.31838 E-3

Table B-1: Computation of Friction Coefficients
Test 5 (Continued)

MATRIX ØF FRICTIØN CØEFFICIENTS C SUB F

6.84784 E-2	.163775	.380506	.874031	2.15315
3.90077	3.72225			
2.75495 E-2	6.70033 E-2	.145074	.333523	.743812
1.2554	1.53341			
1.95994 E-2	4.23792 E-2	9.95308 E-2	.251087	.502898
.997868	1.42928			
2.43936 E-2	5.25612 E-2	.173229	.386961	.769667
1.78003	2.02778			

AVERAGE C SUB F= .854499
STANDARD DEVIATIØN= 1.05836

C SUB F TIME AVERAGE AT EACH RAD STA

3.50052 E-2	8.14298 E-2	.199585	.461401	1.04238
1.98352	2.17818			

C SUB F STAND DEVIATIØN AT EACH RAD STA

2.25535 E-2	5.58189 E-2	.124378	.280707	.750191
1.31895	1.06197			

C SUB F AVERAGE ØVER RAD STA AT EACH TIME

1.60899	.586539	.47752	.744946

C SUB F STAND DEVIATIØN AT EACH TIME

1.65959	.6069	.543206	.833794

Table B-2: Computation of Friction Coefficients
Test 10

TEST NO = 10
NOZ RAD = .1108 FT MACH NO = 2.68
CHAM TEMP = 516 DEG R CHAM VISC = 4.00000 E-7 LB SEC/SQ FT
CHAM PRESS= .6 PSI GAS CONS = 12430 SQ FT/SQ SEC DEG R
DRAG COEFF= 2 HEAT RATIO= 1.67
SOIL DENS = 5.23 SLUG/CU FT GRAV = 32.2 FT/SQ SEC
PART DIA = .0259 FT OR = 7896.34 MICRONS
COHESION = 0 PSF
PACK CONS = .4 FRICT ANG = 65 DEG
DESCEN VEL= 1.11 FT/SEC

NOZZLE HEIGHTS , FEET
.174 .117 .117

TIME , SEC
2.6 3 4

RAD STATIONS , FEET
.0825 .125 .167 .208 .25
.292 .333 .375

EROSION DEPTHS , FEET
.054 .071 .078 .069 .07
.062 .054 .0083

.147 .144 .142 .139 .131
.127 .092 .061

.244 .235 .221 .211 .196
.166 .107 .09

Table B-2: Computation of Friction Coefficients
Test 10 (Continued)

EROSION PROFILE SLOPES

.4	.142012	-1.20482 E-2	-4.81928 E-2	-4.16667 E-2
-9.63855 E-2	-.323494	-1.0881		
-7.05882 E-2	-2.95858 E-2	-3.01205 E-2	-6.62651 E-2	-7.14286 E-2
-.23494	-.39759	-.738095		
-.211765	-.136095	-.144578	-.150602	-.267857
-.536145	-.457831	-.404762		

EROSION RATES , FT/SEC

.2325	.1325	.16	.175	.1525
.1625	.095	.13175		
6.78571 E-2	5.85714 E-2	5.10714 E-2	5.07143 E-2	.045
3.71429 E-2	1.89286 E-2	2.91786 E-2		
.097	.091	.079	.072	.065
.039	.015	.029		

VALUES OF NON ZERO C SUB F= 24

MOMENTUM FACTORS AT EACH NOZ HEIGHT

2.10411 E-3	2.55893 E-3	2.55893 E-3

MATRIX OF FRICTION COEFFICIENTS C SUB F

.100835	.15257	.270212	.570438	1.19341
2.39423	3.07141	3.62272		
5.22117 E-2	.138822	.428704	1.19992	3.19397
5.79137	9.39508	13.9903		
5.48275 E-2	.141546	.412327	1.14146	2.54013
4.16024	8.68753	19.1763		

Table B-2: Computation of Friction Coefficients
Test 10 (Continued)

AVERAGE C SUB F= 3.41169
STANDARD DEVIATION= 4.88404

C SUB F TIME AVERAGE AT EACH RAD STA

6.92914 E-2	.144313	.370414	.970606	2.30917
4.11528	7.05134	12.2631		

C SUB F STAND DEVIATION AT EACH RAD STA

2.73489 E-2	7.27938 E-3	8.71633 E-2	.347786	1.02008
1.69902	3.46483	7.91935		

C SUB F AVERAGE OVER RAD STA AT EACH TIME

1.42198	4.2738	4.5393

C SUB F STAND DEVIATION AT EACH TIME

1.41269	5.11665	6.5859

Table B-3: Computation of Friction Coefficients

Test 39

TEST NØ = 39
NØZ RAD = .1108 FT MACH NØ = 2.68
CHAM TEMP = 512.6 DEG R CHAM VISC = 4.00000 E-7 LB SEC/SQ FT
CHAM PRESS= 1.87 PSI GAS CØNS = 12430 SQ FT/SQ SEC DEG R
DRAG CØEFF= 2 HEAT RATIØ= 1.67
SØIL DENS = 4.85 SLUG/CU FTGRAV = 32.2 FT/SQ SEC
PART DIA = .00162 FT ØR = 493.902 MICRØNS
CØHESIØN = 0 PSF
PACK CØNS = .575 FRICT ANG = 27 DEG
DESCEN VEL= 2.12 FT/SEC

NØZZLE HEIGHTS ,FEET

.705	.599	.493	.397	.312
.312	.312			

TIME ,SEC

1.5	1.55	1.6	1.65	1.7
1.75	1.8			

RAD STATIØNS ,FEET

.167	.208	.25	.292	.333
.375	.416	.458	.5	

ERØSIØN DEPTHS ,FEET

.05	.042	.021	0	0
0	0	0	0	
.083	.068	.043	.013	0
0	0	0	0	
.138	.101	.064	.043	.029
.006	0	0	0	
.167	.133	.107	.085	.067
.042	.012	0	0	
.19	.158	.14	.108	.081
.058	.035	0	0	
.232	.211	.182	.149	.122
.107	.06	0	0	
.262	.242	.22	.192	.16
.125	.08	.008	0	

Table B-3: Computation of Friction Coefficients
Test 39 (Continued)

EROSION PROFILE SLOPES

-.195122	-.174699	-.25	-.126506	0
0	0	0	0	
-.365854	-.240964	-.327381	-.259036	-7.83133 E-2
0	0	0	0	
-.902439	-.445783	-.345238	-.210843	-.222892
-.174699	-3.61446 E-2	0	0	
-.829268	-.361446	-.285714	-.240964	-.259036
-.331325	-.253012	-7.14286 E-2	0	
-.780488	-.301205	-.297619	-.355422	-.301205
-.277108	-.349398	-.208333	0	
-.512195	-.301205	-.369048	-.361446	-.253012
-.373494	-.644578	-.357143	0	
-.487805	-.253012	-.297619	-.361446	-.403614
-.481928	-.704819	-.47619	-.190476	

EROSION RATES, FT/SEC

.66	.52	.44	.26	0
0	0	0	0	
.44	.295	.215	.215	.145
.03	0	0	0	
.42	.325	.32	.36	.335
.21	.06	0	0	
.26	.285	.38	.325	.26
.26	.175	0	0	
.325	.39	.375	.32	.275
.325	.24	0	0	
.36	.42	.4	.42	.395
.335	.225	.04	0	
.6	.62	.76	.86	.76
.36	.4	.16	0	

Table B-3: Computation of Friction Coefficients
Test 39 (Continued)

VALUES ØF NØN ZERØ C SUB F= 47

MØMENTUM FACTØRS AT EACH NØZ HEIGHT

.010157	.010327	1.07016 E-2	1.13307 E-2	1.22833 E-2
1.22833 E-2	1.22833 E-2			

MATRIX ØF FRICTIØN CØEFFICIENTS C SUB F

3.72153	2.62118	2.08364	1.26309	0
0	0	0	0	
1.59943	1.0343	.734119	.784264	.622601
.159435	0	0	0	
.782234	.746591	.809163	1.08944	1.19833
.957008	.389197	0	0	
.350844	.501847	.819354	.912152	.949753
1.22011	1.19602	0	0	
.327196	.602982	.805637	.961932	1.27693
2.33727	2.41218	0	0	
.40459	.649169	.821828	1.25568	1.91053
2.20157	1.75596	.615233	0	
.679245	.981183	1.62945	2.56638	3.23458
2.1582	2.9764	2.13298	0	

Table B-3: Computation of Friction Coefficients
Test 39 (Continued)

AVERAGE C SUB F= 1.30304
STANDARD DEVIATIØN= 1.13615

C SUB F TIME AVERAGE AT EACH RAD STA

1.12358	1.01961	1.10046	1.26185	1.53212
1.5056	1.74595	1.3741	0	

C SUB F STAND DEVIATIØN AT EACH RAD STA

1.22733	.732592	.533715	.601649	1.16033
1.10122	1.59671	3.25462	0	

C SUB F AVERAGE ØVER RAD STA AT EACH TIME

2.42236	.822358	.853138	.850011	1.2463
1.20182	2.0448			

C SUB F STAND DEVIATIØN AT EACH TIME

3.29268	.795763	.559021	.589756	1.09473
.818152	1.19079			

Table B-4: Computation of Friction Coefficients

Test 55

```
TEST NØ = 55
NØZ RAD   = .1108   FT          MACH NØ    = 2.68
CHAM TEMP = 508.6   DEG R       CHAM VISC = 4.00000 E-7   LB SEC/SQ FT
CHAM PRESS= 4.72    PSI         GAS CØNS  = 12430   SQ FT/SQ SEC DEG R
DRAG CØEFF= 2                   HEAT RATIØ= 1.67
SØIL DENS = 4.85    SLUG/CU FTGRAV    = 32.2    FT/SQ SEC
PART DIA  = .0042   FT          ØR        = 1280.49 MICRØNS
CØHESIØN  = 0    PSF
PACK CØNS = .575                FRICT ANG  = 27   DEG
DESCEN VEL= 2.8     FT/SEC

NØZZLE HEIGHTS ,FEET
 1.507          1.367          1.227          1.087          .947
 .807


TIME ,SEC
 .85            .9             .95            1              1.05
 1.1


RAD STATIØNS ,FEET
 .167           .208           .25            .292           .333
 .375           .416


ERØSIØN DEPTHS ,FEET
 .061           .066           .066           .062           .062
 .053           .014

 .087           .092           .091           .083           .083
 .065           .036

 .107           .108           .105           .096           .092
 .086           .061

 .123           .125           .125           .125           .108
 .093           .083

 .175           .171           .154           .133           .123
 .107           .09

 .236           .229           .218           .194           .152
 .121           .104
```

Table B-4: Computation of Friction Coefficients
Test 55 (Continued)

ERØSIØN PRØFILE SLØPES

.121951	3.01205 E-2	-2.38095 E-2	-2.40964 E-2	-5.42169 E-2
-.289157	-.95122			
.121951	2.40964 E-2	-5.35714 E-2	-4.81928 E-2	-.108434
-.283133	-.707317			
2.43902 E-2	-1.20482 E-2	-7.14286 E-2	-7.83133 E-2	-.060241
-.186747	-.609756			
4.87805 E-2	1.20482 E-2	0	-.10241	-.192771
-.150602	-.243902			
-.097561	-.126506	-.22619	-.186747	-.156627
-.198795	-.414634			
-.170732	-.108434	-.208333	-.39759	-.439759
-.289157	-.414634			

ERØSIØN RATES ,FT/SEC

.52	.52	.5	.42	.42
.24	.44			
.23	.21	.195	.17	.15
.165	.235			
.18	.165	.17	.21	.125
.14	.235			
.34	.315	.245	.185	.155
.105	.145			
.565	.52	.465	.345	.22
.14	.105			
1.22	1.16	1.28	1.22	.58
.28	.28			

Table B-4: Computation of Friction Coefficients
Test 55 (Continued)

VALUES ØF NØN ZERØ C SUB F= 42

MØMENTUM FACTØRS AT EACH NØZ HEIGHT

6.41955 E-3	6.52726 E-3	6.68002 E-3	6.89229 E-3	7.18541 E-3
7.59268 E-3				

MATRIX ØF FRICTIØN CØEFFICIENTS C SUB F

4.76392	4.69869	4.10634	3.07429	2.84698
1.56646	1.85142			
1.70322	1.53887	1.3223	1.02779	.857077
.876812	.972399			
1.20739	.962154	.88762	.970523	.550759
.591106	.822769			
1.56019	1.27718	.896558	.652501	.524161
.35125	.463362			
2.0168	1.58286	1.2657	.883676	.552807
.355216	.263529			
2.93292	2.4129	2.44705	2.14212	1.00965
.532304	.535882			

AVERAGE C SUB F= 1.4728
STANDARD DEVIATIØN= 1.125

C SUB F TIME AVERAGE AT EACH RAD STA

2.36407	2.07878	1.82093	1.45848	1.0569
.712191	.818227			

C SUB F STAND DEVIATIØN AT EACH RAD STA

1.31334	1.37131	1.25679	.946762	.898959
.460783	.566501			

C SUB F AVERAGE ØVER RAD STA AT EACH TIME

3.27259	1.1855	.856046	.817887	.988656
1.71612				

C SUB F STAND DEVIATIØN AT EACH TIME

1.29769	.337899	.228512	.45189	.660171
.997941				

TRW SYSTEMS

INTEROFFICE CORRESPONDENCE

TO: File

CC: J. C. McMunn

68-3340.4-23

DATE: 24 May 1968

SUBJECT: Comparison of Friction Coefficient and Particle Reynolds Number

FROM: R. E. Hutton
BLDG R1 ROOM 1004 EXT 63610

References:

1. "Friction Coefficients Calculated from Erosion Profiles Using Roberts' Theory," TRW Memorandum 68-3343.5-49, J. C. McMunn to File, 23 May 1968.

2. H. Schlichting, Boundary Layer Theory, Pergamon Press, New York, 1955.

Reference 1 presented those values of the friction coefficient C_f (in Roberts' theory) for the theory to be in agreement with the rate of soil erosion observed during four erosion tests. The C_f values were computed over a range of radial locations and time periods. These results showed that C_f varied both with time and radial location. Mean values and standard deviations based on a normal distribution of C_f were also computed; and it was found that the standard deviation was roughly the same magnitude as the mean value of C_f.

This memorandum presents the results of an investigation to determine whether there exists a correlation of C_f with the particle Reynolds number, defined as

$$R_D = \frac{\rho u D}{\mu} \tag{1}$$

In this equation D is the soil particle diameter and ρ, u and μ are the local values of gas mass density, radial velocity and viscosity at each radial station and time. The values of R_D corresponding to each C_f value were determined and the results plotted in Figure 1. The figure indicates considerable scatter in the values of C_f. However, there does appear to be some correlation with C_f, in that generally, C_f decreases with increasing Reynolds number. It might be noted that the values of C_f are larger for the gravel (Test 10) than on the other three tests on glass beads. This may be because the gravel is rougher. However, the larger C_f values on Test 10 may be coincidental and more test data

should be examined before drawing general conclusions concerning the influence of particle roughness on friction coefficient. Clearly, these results indicate a constant value of C_f, such as 0.2, would be inappropriate. Apparently a better approximation would be to consider C_f to depend on Reynolds number.

Stokes' theory for a spherical particle immersed in a flowing fluid indicates the drag coefficient depends on the Reynolds number according to the equation

$$C_D = \frac{24}{R_D} \tag{2}$$

Equation 1 is plotted in Figure 1 along with the experimentally determined drag coefficient presented in Reference 2 (Figure 1.5, page 16). A comparison of the distribution of C_f values indicates the variation is more like that given by Stokes' theory. By assuming the friction coefficient varies inversely with Reynolds number and writing

$$C_f = \frac{K}{R_D} \tag{3}$$

A least squares fit of all the data gives K = 35. Equation (3) with K = 35 is also plotted in Figure 1. If Test 10 is omitted the value of K determined for the three tests on glass beads is K = 21. The values of K for each of the individual tests are K = 12, 143, 56 and 67 for Tests 5, 10, 39 and 55 respectively.

Since the value of K for all the data was close to Stokes' theory, it is recommended that the nominal value of C_f be that given by Stokes' theory, namely

$$C_f = \frac{24}{R_D} \tag{4}$$

with R_D computed from Equation (1) corresponding to the local flow variables at each radial station and time. Statistical theory can be used to account for the random variations of C_f from the nominal value. Recalling that C_f cannot be

negative, and an examination of the C_f data in Figure 1, suggests that C_f may approximate a log normal distribution about the nominal value given in (4). By assuming such a distribution actually exists the values of C_f can be computed based on a given probability and for a desired confidence interval.

The standard deviation S for the log normal distribution about the mean value in Equation (4) is

$$S^2 = \frac{1}{N} \sum_{i=1}^{N} (\log C_{fi} - \log 24 + \log R_{Di})^2 \qquad (5)$$

For the 141 data points in Figure 1 the value of S to the base e is

$$S = 1.2414$$

If it is required that there is a 90 per cent probability that C_f lies between $C_{f\ max}$ and $C_{f\ min}$ and a 90 per cent confidence is required for these limits, log normal distribution tables for 141 data points gives k = 1.790. Thus, kS = 2.222 and $e^{2.222} = 9.224$. Then

$$C_{f\ max} = 9.224 \left(\frac{24}{R_D}\right) = \frac{222}{R_D} \qquad (6)$$

$$C_{f\ min} = \frac{1}{9.224} \left(\frac{24}{R_D}\right) = \frac{2.6}{R_D} \qquad (7)$$

Figure 2 shows the same C_f and R_D data in Figure 1 with the mean value of C_f given by (4) and the limit values given by (6) and (7) superimposed.

Finally then, it is recommended that the "best" estimate of the erosion contours be based on the nominal C_f value given in (4). While (6) will be used to predict a maximum erosion profile which will be exceeded no more than 10 per cent of the time with a 90 per cent confidence.

FIGURE 1

Friction Coefficient vs. Reynolds Number

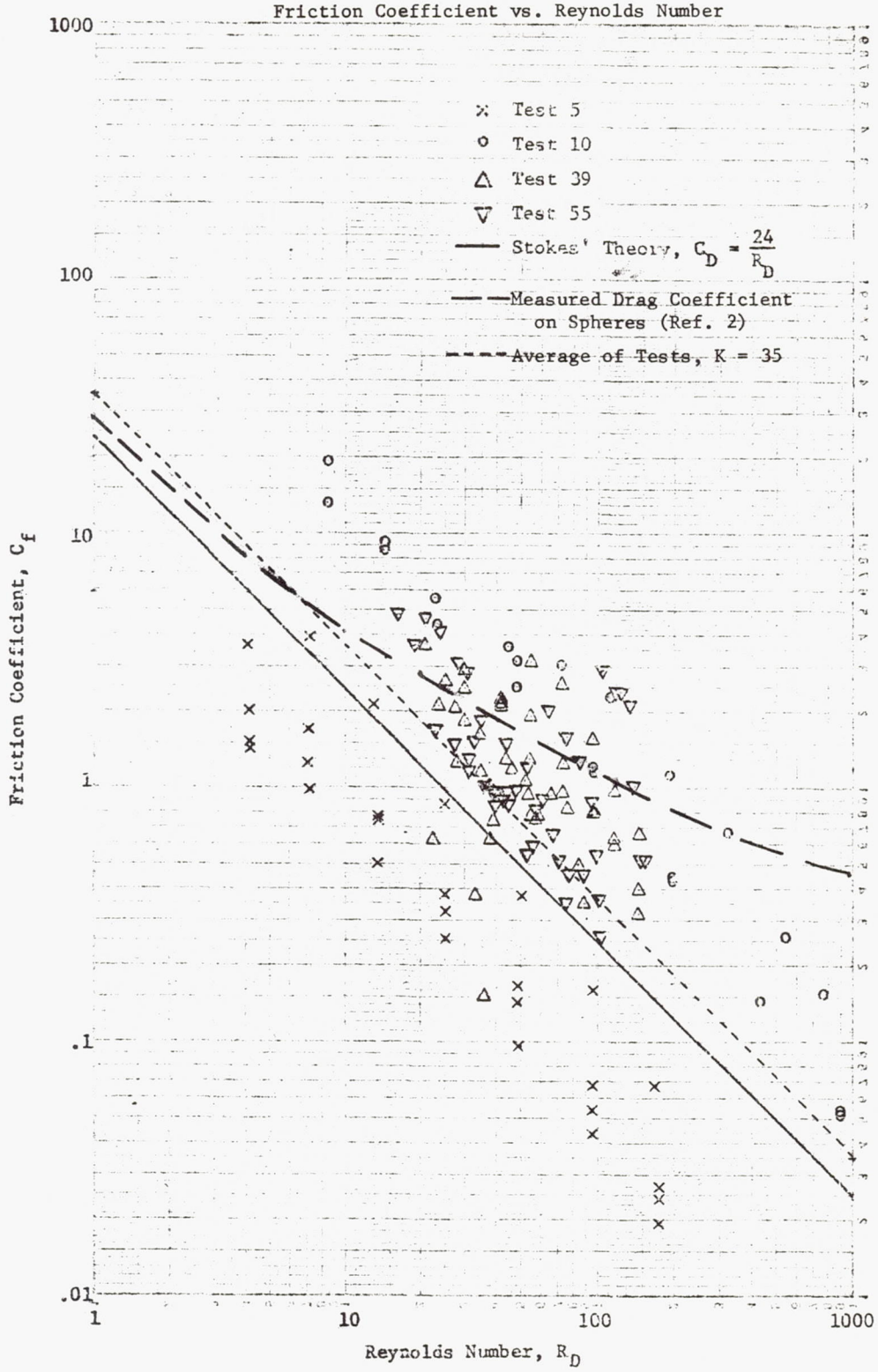

FIGURE 2
Variation of Nominal Friction
Coefficient with Reynolds Number